

LOCKHEED MARTIN ENERGY RESEARCH LIBRARIES



3 4456 0515553 2

CENTRAL RESEARCH LIBRARY
DOCUMENT COLLECTION

3

ORNL-4366
UC-4 - Chemistry

OAK RIDGE NATIONAL LABORATORY
CENTRAL RESEARCH LIBRARY
DOCUMENT COLLECTION

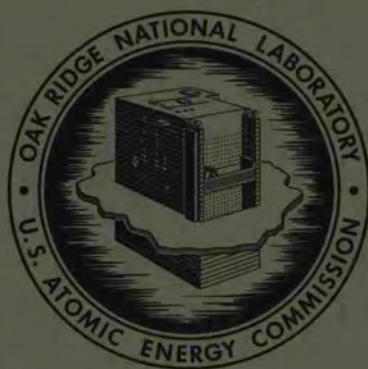
LIBRARY LOAN COPY

DO NOT TRANSFER TO ANOTHER PERSON

If you wish someone else to see this
document, send in name with document
and the library will arrange a loan.

ORNL-4366
UC-4 - Chemistry

CHEMICAL TECHNOLOGY DIVISION
UNIT OPERATIONS SECTION
QUARTERLY PROGRESS REPORT
JULY-SEPTEMBER 1968



OAK RIDGE NATIONAL LABORATORY
operated by
UNION CARBIDE CORPORATION
for the
U.S. ATOMIC ENERGY COMMISSION

Printed in the United States of America. Available from Clearinghouse for Federal
Scientific and Technical Information, National Bureau of Standards,
U.S. Department of Commerce, Springfield, Virginia 22151
Price: Printed Copy \$3.00; Microfiche \$0.65

LEGAL NOTICE

This report was prepared as an account of Government sponsored work. Neither the United States, nor the Commission, nor any person acting on behalf of the Commission:

- A. Makes any warranty or representation, expressed or implied, with respect to the accuracy, completeness, or usefulness of the information contained in this report, or that the use of any information, apparatus, method, or process disclosed in this report may not infringe privately owned rights; or
- B. Assumes any liabilities with respect to the use of, or for damages resulting from the use of any information, apparatus, method, or process disclosed in this report.

As used in the above, "person acting on behalf of the Commission" includes any employee or contractor of the Commission, or employee of such contractor, to the extent that such employee or contractor of the Commission, or employee of such contractor prepares, disseminates, or provides access to, any information pursuant to his employment or contract with the Commission, or his employment with such contractor.

ORNL-4366

Contract No. W-7405-eng-26

UNIT OPERATIONS SECTION QUARTERLY PROGRESS REPORT

July-September 1968

CHEMICAL TECHNOLOGY DIVISION

M. E. Whatley

P. A. Haas

L. E. McNeese

A. D. Ryon

C. D. Watson

APRIL 1970

OAK RIDGE NATIONAL LABORATORY
Oak Ridge, Tennessee
Operated by
UNION CARBIDE CORPORATION
for the
U. S. ATOMIC ENERGY COMMISSION

LOCKHEED MARTIN ENERGY RESEARCH LIBRARIES

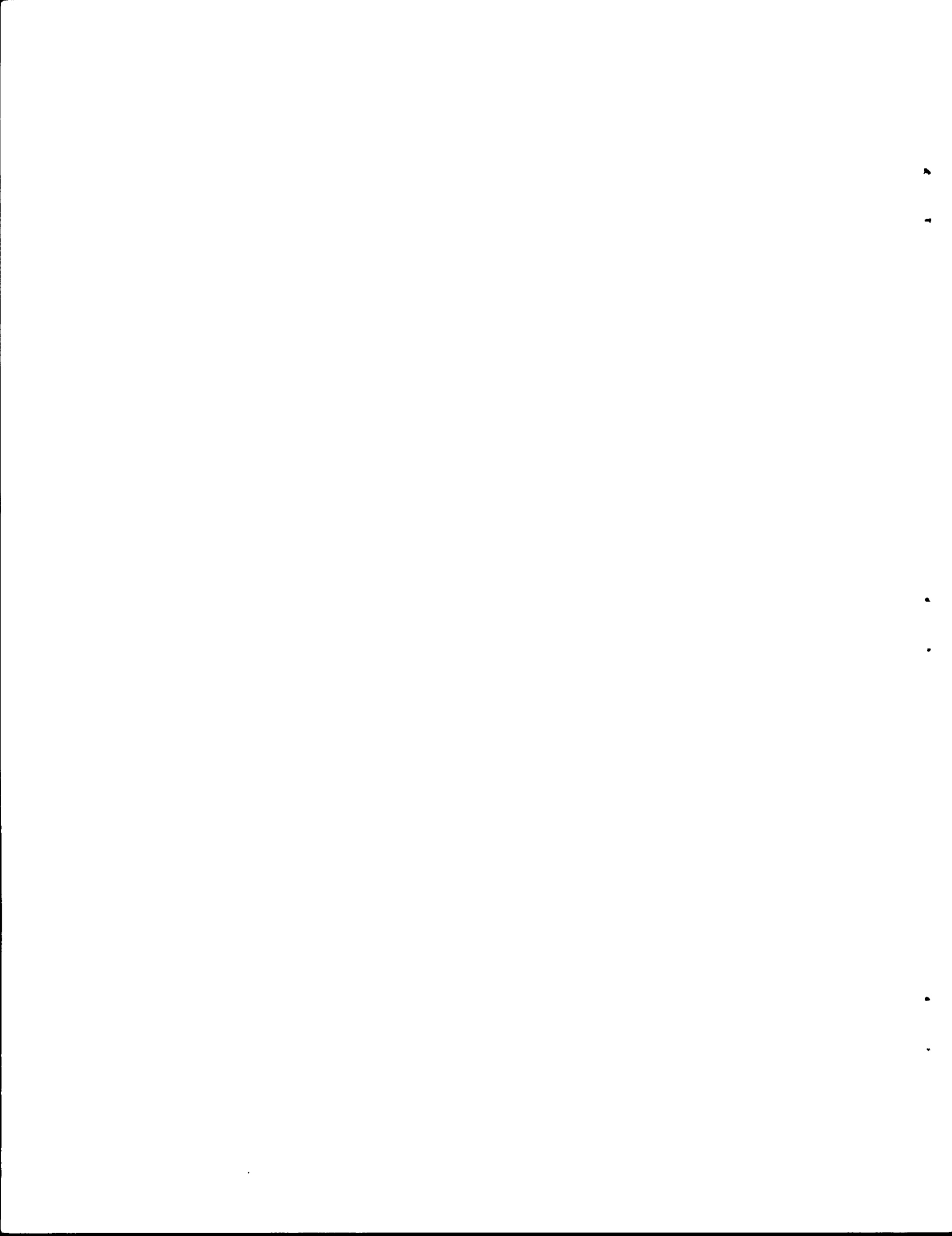


3 4456 0515553 2



CONTENTS

	<u>Page</u>
ABSTRACTS	1
1. ENGINEERING SEPARATION OF MACROMOLECULAR BIOLOGICAL SUBSTANCES	3
1.1 Prediction of Solute Resolution and Gradient Effects in Elution Chromatography in Craig Extractors	3
1.2 Appendix	18
2. SOL-GEL DEVELOPMENT STUDIES	22
2.1 Preparation of UO_2 Sols by Solvent Extraction	22
2.1.1 Preparation of U(IV) Nitrate Solution	25
2.1.2 Operation of the Solvent-Extraction Equipment	30
2.1.3 Evaporation of Sol	33
2.2 Two-Fluid Nozzles as Sol Dispersers Under Turbulent Flow Conditions	35
3. MOLTEN-SALT REACTOR PROCESSING STUDIES	41
3.1 Distillation of Molten Salt	42
3.2 Gas-Lift Pumping of Liquid Metals	47
3.3 Simulated Salt-Metal Contactor Studies	57
3.3.1 Use of Simulated System for Contactor Development	57
3.3.2 Experimental Equipment and Method	59
3.3.3 Visual Observation of Column Operation	61
3.3.4 Experimentally Measured Flooding Rates	70
3.3.5 Dispersed-Phase Holdup	76
3.3.6 Pressure Drop in the Continuous Phase	81



ABSTRACTS

1. ENGINEERING SEPARATION OF MACROMOLECULAR BIOLOGICAL SUBSTANCES

Key parameters for the successful separation of solutes in the chromatographic elution of macromolecules have been identified by means of a mathematical analysis based on the Craig type of solvent extraction.

2. SOL-GEL DEVELOPMENT STUDIES

2.1 Preparation of UO_2 Sols by Solvent Extraction

The preparation of UO_2 sols by solvent extraction has been successfully scaled up, and engineering equipment has been operated continuously to produce 6 liters of 0.2 M sol per hour. A 14-liter batch slurry reductor was developed, and was used to produce more than 40 kg of U(IV) nitrate solution that was suitable as feed for the solvent-extraction process. In the extraction process, a 30-min interstage digestion step carried out at about 60°C produced the best-quality sol.

2.2 Development of Two-Fluid Nozzle

The development of processes and equipment for sol-gel ceramic fuels was continued. The two-fluid nozzle in conjunction with turbulent flow conditions was applied to the preparation of sol droplets 20 to 300 μ in diameter, and a dimensionless correlation was derived for the results.

3. MOLTEN-SALT REACTOR PROCESSING STUDIES

Information obtained from the nonradioactive operation of the MSRE Distillation Experiment is summarized. Calculations indicate that distillation of 10 to 40% of MSBR fuel salt will produce a significant increase in the free-fluoride content, which will improve the rare-earth: thorium separation factor in the subsequent reductive extraction.

A series of experiments to test the feasibility of gas-lift pumping of liquid metals such as bismuth was made with mercury.

Measurements of dispersed-phase holdup, continuous-phase pressure drop, and throughput at flooding have been made for the countercurrent flow of water and mercury in a 1-in.-diam column containing various types and sizes of packing materials.

Previous Reports in This Series for the Year 1968

January-March

ORNL-4364

April-June

ORNL-4365

1. ENGINEERING SEPARATION OF MACROMOLECULAR BIOLOGICAL SUBSTANCES

1.1 Prediction of Solute Resolution and Gradient Effects in Elution Chromatography in Craig Extractors

W. S. Groenier A. D. Ryon

The elution operation of the Craig solvent extractor was analyzed mathematically to enable us to predict its performance for the separation of solutes. The analysis should also be helpful in simulating the transport of macromolecules in elution chromatography.

During each cycle of operation of a Craig extractor, two immiscible liquid phases are mixed in each stage, allowed to settle, and then separated completely. The heavy phase in each stage is stationary, while the light phase progresses from one stage to the next. By this method, the portion of heavy phase in each stage is successively contacted in a stepwise manner with new portions of light phase. The analogy between such extractions and elution chromatography is straightforward when one considers Craig extractors to have a sufficient number of stages to account for chromatographic adsorption sites and enough cycles to approximate the continuous operation of an elution column.

Craig extractors perform mass-transfer operations as follows: First, a portion of the heavy phase is added to each stage. Then, the feed (i.e., the light phase) is admitted to stage 1 in cycle 1. On contact of the two phases, some solute is transferred from the feed to the heavy phase in that stage. In succeeding cycles, the feed progresses to other stages and is further depleted of solute, while fresh portions of the light phase (but containing no solute) are admitted to stage 1. These additions serve to wash the solute through the device by reextracting some solute in each stage. Now if the original feed contains more than one solute, and if each solute exhibits a different mass distribution to the opposite phase, these solutes will be washed out of the contactor in different cycles and will, therefore, be separated. A Gaussian concentration distribution of solutes is obtained if we assume constant dis-

tribution coefficients and phase ratios. The sharpness of the emerging concentration peak and the overlap of emerging concentration distributions are of interest, since clean separation of solutes demands minimum overlap, and significant product concentration demands a high concentration peak.

To more closely fit Craig-type extractions to conditions observed with real chromatographic columns, we deviated from normal operation as follows: Allowances were made for the case in which solute is delayed in the column packing by some stronger adsorbing medium. This can be expressed as an incomplete phase separation in the extraction analogy. Also, in order to wash all solutes through the column in a reasonable period of time, the salt content of the wash solution (weak sodium chloride solution) was usually altered in a programmed manner to hasten emergence of the last solute. This type of operation, known as gradient elution, was treated in the extraction analogy by having the mass distribution coefficient vary in a programmed manner with each cycle. The influence of such a gradient on concentration distribution overlap was determined.

In Fig. 1.1, a schematic diagram of the process is shown. All of the stages retain heavy phase. Note the manner in which feed and wash solutions proceed through the stages with succeeding cycles. The path of feed or any solvent portion is labeled as a traverse.

The mathematical treatment of this system involves the successive application of a mass balance around each stage, utilizing the definition of the mass distribution coefficient, k . For any stage s , during any cycle c , the solute composition of the heavy phase within the stage changes from $y_{c-1,s}$ to $y_{c,s}$, and the solute composition of the feed or wash solution portion changes from $x_{c-1,s}$ to $x_{c,s+1}$. We define the phase ratio, R , as the ratio of feed or wash solution volume to the heavy-phase volume in each stage. The extraction factor, E , is defined as k/R . Thus,

$$k = E R = \frac{y_{c,s}}{x_{c,s+1}} .$$

The single-stage separation factor, α , is k_1/k_2 .

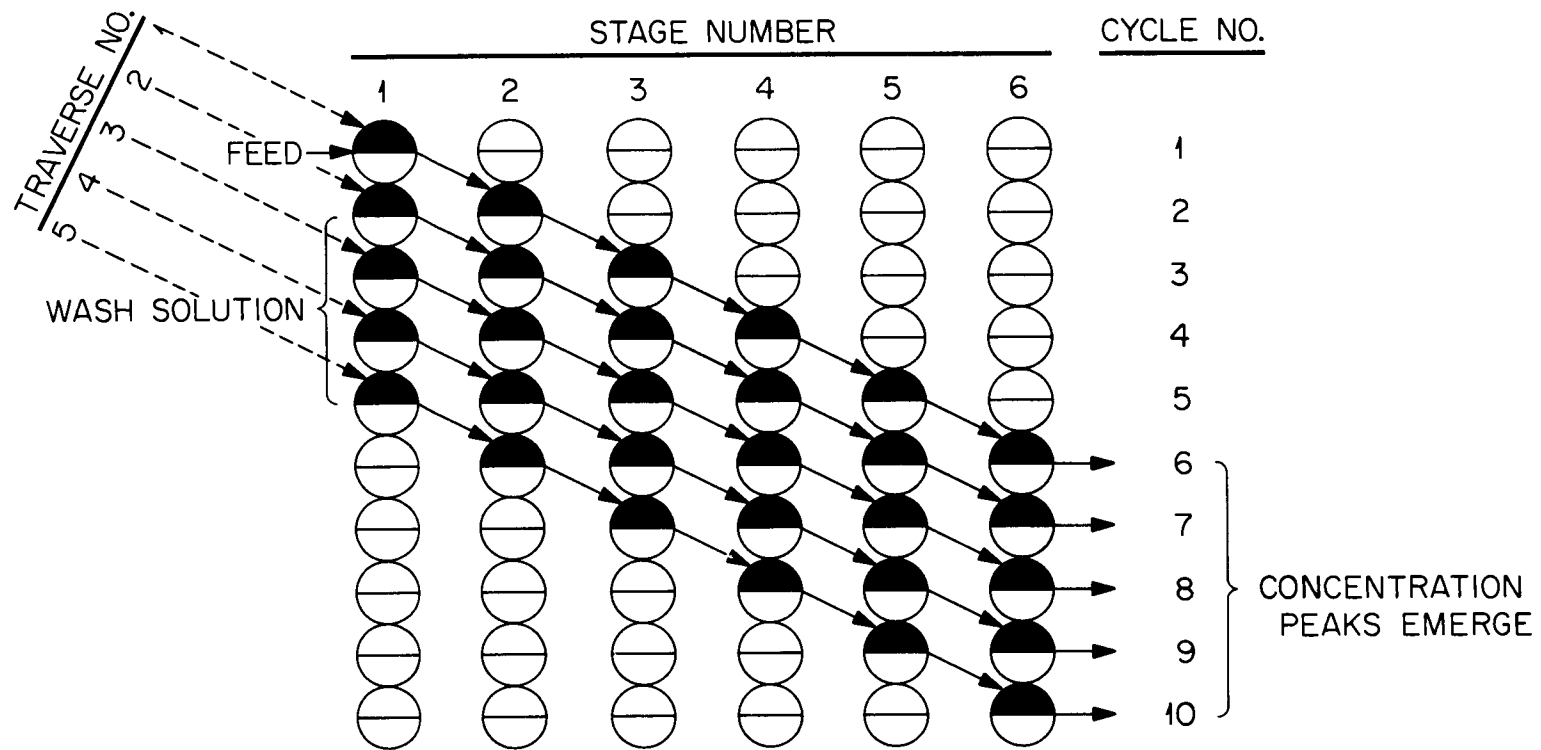


Fig. 1.1 Representation of Stagewise Elution Experiment.

The stage product compositions in terms of inlet compositions are:

$$x_{c,s+1} = \frac{1}{1+E} \left[\frac{R x_{c-1,s} + y_{c-1,s}}{R} \right]$$

$$y_{c,s} = \frac{1}{1-E} \left(R x_{c-1,s} + y_{c-1,s} \right).$$

A computer program (ELUGRA) was written to perform the above calculations for systems of up to 1000 stages involving up to 3 solutes and 1000 traverses (2000 cycles). Provisions were made for both linear and logarithmic gradients and for incomplete phase separation. The program, along with instructions for its use, is presented in the Appendix (Sect. 1.2).

Typical elution curves for three solutes (A, B, and C) are shown in Fig. 1.2. These curves demonstrate the general advantages of gradient elution: higher peak concentrations are obtained, and fewer traverses are required. However, some loss of resolution occurs, as shown by increased overlapping of solute peaks.

The large volume of data obtained using ELUGRA has been summarized in Figs. 1.3 through 1.11. These graphs show the effects of distribution coefficient, completeness of phase separation, phase ratio, and number of stages on the sharpness of the emerging solute concentration peak (measured as an average concentration and expressed as a percentage of the feed concentration), the number of traverses required to wash the solute through the extractor (the last traverse yields product containing less than 1 ppm of solute), and the amount of overlap exhibited by the concentration distributions.

For constant distribution coefficients, the number of required traverses varies nearly linearly with the value of k (Fig. 1.3). Average product values are highest when k is very small and decrease rapidly as k increases to about 1. In a 10-stage extractor, an average product that is only 0.5% of the feed concentration is obtained when k is about 8. The overlapping of concentration distributions is greatest when the k values for the products are similar and when the separation factors are small (Fig. 1.4).

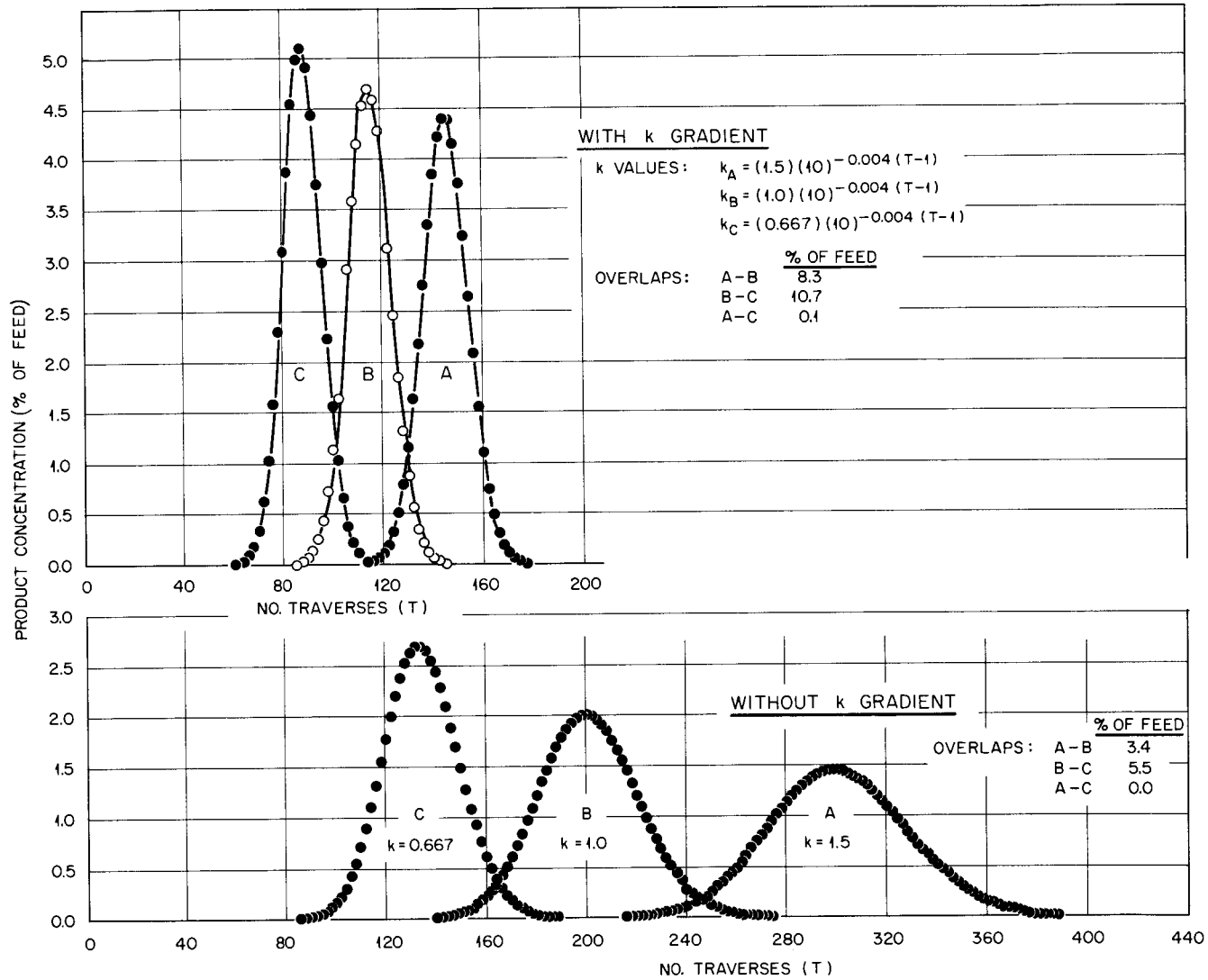


Fig. 1.2 Typical Product Profiles. Conditions: 200 stages, 100% phase separation, R = 1.0.

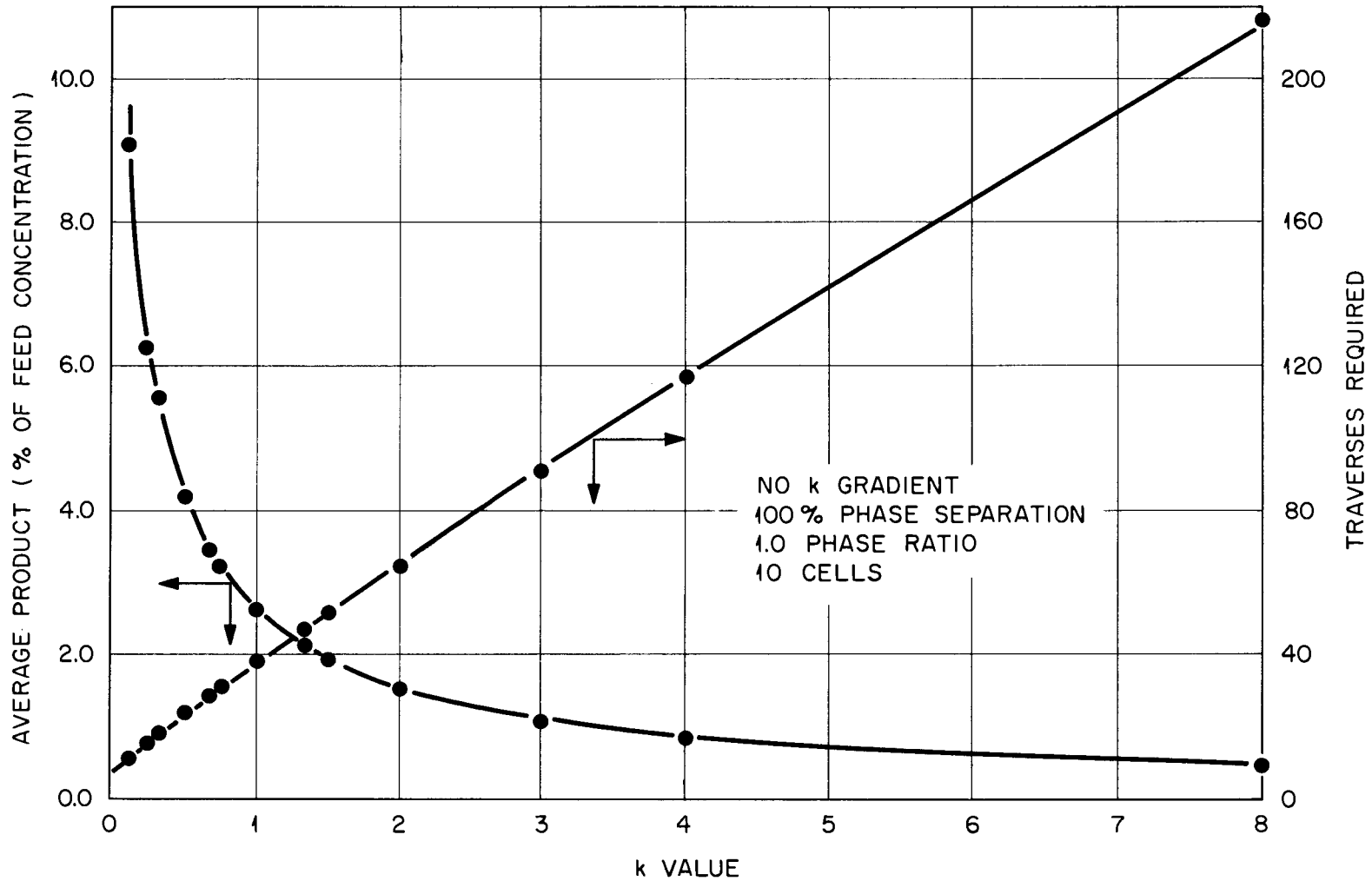


Fig. 1.3 Effect of Distribution Coefficient, k , on Average Product Concentration and on Number of Traverses Required. Conditions: constant k ; 100% phase separation; $R = 1.0$; 10 stages.

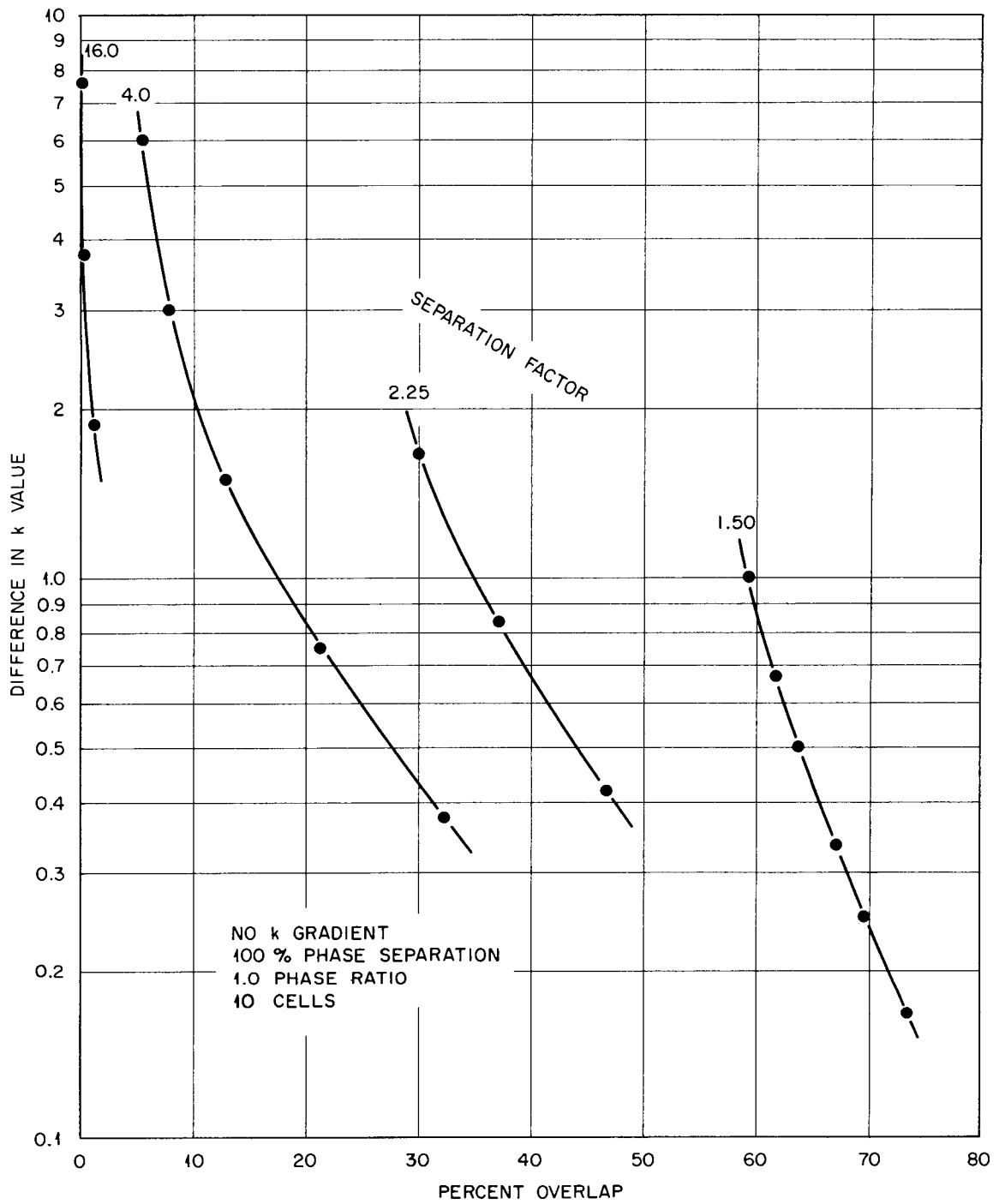


Fig. 1.4 Effect of Separation Factor and k Difference on Percent Overlap. Conditions: constant k; 100% phase separation; $R = 1.0$; 10 stages.

ORNL DWG 69-12174

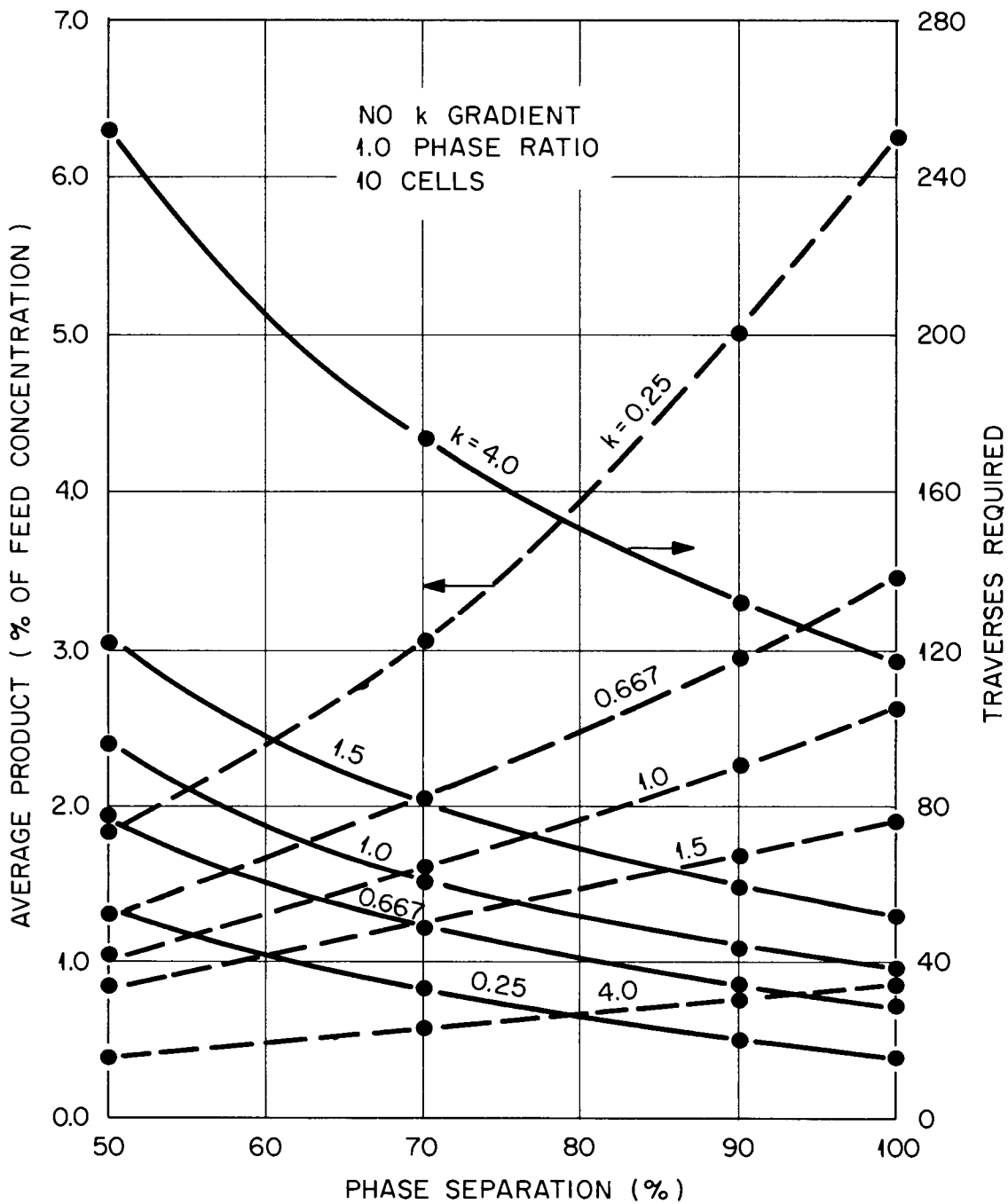


Fig. 1.5 Effect of Degree of Phase Separation on Average Product Concentration and on Number of Traverses Required. Conditions: constant k ; $R = 1.0$; 10 stages.

ORNL DWG 69-12175

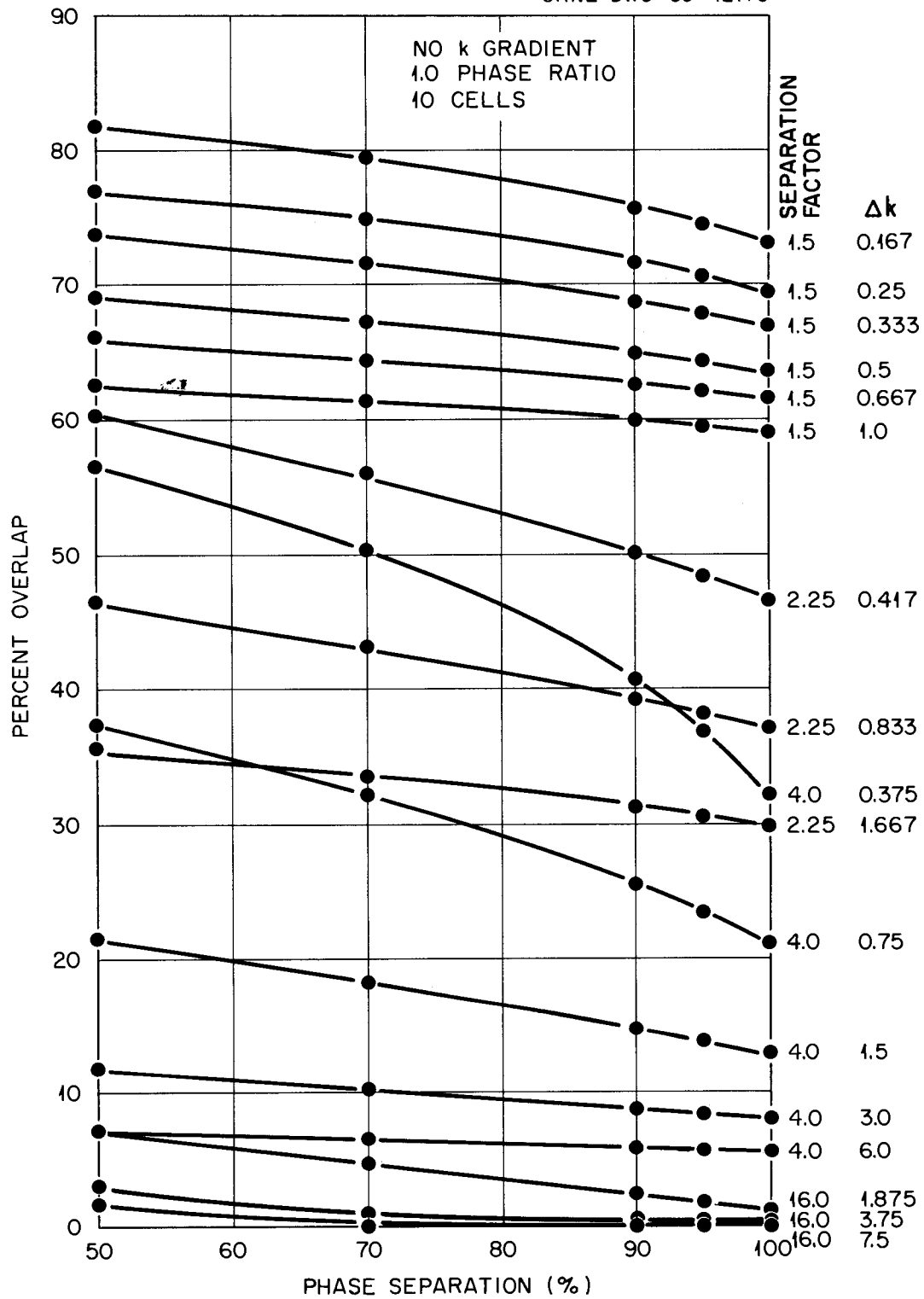


Fig. 1.6 Effect of Degree of Phase Separation and Separation Factor on Percent Overlap. Conditions: constant k; R = 1.0; 10 stages.

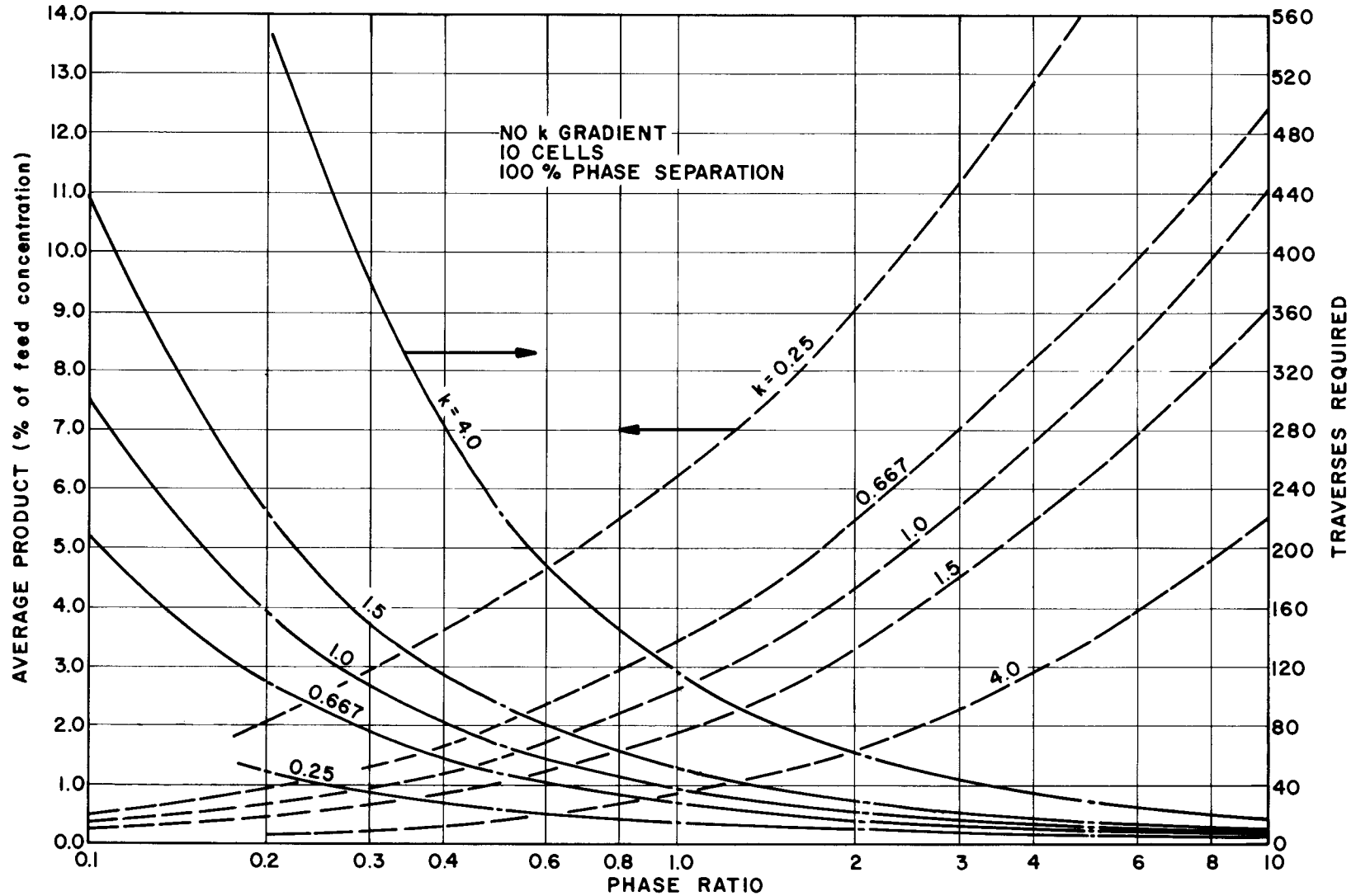


Fig. 1.7 Effect of Phase Ratio on Average Product Concentration and on Number of Traverses Required. Conditions: constant k ; 10 stages; 100% phase separation.

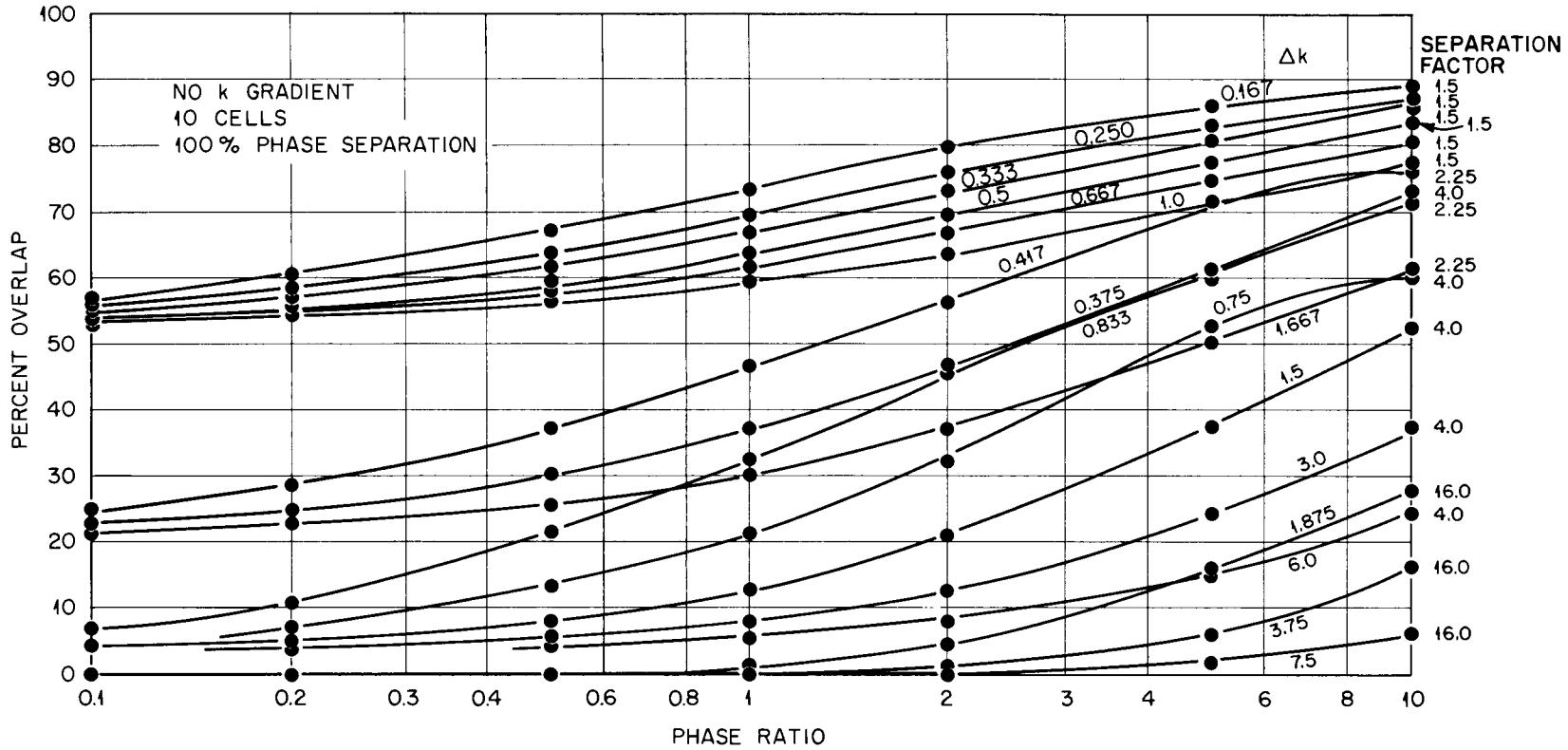


Fig. 1.8 Effect of Phase Ratio and Separation Factor on Percent Overlap. Conditions: constant k; 10 stages; 100% phase separation.

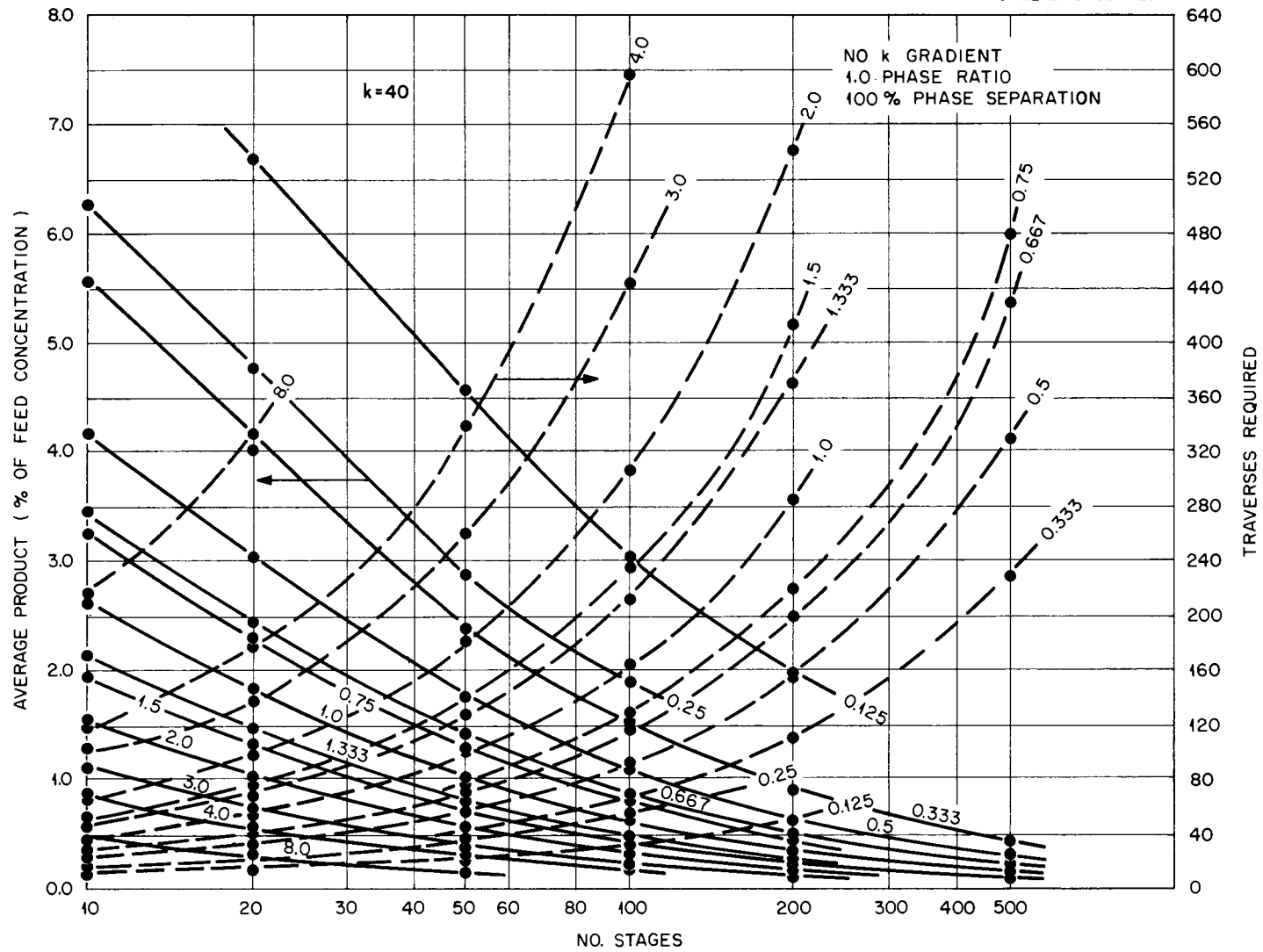


Fig. 1.9 Effect of Number of Stages on Average Product Concentration and on Number of Traverses Required. Conditions: constant k ; $R = 1.0$; 100% phase separation.

ORNL DWG 69-12178

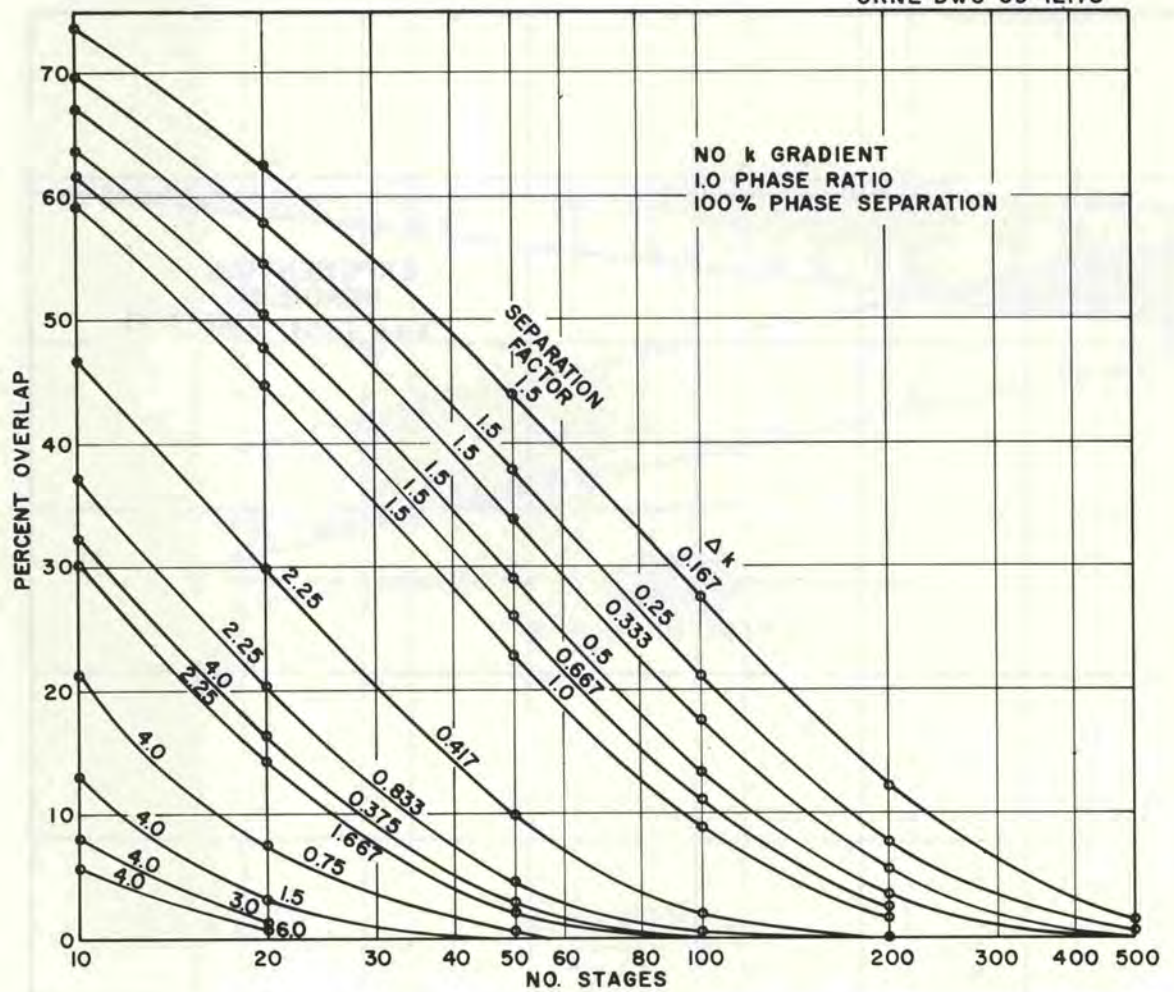


Fig. 1.10. Effect of Number of Stages and Separation Factor on Percent Overlap. Conditions: constant k ; $R = 1.0$; 100% phase separation.

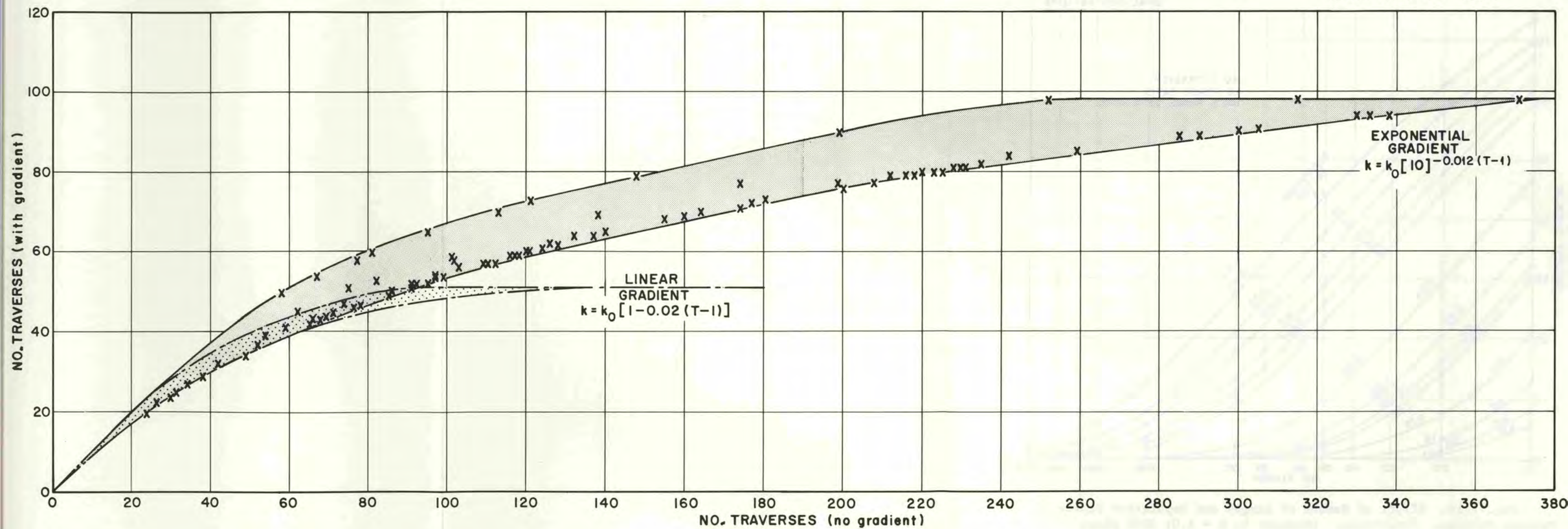


Fig. 1.11 Effect of a Varying Mass Distribution Coefficient (Gradient Elution) on the Number of Traverses Required to Complete an Elution.

The effects of incomplete phase separation are shown in Figs. 1.5 and 1.6. Whereas poor phase separation causes rather large increases in the number of traverses required (producing large decreases in average product concentration), the effect on overlap is small. A greater effect is noted when the phase ratio is varied (Figs. 1.7 and 1.8).

Increasing the number of stages (Fig. 1.9 and 1.10) disperses the solute peak and requires a larger number of traverses in order to recover all the product. The average concentration of the product is lower in this case, but resolution is improved considerably.

Gradient elution serves to hasten the emergence of slow components (strongly adsorbed ones). Fewer traverses are required when a gradient is used (Fig. 1.11). However, the overlapping of distributions is somewhat greater.

The calculated effects shown here, along with subsequent use of the ELUGRA program, will allow a better interpretation of chromatographic elution data and make possible more efficient planning of elution experiments.

1.2 Appendix

The listing for program ELUGRA is given on pp. 19-21. The following program cards are required for this program:

First Card:

Columns	1 - 16	Job Title
	17 - 24	Number of Stages, NS
	25 - 32	Number of Traverses, NT
	33 - 40	Number of Extractable Components, NC
	41 - 48	Job Index, DEX (see footnote "a")
	49 - 56	Phase Ratio, PR (ratio of feed or wash solution volume to heavy-phase volume)
	57 - 64	% Phase Separation, BM
FORMAT		(2A8, 3I8, 3F8.0)

Succeeding Cards: (One for each component, a total of NC)

Columns	1 - 8	Extraction Distribution Factor Index, INDEX (see footnote "b")
	9 - 16	Constant, EXF
	17 - 24	Constant, EXG
FORMAT		(I8, 2F8.1)

"a" DEX is -1.0: Allows program to determine the number of traverses required to get product concentrations down to less than 1 ppm. For this case, leave columns 25-32 (NT) blank. Print-out includes only the product concentrations from each traverse.

DEX is 0.0: Print-out includes only the product concentrations for all traverses 1 through NT.

DEX is -1: Print-out includes both phase concentrations in each stage for all traverses 1 through NT.

"b" INDEX is -1: For a linear gradient according to $k = \text{EXF} - \text{EXG}(T-1)$, where T is the traverse number.

INDEX is 0: For a constant value of k. $k = \text{EXF}$.

INDEX is 1: For an exponential gradient according to $k = \text{EXF}(10)^{-\text{EXG}(T-1)}$, where T is the traverse number.

```

PROGRAM ELUGRA
C CONCENTRATION GRADIENTS IN CRAIG-TYPE ELUTION EXPERIMENTS
DIMENSION JUNK(10),N(1000),CON(2,1000),CON(3,1000),NTX(3)
2 READ 900,JUNK
  DECODE(80,901,JUNK) TAT1,TAT2,NS,NT,NC,DEX,PR,BM
  IF(DEX)3,4,4
3 NT = 1000
4 NTT = NT + NS = 1
  PRINT 902,PR,TAT1,TAT2,NS,NT,NTT,NC,BM
  PRINT 906
  R = PR
  BM = BM/100.0
  DO 5 J=1,NS
5 N(J) = J
  DO 890 I=1,NC
  SUM = 0.0
  DO 10 K=1,NS
10 CON(2,K) = 0.0
  TOT = 1000.0
  READ 903,INDEX,EXF,EXG
  IF(INDEX)30,20,46
20 PRINT 904,EXF,I
  EXH = EXF/(PR + EXF)
  GO TO 49
30 PRINT 905, I,EXG,EXF
  GO TO 49
46 PRINT 910, I,EXF,EXG
49 EX = EXF
  DO 800 II=1,NT
  DO 100 J=1,NS
  IF(INDEX)60,50,73
50 CON(2,J) = TOT*EXH
  IF(CON(2,J)=0.0001)53,53,55
53 CON(2,J) = 0.0
55 CON(1,J) = CON(2,J)/EXF
  GO TO 70
60 T = II
  EXF = -EXG*(T-1.0) + EX
  EXH = EXF/(PR + EXF)
  GO TO 50
73 T = II
  EXF = EX *10.0**(-EXG*(T-1.0))
  EXH = EXF/(PR + EXF)
  GO TO 50
70 IF(BM=1.0)75,90,90
75 IF(NS=J)79,79,78
78 KK = J + 1
  TOT = CON(1,J)*R*BM + CON(2,KK) + CON(1,KK)*R*(1.-BM)
  GO TO 100
79 TOT = CON(2,1) + CON(1,1)*R*(1.-BM)
  GO TO 100
90 IF(NS=J)92,92,91
91 KK = J+1
  TOT = CON(1,J)*R + CON(2,KK)
  GO TO 100
92 TOT = CON(2,1)

```

```

100 CONTINUE
    IF(DEX)105,110,120
105 IF(II)110,110,106
106 IF(CON(1,NS)=0.0100)108,108,110
108 IN = II = 1
    CCC = CNO(1,IN)/(R*BM)
    IF(CON(1,NS)=CCC)109,110,110
109 NTX(I) = II
    CNO(I,II) = CON(1,NS)*R*BM
    SUM = SUM + CNO(I,II)
    IF(I=1)805,805,500
500 IJ = II + 1
    DO 600 M=IJ,NT
    CNO(I, M) = 0.0
600 CONTINUE
    GO TO 805
110 CNO(I,II) = CON(1,NS)*R*BM
    SUM = SUM + CNO(I,II)
    GO TO 800
120 PRINT 908,II,EXF
    PRINT 909,(N(J),CON(1,J),CON(2,J),J=1,NS)
800 CONTINUE
805 IF(DEX)810,810,890
810 NT = NTX(I)
    PRINT 911,NTX(I)
    NN = NTX(I)
    PRINT 912,(CNO(I,II),II=1,NN)
    SUM = SUM/NTX(I)
    PRINT 907,SUM
890 CONTINUE
    SUM1 = 0.0
    SUM2 = 0.0
    SUM3 = 0.0
    IF(DEX)510,510,2
510 DO 899 I=1,NT
    IF(CNO(1,I)=CNO(3,I))891,891,892
891 SUM3 = SUM3 + CNO(1,I)
    GO TO 893
892 SUM3 = SUM3 + CNO(3,I)
893 IF(CNO(1,I)=CNO(2,I))894,894,895
894 SUM2 = SUM2 + CNO(1,I)
    GO TO 896
895 SUM2 = SUM2 + CNO(2,I)
896 IF(CNO(2,I)=CNO(3,I))897,897,898
897 SUM1 = SUM1 + CNO(2,I)
    GO TO 899
898 SUM1 = SUM1 + CNO(3,I)
899 CONTINUE
    SUM1 = SUM1/I0.
    SUM2 = SUM2/I0.
    SUM3 = SUM3/I0.
    PRINT 913,SUM1,SUM2,SUM3
    GO TO 2
900 FORMAT(10A8)
901 FORMAT(2A8,3I8,3F8.0)
902 FORMAT(34H|CONCENTRATION GRADIENTS FOR A/B =,F8.4,|X,|9HCRAIG=TYPE

```

```

1 ELUTIONS//10X,2A8/20X,18,2X,13HCONTACT CELLS/20X,18,2X,9HTRAVERSE
28/20X,18,2X,6HCYCLES/20X,18,2X,10HCOMPONENTS/20X,F8,2,2X,18HPERCENT
3T SEPARATION)
903 FORMAT(18,2F8,1)
904 FORMAT(1H0,10X,20HDISTRIBUTION COEF = ,F8.4,5X,13HFOR COMPONENT,18
1)
905 FORMAT(1H0,10X,31HDISTRIBUTION COEF FOR COMPONENT,18,5X,16HVARIES
1LINEARLY,/15X,4HK = ,F8.4,5X,27HTIMES (TRAVERSE NO.=1) PLUS,F8.4)
906 FORMAT(1H0,10X,38MA = MOBILE PHASE, B = STATIONARY PHASE)
907 FORMAT(14,5X,11HAVERAGE X = ,F8.4)
908 FORMAT(14H0TRAVERSE NO. ,18,10X,4HK = ,F8.4/5X,4HCELL,7X,1HX,12X,
11HY,14X,4HCELL,7X,1HX,12X,1HY,14X,4HCELL,7X,1HX,12X,1HY)
909 FORMAT(3(18,5X,F8.4,5X,F8.4,5X))
910 FORMAT(1H0,10X,31HDISTRIBUTION COEF FOR COMPONENT,18,5X,10HVARIES
1AS /15X,4HK = ,F8.4,5X,32HTIMES 10 TO THE =A TIMES B POWER/15X,10H
2WHERE A = ,F8.4,5X,30HAND B = TRAVERSE NO. MINUS 1.0)
911 FORMAT(76H0VALUES OF X%A FROM LAST CELL (WEIGHT UNITS OF SOLUTE, 1
1000 UNITS INITIALLY),18,2X,9HTRAVERSES)
912 FORMAT(10(F8.4,4X))
913 FORMAT(1H,5X,27H0OVERLAPS COMPONENTS 2=3,F8.4/19X,14HCOMPONENT
1S 1=2,F8.4/19X,14HCOMPONENTS 1=3,F8.4)
END ELUGRA

```

2. SOL-GEL DEVELOPMENT STUDIES

P. A. Haas

The objective of these studies is to develop optimum sol-gel processes for the preparation of ceramic fuels containing uranium, plutonium, thorium, and their mixtures. The present emphasis is on the preparation of urania or urania-thoria sols, and the subsequent use of these sols in preparing oxide microspheres.

Several flowsheets have been developed for preparing UO_2 sols. All of these processes use uranyl nitrate solution as the starting material, and involve the following conversions:

1. Reduction of uranyl nitrate to uranous nitrate by hydrogen in the presence of a catalyst.
2. Formation of a hydrated uranous oxide.
3. Removal of nitrate ion, and other anions or cations.
4. Dispersion of the hydrated uranous hydroxide as colloidal crystallites.

The suitability of the sol for preparing UO_2 microspheres depends on the preparation conditions and on the operating conditions in the sphere-forming system. This quarter we report on the preparation of UO_2 sols by solvent extraction, and the forming of spheres via a two-fluid nozzle under turbulent flow conditions.

2.1 Preparation of UO_2 Sols by Solvent Extraction

F. L. Daley A. D. Ryon

The process for preparing UO_2 sols by solvent extraction has been successfully scaled up and operated continuously in engineering experiments. Forty runs have been made, each producing about 2 kg of UO_2 in the form of a dilute (about 0.2 M) sol. Laboratory studies to characterize the sol and to aid in the engineering studies are still in progress. We

have studied three operating parameters that affect sol properties: the method for preparing the initial U(IV) solution, nitrate-to-uranium mole ratio during digestion, and digestion temperature.

The basic method for preparing UO_2 sol by solvent extraction (Fig. 2.1) was developed from laboratory batch studies.¹ It consists of extracting nitrate from an aqueous solution of U(IV) nitrate-formate with a long-chain amine (e.g., Amberlite LA-2*) dissolved in a liquid paraffin. Digestion of the resulting nitrate-deficient solution produces the UO_2 sol. Final nitrate adjustment is obtained in subsequent extractions. The amine, which is regenerated by contact with sodium carbonate is recycled.

The equipment for the engineering study of the process is the same as that used for preparing ThO_2-UO_3 sol.² The contacting devices for extraction, water scrubbing, and amine regeneration are mixer-settlers designed to be geometrically safe with regard to criticality. Each mixer has six compartments which, with cocurrent flow of the organic and aqueous phases, give the same effect as mixing vessels in series. The phases separate in the settler section below the mixer. The position of the interface is controlled by adjustable weirs on both the organic-phase outlet and the aqueous-phase outlet. Maintaining the interface below the mixer helps to produce a water-in-oil type of dispersion, which is important in minimizing emulsions. At shutdown the aqueous phase is drained out of the mixer, so that at subsequent startup the incoming aqueous phase is readily dispersed into the organic phase. The digester is an enlargement of the aqueous-phase jackleg on the first extraction mixer-settler. The temperature in each extractor and in the digester is controlled by circulating water through internal coils. The design capacity of the equipment is 6 liters of sol per hour; the capacity is determined by the size of the digester and the required residence time in the digester (30 min).

* Product of Rohm and Haas Co.

¹ Chem. Technol. Div. Ann. Progr. Rept. May 31, 1967, ORNL-4145, p. 184.

² M. E. Whatley et al., Unit Operations Section Quarterly Progress Report, July-September 1967, ORNL-4234, pp. 57-79.

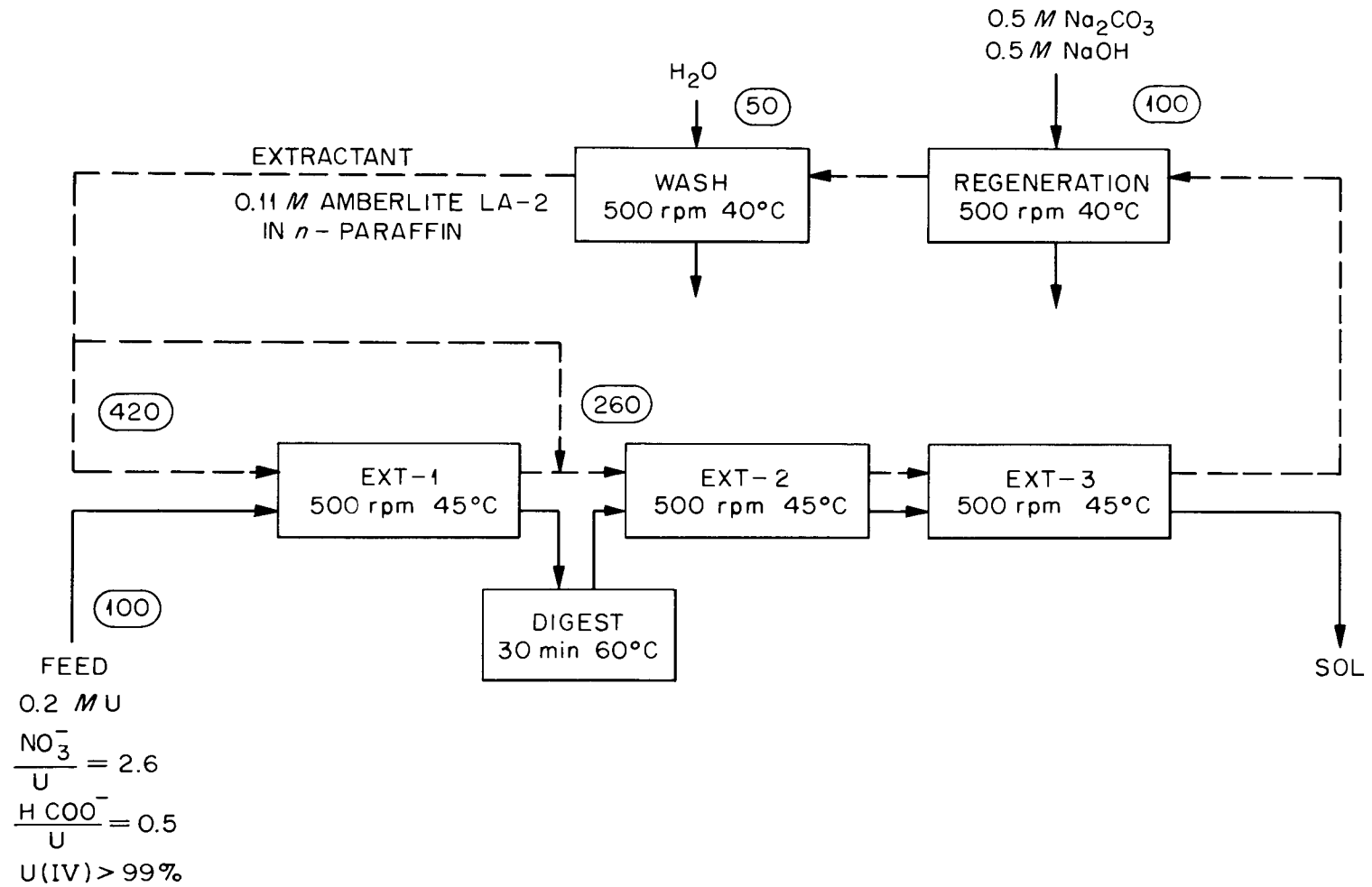


Fig. 2.1 Reference Flowsheet for the Preparation of UO₂ Sol by Solvent Extraction.

2.1.1 Preparation of U(IV) Nitrate Solution

During the laboratory studies, U(IV) nitrate solution was prepared by contacting 0.2 M $\text{UO}_2(\text{NO}_3)_2$ -- 0.1 M HCOOH with hydrogen, using platinized Al_2O_3 powder as the catalyst. Although this procedure usually produced good results, it did not appear very practical for the larger engineering tests because of the time required for removing (by settling and filtration) the catalyst. Consequently, several alternative methods of reduction were evaluated. One of these consisted of continuous reduction in a pressurized fixed bed of platinized Al_2O_3 pellets. Attempts to make sol by using U(IV) nitrate solution prepared in this reductor failed because the material became viscous in the second extraction stage. Another method involved batch operation of the fixed catalyst bed at approximately atmospheric pressure. This allowed better control of the reduction and, in turn, resulted in an improved product sol. However, the sol tended to thicken, or gel, on concentration (by vacuum evaporation) to 1 M. We believe that this tendency was caused by the presence of a nitrogen-bearing basic material, which behaved like ammonia during chemical analysis but degraded on standing, in the U(IV) nitrate solution. [Ammonia, on addition (NH_3/U mole ratio = 0.02) to laboratory-prepared U(IV) nitrate solution, has been shown to cause thickening of the sol which is subsequently formed by batch extraction.]

Most of the recent runs have been made by using U(IV) feed that was prepared in a slurry-type reductor, where finely divided PtO_2 catalyst is suspended in a well-mixed uranium nitrate solution and the hydrogen enters through a sparger. Since the catalyst is reduced to metal that becomes flocculated in the presence of excess hydrogen, it settles very rapidly and is readily retained on a filter when reduction of the uranium is nearly complete. The filter consists of a flat disk of porous stainless steel (10- μ pore) that forms the bottom of the reductor. The reduction is monitored by measuring the redox potential of the solution, using a platinum electrode vs a glass reference electrode. (Other reference electrodes such as silver--silver chloride or calomel can also be used, but are not as rugged and trouble-free as glass.) The end

point is readily detected as a sharp break in emf, which occurs when reduction has progressed to between 96 and 100% U(IV). The feed composition was fixed at $0.6 \text{ M } \text{UO}_2(\text{NO}_3)_2$ -- $0.4 \text{ M } \text{HNO}_3$ -- $0.3 \text{ M } \text{HCOOH}$; the NO_3^-/U and HCOOH/U mole ratios were 2.6 and 0.5, respectively.

Both a small laboratory slurry reductor (1.6-liter capacity) and a larger unit (14-liter capacity, Fig. 2.2) have been evaluated as devices for supplying feed for engineering tests of the solvent-extraction process. About 10 kg of uranium was reduced in the small reductor, thus demonstrating the feasibility of the slurry catalyst. The design and construction of the larger reductor were based on laboratory data. The results of 20 runs (Table 2.1), which produced a total of 40 kg of U(IV), indicate excellent performance. (Reduction time is not definitely known for runs 1 and 2; reduction was not complete in run 23, which was attempted with diluted hydrogen.) The catalyst (initial charge, 30 kg of PtO_2^*) has shown no sign of loss in activity or of decrease in filtration efficiency (filtration time by gravity was 12 min for 14 liters). No subsequent additions have been required. Reduction of greater than 99.5% of the uranium was easily obtained; very little ammonia was formed (NH_3/U mole ratio < 0.002). The rate of uranium reduction increased linearly with hydrogen flow rate (Fig. 2.3) from 1.8 moles/hr at a hydrogen flow rate of 41 liters/hr (95% utilization) to 3.4 moles/hr at a hydrogen flow rate of 100 liters/hr (80% utilization). The rate of uranium reduction also increased with agitator speed (Fig. 2.4), from an average of 2 moles/hr at an agitator speed of 570 rpm to 2.7 moles/hr at 1070 rpm. Doubling the amount of uranium present by doubling the volume of solution processed had virtually no effect on the rate of uranium reduction. One run (run 19) at 50°C showed only a slightly higher reduction rate than that for the remainder of the runs at 30 to 35°C . An attempt was made (run 23) to effect reduction by using a mixture of argon--4% H_2 . This gas has the obvious advantage of being non-explosive; however, the rate of uranium reduction was very slow when it was used (i.e., only 10% was reduced after 6 hr as compared with complete reduction in 2 hr with pure hydrogen).

* Adams catalyst obtained from Englehard Industries Div. of Englehard Minerals and Chemicals Corp., Newark, N. J.

ORNL DWG 68-4113

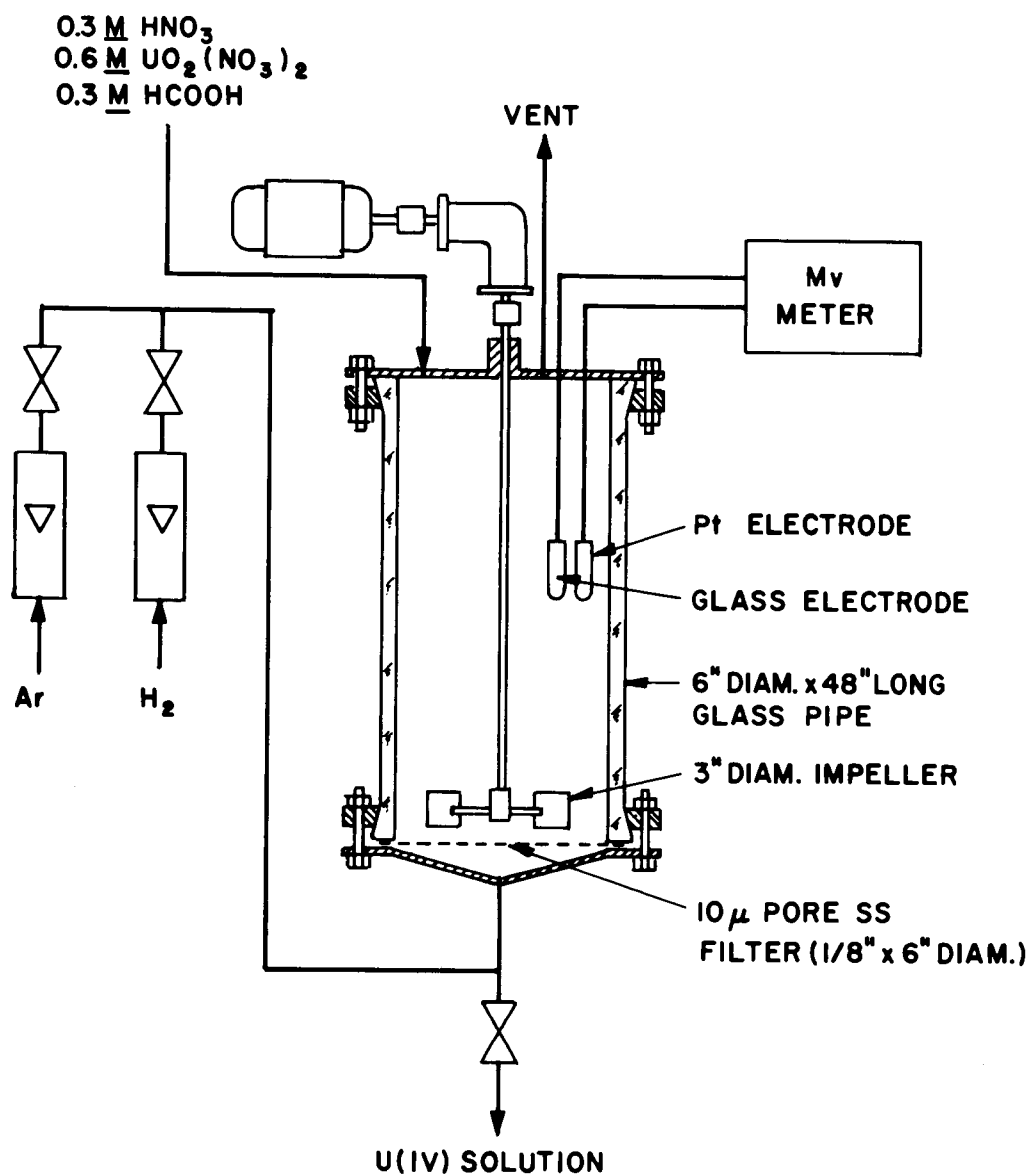


Fig. 2.2 Batch Slurry Uranium Reductor. Capacity, 14 liters.

Table 2.1. Batch Reduction of Uranyl Nitrate with Hydrogen, Using Platinum as Slurry Catalyst

Feed: 0.6 M $\text{UO}_2(\text{NO}_3)_2$ --0.4 M HNO_3 --0.3 M HCOOH
 Temperature: 30-35°C except when noted

Run No.	Vol. (liters)	Agitator Speed (rpm)	H ₂ Flow Rate $\frac{\text{ℓ}}{\text{hr}}$ (STP)		Percent Excess H ₂	Reduction Rate (mole U/hr)	Reduction Time (min)	Filter Time (min)
			In	Out				
1	7	1070	41	---	---	---	210 ^a	6
2	7	1070	41	---	---	---	229 ^a	6
3	7	1070	70	---	---	2.2	115	6
4	7	1070	70	---	---	2.0	124	6
5	14	1070	70	---	---	2.4	206	12
6A	14	1070	41	2	5	1.8 ^b	---	---
6B	14	1070	70	9	15	2.4	213	12
7	14	1070	70	9	15	2.6	194	13
8	14	1070	70	9	15	2.6	193	13
9A	14	570	70	23	49	2.1 ^b	---	---
9B	14	820	70	14	25	2.5 ^b	---	---
9C	14	1070	70	9	15	2.7 ^b	220	---
10	14	570	70	28	67	1.9	267	---
11	14	1070	70	6	9	2.4	210	12
12	14	1070	70	9	15	2.6	192	---
13	14	1070	70	---	---	2.2	232	12
14	14	1070	70	---	---	2.6	193	---
15	14	1070	70	9	15	2.6	191	13
16	14	1070	70	9	15	2.7	184	12
17	14	1070	70	9	15	2.6	193	13
18	14	1070	100	17	20	3.4	150	13
19	14	1070	100	17	20	3.7 ^c	135	20
20	8.4	1070	100	22	28	3.1	95	10
21	8.4	1070	100	---	---	3.4	88	11
22	14	1070	100	30	30	3.4	147	20
23	7	1070	60	---	---	d	> 300	---

^a Run without end-point-detection instruments.

^b Rate calculated from H₂ flow rate.

^c Temperature was 50°C.

^d Attempted reduction with Argon--4% H₂.

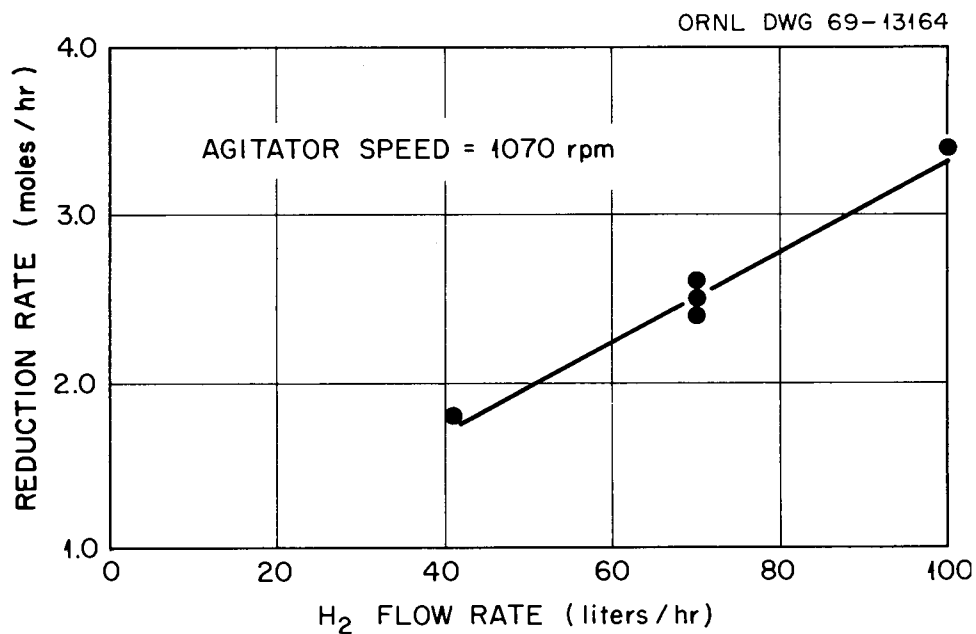


Fig. 2.3 Effect of Hydrogen Flow Rate on Rate of Reduction of Uranyl Nitrate.

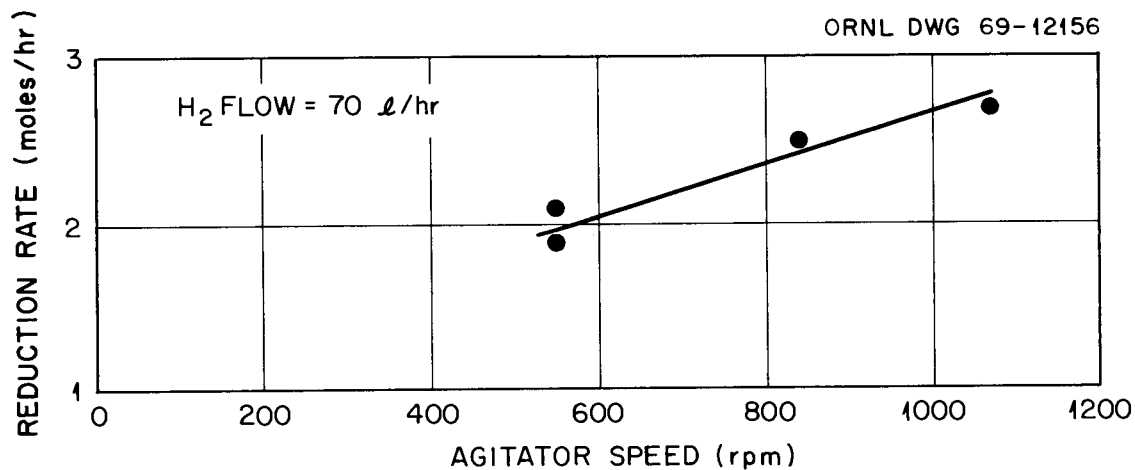


Fig. 2.4 Effect of Agitator Speed on the Rate of Reduction of Uranyl Nitrate.

2.1.2 Operation of the Solvent-Extraction Equipment

About 40 runs have been made (Table 2.2) to demonstrate the operation of the solvent extraction equipment. As was noted in the section on the preparation of U(IV) nitrate solutions, a number of the runs were made to test various feed solutions. In the last 20 runs, for which the feed was prepared by batch slurry catalyst, about 1000 liters of 0.2 M UO_2 sol was produced. The equipment operated satisfactorily at the design rate of 6 liters of sol per hour. No emulsions or entrainment difficulties were encountered. The entrainment of extractant in the sol product was consistently less than 0.1 vol %. The small amount of entrained sol in the used extractant can be removed by scrubbing with water to prevent loss of uranium to the waste stream. Although three extractors were used in most of the runs, only two are needed because the nitrate content of the sol changes only slightly in the third extractor. Approach to chemical equilibrium in the extractor has been consistently greater than 90% at a mixer speed of 500 rpm.

Variation of the uranium concentration from 0.15 to 0.3 M (the reference concentration is 0.2 M) did not cause any difficulty, and good-quality sols were produced; however, two attempts to prepare a sol having a uranium concentration of 0.6 M were unsuccessful because the product material thickened in the second extractor.

The temperature at which the digestion step (see Fig. 2.1) was carried out was found to be an important variable (Table 2.3). At 50°C the sol contains a significant amount of amorphous UO_2 (as determined by x-ray diffraction). The sol gels at a uranium concentration of about 0.5 M if it is evaporated immediately after preparation; however, after aging overnight it can be concentrated to greater than 1.0 M and will remain fluid for more than 30 days. When the digestion temperature is increased to 60°C, the sol contains more UO_2 crystallites, and the fresh sol can be concentrated without gelling. To minimize oxidation of the uranium at the higher digestion temperature, the laboratory flowsheet was modified to include the use of an excess of amine in the first stage.

Table 2.2. Summary of UO₂ Sol Runs

Run No.	Comments on Feed ^a	Flow Rate (ml/min)					Digestion Temperature (°C)	U Concn. in Sol (M)	NO ₃ ⁻ /U Mole Ratio in Product from First Extractor	Sol Properties						
		Feed	Extractant to First Stage	Extractant to Second Stage	0.5 M Na ₂ CO ₃ -- 0.5 M NaOH	H ₂ O				Conductivity at 35°C (millimhos/cm)	NO ₃ ⁻ /U Mole Ratio	C/U Atom Ratio	% U ⁴⁺	Shelf Life of 1 M Sol (days)	Crystallite Size (Å)	% Crystallized After 1-3 weeks
1	1	50	120	180	80	20	55	0.20	0.32	---	0.05	0.44	88	0	---	---
2	1	70	120	180	80	--	50	0.20	---	---	---	---	---	0	---	---
3	1	90	260	230	60	--	50	0.20	---	---	---	---	---	0	---	---
4	2	90	300	240	65	--	50	0.20	0.72	---	0.21	0.15	88	---	---	---
5	2	90	300	240	65	--	50	0.20	0.98	---	0.11	0.15	85	0	---	---
6	3	90	300	240	65	--	50	0.20	0.68	---	0.07	0.50	93	---	---	---
7	2	50	375	375	90	--	50	0.20	1.4	---	0.24	0.40	88	0	---	---
8A	4	140	400	400	90	40	50	0.20	1.0	5.0	0.25	0.54	93	11	34	---
8B	4	140	400	400	110	40	50	0.30	1.1	5.0	0.20	0.46	91	3	34	---
8C	5	100	285	375	100	50	50	0.15	0.50	3.5	0.24	0.68	96	8	34	---
8D	6	90	400	400	100	50	50	0.30	0.77	3.8	0.12	0.49	87	< 1	40	---
8E	6	90	400	400	100	50	50	0.30	0.91	3.2	0.09	0.50	89	6	39	---
8F	6	110	400	400	100	50	50	0.30	0.82	3.4	0.11	0.50	88	4	37	---
9A	7	190	400	400	100	50	50	0.25	0.99	---	0.25	0.46	88	0	---	---
9B	8	140	400	400	100	50	50	0.15	0.93	---	0.25	0.47	92	3	---	---
10	4	100	420	260	100	50	50	0.20	1.11	---	0.16	0.51	88	1	---	---
11	9	100	420	260	100	50	50	0.20	0.45	---	0.18	0.52	96	16	---	---
12	4	100	420	260	100	50	50	0.20	0.52	---	0.15	0.26	90	< 1	---	---
13A	4	100	420	260	100	50	50	0.20	0.50	---	0.17	0.34	90	3	---	---
13B	10	100	420	260	100	50	50	0.20	0.46	---	0.17	0.34	90	2	---	---
14A	4	100	420	260	100	50	50	0.20	0.51	---	0.27	0.42	95	9	38	50
14B	4	100	420	260	100	50	65	0.20	0.49	---	0.12	0.42	90	3	42	100
15A	9	100	420	260	100	50	50	0.20	0.41	---	0.17	0.44	96	13	38	40
15B	11	100	420	260	100	50	50	0.20	0.44	---	0.24	0.44	96	17	39	50
16A	9	100	420	260	100	50	50	0.20	0.43	2.1	0.26	0.50	97	50	40	100
16B	9	100	420	260	100	50	65	0.20	0.42	1.3	0.08	0.50	93	90	41	100
17A	9	100	420	260	100	50	50	0.20	0.42	---	0.26	0.55	99	43	---	---
17B	12	100	420	260	100	50	50	0.20	0.37	1.8	0.17	1.12	99	90	49	100
18	9	100	420	260	100	50	50	0.20	0.55	2.1	0.24	0.43	95	40	---	---
19	13	100	420	260	100	50	50	0.20	0.34	1.7	0.24	0.62	99	60	---	---
20	13	100	350	210	100	50	60	0.20	0.44	1.9	0.09	0.43	93	35	---	---
21	13	100	350	210	100	50	60	0.20	0.41	1.9	0.09	0.52	99	36	---	---
22	13	100	350	210	100	50	60	0.20	0.43	1.8	0.10	0.51	94	60	---	---
23	13	100	420	260	100	50	60	0.20	0.38	1.9	0.09	0.50	--	25	---	---
24	13	100	350	210	100	50	50	0.20	0.41	2.1	0.24	0.50	97	50	---	---
25	14	50	420	260	100	50	60	0.6	---	---	---	---	---	---	---	---
26	14	50	420	260	100	50	60	0.6	1.10	---	0.65	0.49	85	---	---	---
27	13	100	340	180	100	50	60	0.2	0.65	4.5	0.13	0.50	89	50	---	---
28	13	100	390	130	100	50	60	0.2	0.51	5.4	0.14	0.52	91	50	---	---
29	13	100	390	240	100	50	60	0.2	0.53	3.3	0.10	0.51	91	50	---	---
30	13	100	390	270	100	50	60	0.2	0.55	3.2	0.09	0.51	91	10	---	---
31	13	100	390	270	100	50	60	0.2	0.55	2.7	0.09	0.51	91	25	---	---
32	13	100	390	270	100	50	60	0.2	0.52	2.9	0.09	0.51	91	15	---	---
33A	13	100	420	260	100	50	70	0.2	0.47	2.8	0.07	0.40	91	8	---	---
33B	13	100	390	290	100	50	70	0.2	0.60	2.8	0.07	0.49	88	4	---	---
34A	13	100	290	370	100	50	50	0.2	1.0	2.7	0.11	0.50	94	7	---	---
34B	13	100	290	370	100	50	60	0.2	1.0	3.0	0.08	0.50	85	5	---	---
35	15	50	390	270	100	50	60	0.2	0.73	2.8	0.10	0.50	87	14	---	---
36	15	50	390	270	100	50	60	0.2	0.72	3.4	0.09	0.50	88	26	37	70

^a Comments on feed:

1. Prepared in continuous-flow pressurized fixed-bed reductor.
2. Prepared in batch fixed-bed reductor.
3. Prepared in batch platinum-slurry reductor at a uranium concentration of 1 M.
4. Prepared in continuous platinum-slurry reductor at a uranium concentration of 1 M.
5. Same as 4, except uranium concentration in feed to solvent extractor was 0.15 M.
6. Same as 4, except uranium concentration in feed to solvent extractor was 0.30 M.
7. Same as 2, except uranium concentration in feed to solvent extractor was 0.25 M.
8. Same as 2, except uranium concentration in feed to solvent extractor was 0.15 M.
9. Prepared in batch platinum-slurry reductor at a uranium concentration of 0.06 M.
10. Same as 9, except feed to solvent extractor was 0.005 M in hydrazine.
11. Same as 9, except feed to solvent extractor was 0.01 M in hydrazine.
12. Same as 9, except feed to solvent extractor was 0.01 M in hydrazine.
13. Prepared in large-scale (14-liter) platinum-slurry reductor at a uranium concentration of 0.6 M.
14. Same as 13, except uranium concentration in feed to solvent extractor was 0.6 M.
15. Same as 13, except uranium concentration in feed to solvent extractor was 0.4 M, and scrub solution was blended with feed to give a uranium concentration of 0.2 M in stream entering first extractor.

Table 2.3. Effect of Digestion Temperature and Excess Amine on Properties of UO₂ Sol

Run No.	Digestion Temp. (°C)	Excess Amine (%)	0.2 M Sol			Shelf Life of 1 M Sol (days)
			NO ₃ ⁻ /U Mole Ratio	Conductivity (millimhos/cm)	% U(IV)	
15A	50	50	0.17	---	96	13
15B	50	50	0.24	---	96	17
16A	50	50	0.26	2.1	97	50
17A	50	50	0.26	---	99	43
18	50	50	0.24	2.1	95	40
19	50	50	0.24	1.7	99	60
24	50	50	0.24	2.1	97	50
23	60	65	0.09	1.9	--	25
20	60	50	0.09	1.9	93	35
21	60	50	0.09	1.9	99	36
22	60	50	0.10	1.8	94	60
29	60	50	0.10	3.3	91	50
30	60	50	0.09	3.2	91	10
31	60	50	0.09	2.7	91	25
32	60	50	0.09	2.9	91	15
34B	60	35	0.08	3.0	85	5
35	60	35	0.10	2.8	87	14
36	60	35	0.09	3.4	88	26
27	60	20	0.13	4.5	89	50
28	60	20	0.14	5.4	91	50
16B	65	50	0.08	1.3	93	41
33A	70	35	0.07	2.8	91	15
33B	70	35	0.07	2.8	88	8

This amine extracts sufficient nitrate to give a NO_3^-/U mole ratio of less than 0.5. Sol prepared at a digester temperature of 70°C has a shorter shelf life after concentration, perhaps because extensive oxidation of uranium occurs even at the low NO_3^-/U mole ratio. The digester temperature also affects the NO_3^-/U mole ratio of the sol product; for example, the ratio averages 0.24, 0.10, and 0.07 when digestion is carried out at 50, 60, and 70°C , respectively. The addition of 20 to 65% excess amine (i.e., 20 to 65% more than the stoichiometric quantity required to extract the nitrate from the feed) appears to have very little effect on the nitrate content of the sol. The average size of the UO_2 crystallites in the sol product is 35 to 40 A and does not seem to depend on either the temperature of the digester or the period of aging.

2.1.3 Evaporation of Sol

Dilute sol ($\sim 0.2 \text{ M}$) must be concentrated until it is about 1 M in uranium in order to facilitate the formation of microspheres. Vacuum evaporation is used to avoid overheating the sol; the temperature is kept below about 35°C . Because the sol is quite sensitive to oxidation, exposure to air is a common cause of thickening or, in extreme cases, flocculation of the sol.

Representative samples from each run were concentrated to 1 M in uranium in a rotating, evacuated 500-ml flask,^{*} in order to determine the effects of variables on the shelf life on the concentrated sol. Most of the sols prepared according to the reference flowsheet remained fluid at a uranium concentration of 1 M for 50 days or more.

Several batches (each containing 2 kg of uranium) of dilute sol were successfully concentrated in the forced-circulation vertical-tube evaporator² to yield 1 M sol for use in forming microspheres. The data are summarized in Table 2.4. The evaporation was satisfactory at the design boilup rate of 15 liters/hr and an absolute pressure of 30 torrs. No foaming or scaling was observed. About 25% of the formic acid was

*"Rotavapor," Rinco Instrument Co., Inc., Greenville, Ill.

Table 2.4. Summary of Data for the Concentration of UO_2 Sol in the Forced-Circulation Vertical-Tube Evaporator

Evaporator Run No.	Sol Run No. ^a	Age Before Evaporation (days)	% U(IV) in			C/U Atom Ratio in		Shelf Life of Evaporator Product (days)
			Fresh Sol	Evaporator Feed	Evaporator Product	Evaporator Feed	Evaporator Product	
7	6	18	93	90.0	90.9	0.38	0.42	---
10	7	16	88	85.9	85.3	0.41	0.26	---
11	8	14	90	88.3	88.0	0.59	0.47	---
12	8	16	90	88.1	88.1	0.51	0.47	---
13	8	21	90	89.0	88.3	---	---	---
14	8	23	90	87.4	86.7	---	---	---
15	10	7	88	88.1	87.0	0.65	0.51	---
16	{ 15B	42	96	---	---	---	---	---
	{ 16A	34	97	---	---	---	---	---
17	{ 16B	46	93	87.0	---	---	---	---
	{ 17A	40	99	---	---	---	---	45
18	18	40	95	88.6	87.7	---	---	4 ^b
19	27	8	89	89.2	88.2	0.51	0.40	10
20	22	20	94	90.4	90.1	0.45	0.40	17
21	21	22	99	90.3	89.6	0.47	0.41	28
22	{ 20	30	93	91.6	89.2	0.46	0.37	> 10
	{ 21	29	99	---	---	---	---	---
23	29	20	91	91.3	89.6	0.53	0.40	> 4
24	30	36	90	88.8	87.6	0.47	0.35	3
25	31	45	91	89.0	88.0	0.50	0.37	---
26	32	57	91	89.2	88.1	0.51	0.34	---
27	{ 35	43	87	---	---	---	---	---
	{ 36	42	88	---	---	---	---	> 1

^aSee Table 2.2 for properties of these sols.

^bAir was inadvertently admitted during the evaporation.

removed from the sol during evaporation. Shelf lives of the large batches of concentrated sol were shorter than the shelf life of the product from the small laboratory evaporator. We believe that this decreased shelf life is the result of oxidation of the uranium, due to leakage of air, during storage (~ 30 days) prior to evaporation and also during evaporation.

2.2 Two-Fluid Nozzles as Sol Dispersers Under Turbulent Flow Conditions

P. A. Haas

We have continued to use the two-fluid nozzle as a sol disperser. During this report period, we employed organic flow rates that are too large to allow varicose dispersion (which gives large sol droplets).^{3,4} Product diameters were determined for a wide range of variables and a variety of sols, and a dimensionless correlation was developed.

To obtain a dispersion of a sol in an alcohol as droplets of a uniform and controlled diameter, a controllable, uniform force should be applied to a uniform configuration of undispersed sol. The formation of the new surface requires energy; however, dispersion is usually a very inefficient operation, and most of the supplied energy is dissipated as fluid friction. An important practical requirement is capacity, and the number of drops per unit weight increases inversely as the cube of the diameter. The viscosity of the sol and the sol-alcohol interfacial tension vary and are thus difficult to control; therefore, disperser control will be simpler if the importance of these variables can be minimized.

In operations employing the two-fluid nozzle, turbulence of the continuous (alcohol) phase flowing through a tube provides a uniform and controllable force for dispersing a sol stream that is introduced into the channel. The degree of turbulence can be varied easily and

³M. E. Whatley et al., Unit Operations Section Quarterly Progress Report, October-December 1967, ORNL-4235.

⁴M. E. Whatley et al., Unit Operations Section Quarterly Progress Report, April-June 1968, ORNL-4365.

reproducibly by varying the alcohol flow rate. The transition from viscous or laminar flow to turbulent flow depends on a dimensionless parameter called Reynolds number. The scale of the turbulence in the two-fluid nozzle and the localized forces that cause dispersion depend on the dimensions of the channel and on the properties of the continuous fluid, as well as on the Reynolds number.

The underlying principle for operation of this disperser is the use of controlled turbulence (as the primary force) to disperse the sol into a flowing alcohol stream. The promotion of turbulence by the sol inlet configuration and the addition of shearing forces to the turbulent forces are unavoidable supplementary effects. The sol stream from a capillary inlet gives a uniform configuration. The force causing dispersion is easily controlled and is more uniform than the somewhat similar forces used in dispersion by agitation or by fluid-driven atomizing nozzles. Information found in the literature on dispersion by agitation indicates that the viscosity of the sol is probably not a controlling variable if it is of the same magnitude as, or less than, that of the alcohol.

The results obtained by operating the two-fluid nozzle under turbulent flow conditions have been correlated using dimensional analyses. The following dimensionless relationship has been developed:

$$\frac{D_{\text{sol}}}{ID} = 1630 \left(\frac{G}{F} \right)^{0.1} Re^{-1.5},$$

where

- D_{sol} = diameter of the sol droplet,
- ID = diameter of the alcohol flow channel,
- G = alcohol flow rate,
- F = sol flow rate,
- Re = Reynolds number for the alcohol.

For our two-fluid nozzle configuration with the sol inlet capillary positioned perpendicular to the axis of the alcohol channel, this expression was valid for Reynolds numbers greater than 600, perhaps due to

promoted turbulence for Reynolds numbers greater than 600 but less than 2000. Terms for ratios of the viscosities and densities of the alcohol and sol were omitted from the equation because we do not have data to determine their contributions. Data to illustrate the range of variables are tabulated in Table 2.5. Substituting commonly used units, the dimensionless relationship presented above becomes:

$$D_{\text{sol}} = 7.0 \cdot 10^6 \frac{ID^{2.5} \mu^{1.5}}{G^{1.4} F^{0.1}},$$

where D_{sol} is expressed in microns, ID in centimeters, G in cubic centimeters per minute, F in cubic centimeters per minute, and μ (the viscosity of the alcohol) in centipoises.

The most important advantage of the two-fluid nozzle - turbulent flow type of operation is that a fairly small fraction of the product is in the form of spheres having diameters smaller than the mean diameter. Other dispersers, which give controllable diameters and practical capacities, produce a much larger fraction of small spheres. The size distributions for products of the same mean size formed during paddle agitator⁵ and two-fluid nozzle operation are compared in Table 2.6 and Fig. 2.5.

⁵M. E. Whatley et al., Unit Operations Section Quarterly Progress Report, July-September 1965, ORNL-3916, pp. 44-50.

Table 2.5. Results Obtained by Using the Two-Fluid Nozzle to Disperse Sol Under Turbulent Flow Conditions

$$\text{Equation: } \frac{D_{\text{sol}}}{ID} = 1630 \left(\frac{G}{F} \right)^{0.1} \text{Re}^{-1.5}$$

Nozzle ID (cm)	Alcohol Flow, G (cm ³ /min)	Alcohol Viscosity, μ (centipoises)	Sol Flow, F (cm ³ /min)	Reynolds Number of Alcohol	Mean Diameter of Sol Droplets, D_{sol} (μ)	Calculated Diameter of Sol Droplets (μ)	Percent Error
0.15	520	2.5	7.6	2440	25	30	20
0.195	330	5.0	4.9	595	230	333	--
	520	5.7	4.9	825	185	214	16
	560	2.2	9.6	2240	40	45	12
	620	5.1	4.9	1100	165	141	14
	860	2.0	9.6	3790	20	21	5
0.200	210	2.3	9.6	785	170	276	--
	240	3.5	9.8	605	300	302	1
	368	4.8	9.8	675	300	268	11
	385	2.2	9.6	1500	80	81	1
	405	2.3	9.6	1510	75	81	8
	430	2.8	9.6	1320	95	99	4
0.265	535	2.65	9.8	1310	145	136	6
	550	2.7	9.8	1320	145	134	8
	650	2.7	3.7	1565	127	117	8
0.28	500	2.7	9.6	1140	180	176	2
0.38	710	3.0	10.0	1070	280	271	3
	740	2.9	7.6	1150	265	251	5

Table 2.6. Size Distributions for ThO₂ Microspheres Prepared by a Paddle Agitator
 Compared with Those Prepared by a Two-Fluid Nozzle

Method of Preparation	Mean Diameter, d_{50} (μ)	Weight Percent Smaller Than			
		0.8 d_{50}	0.6 d_{50}	0.4 d_{50}	0.2 d_{50}
Paddle agitator	92	42	30	24	~18
Two-fluid nozzle (turbulent flow)	90	30	13	7	~ 3
Paddle agitator	78	38	26	~19	~14
Two-fluid nozzle (turbulent flow)	76	28	11	~ 4	< 2

ORNL DWG 69-12141

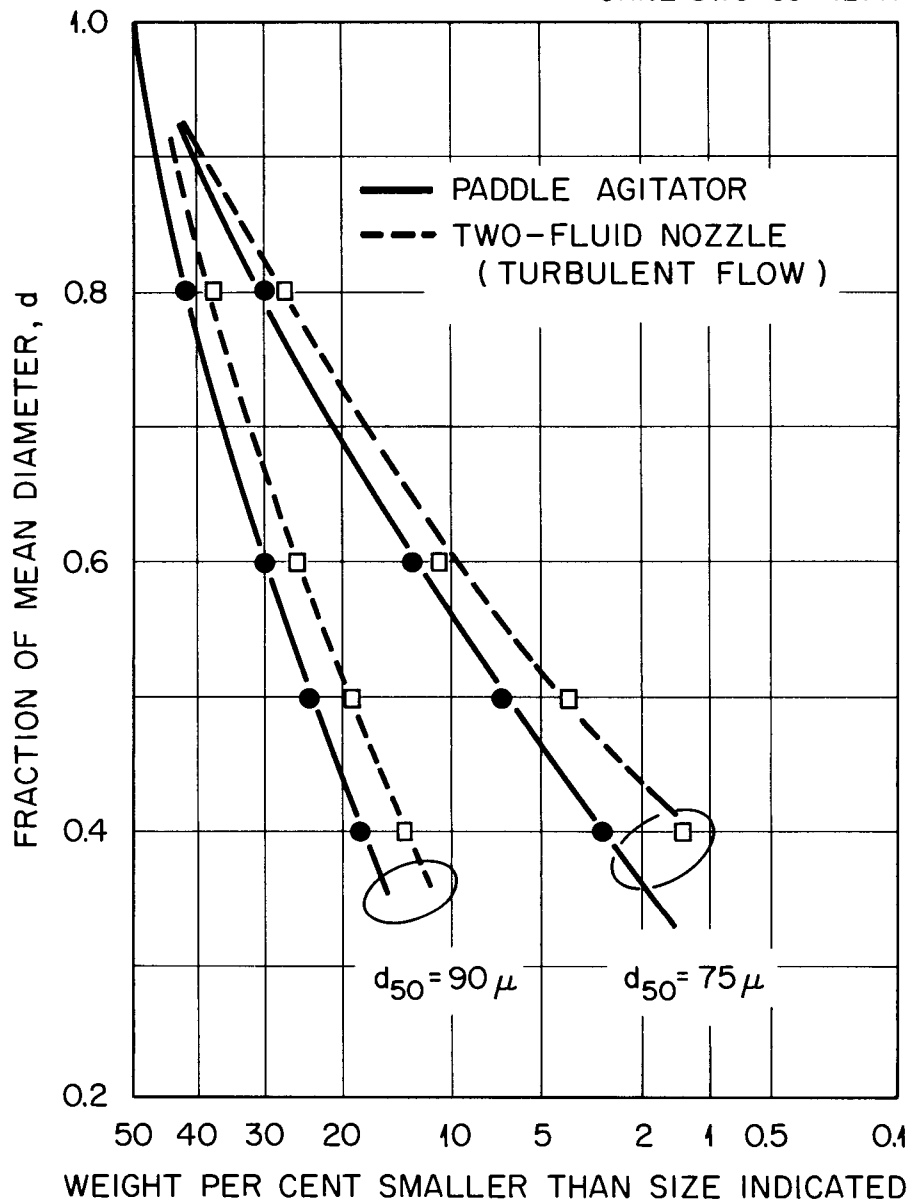


Fig. 2.5 Dispersion in Size of Microspheres Prepared by Agitation and by the Two-Fluid Nozzle Under Turbulent Flow Conditions.

3. MOLTEN-SALT REACTOR PROCESSING STUDIES

L. E. McNeese

A molten-salt breeder reactor (MSBR) will be fueled with a molten fluoride mixture that will circulate through the blanket and core regions and through the primary heat exchanger. A close-coupled processing facility for removing fission products, corrosion products, and fissile materials from the fused fluoride mixture will be an integral part of the reactor system.

Work involving several operations related to MSBR processing is reported. A summary is presented of the nonradioactive operation of the MSRE Distillation Experiment; emphasis is on the application of this information to the adjustment of the composition of single-fluid MSBR fuel salt. It is shown that distillation of 10 to 40% of the fuel salt produces a significant increase in free fluoride, which will, in turn, increase the separation factor for rare earths from thorium in the subsequent reductive extraction.

Gas-lift pumps are being considered for use with liquid bismuth and molten salt for the Flow Electrolytic Cell Facility. A series of room-temperature experiments to test the feasibility of a gas lift for pumping liquid metals such as bismuth was made with mercury.

Multistage equipment for contacting molten salt and liquid bismuth will be required for the removal of protactinium and the rare earths from molten salt by reductive extraction. Initial studies of contactor development are being made with water and mercury, which simulate molten salt and bismuth. Measurements of dispersed-phase holdup, continuous-phase pressure drop, and throughput at flooding have been made for a 1-in.-diam column containing various types and sizes of packing materials.

3.1 Distillation of Molten Salt

J. R. Hightower, Jr. L. E. McNeese
H. D. Cochran, Jr.

The emphasis in the Molten Salt Reactor program has shifted toward a single-fluid breeder reactor, and the potential role of molten-salt distillation in fuel processing has changed considerably. A single-fluid reactor will require the removal of rare-earth fluorides from salt containing considerable quantities of ThF_4 ; however, the relatively low volatility of ThF_4 complicates the removal of rare earths by this method. Nevertheless, distillation of molten salt may be useful in fuel processing as a means for adjusting the salt composition prior to reductive extraction. Another possible area of application is in the partial recovery of salt from the waste stream of a reductive extraction plant.

The conclusions from the nonradioactive tests for the MSRE Distillation Experiment may be summarized as follows:

- (1) Separations were predicted satisfactorily by equilibrium data obtained from laboratory-scale experiments. No evidence of entrainment or concentration polarization was observed.
- (2) Distillation rates at 1000°C are reasonably high and are given approximately by the following empirical expression:

$$R = 1.6 (p_t^2 - p_c^2)^{0.41}, \quad (3.1)$$

where

R = distillation rate (ft^3 salt/ ft^2 day),

p_t = total equilibrium vapor pressure above the liquid in the still pot (mm Hg),

p_c = pressure maintained at the condenser exit (mm Hg).

The correlation (Fig. 3.1) represented by Eq. (3.1) was suggested by the fact that a steady-state mechanical-energy balance for the isothermal flow of an ideal gas through a conduit of constant cross section shows the flow of gas to be a function of the difference in

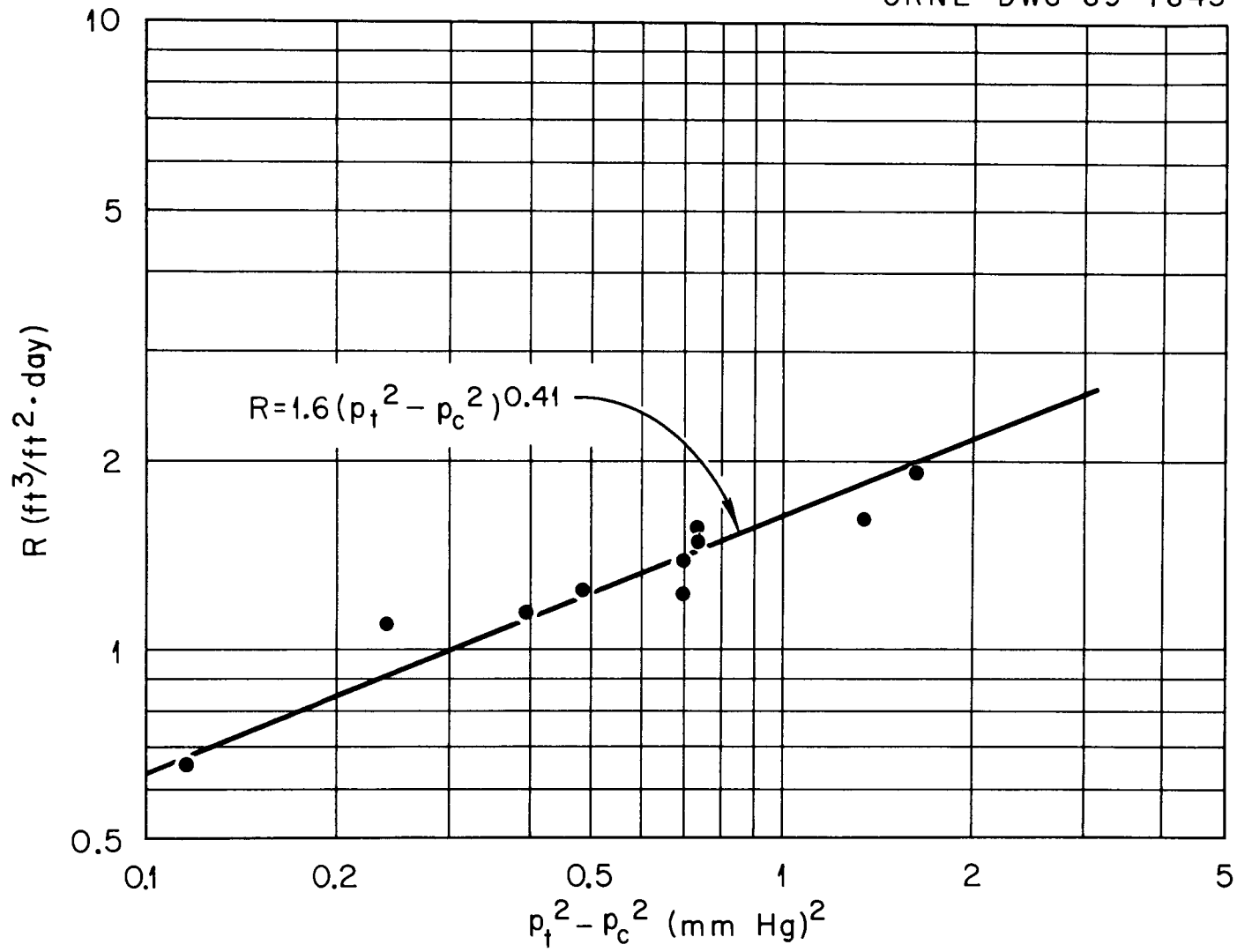


Fig. 3.1 Empirical Correlation of Vaporization Rate vs Driving Force.

the squares of the upstream and downstream pressures. Although the flow path was not isothermal and the condenser cross section was not uniform in the tests summarized in Fig. 3.1, a fair correlation of all the distillation rate data was obtained. The value of p_c ranged from 0.055 to 0.5 mm Hg, and the value of p_t ranged from 0.70 to 1.28 mm Hg.

- (3) The still pot was operated for 300 hr at temperatures in excess of 900°C, including a 45-hr period at temperatures greater than 1000°C, without evidence of serious corrosion or deformation of the Hastelloy N structural material.
- (4) No important difficulties or unexpected results were observed.

Thus we conclude that distillation performance, distillation rates, and separation factors may be predicted from vapor-liquid equilibrium measurements made on a laboratory scale. Calculations were made to show that distillation can be used as a means for adjusting the composition of salts containing thorium prior to reductive extraction. The calculational method and the results are described in the following paragraphs.

Laboratory experiments⁶ have indicated that optimal reductive extraction is obtained with a salt of maximum "free-fluoride" content, a concept advanced by M. A. Bredig. The free-fluoride content, F , for a mixture of LiF , BeF_2 , and ThF_4 is given by:

$$F = (x_{\text{Li}} - 2x_{\text{BeF}_2} - 3x_{\text{ThF}_4}) \times 100, \quad (3.2)$$

where

$$\begin{aligned} x_{\text{Li}} &= \text{mole fraction of lithium,} \\ x_{\text{BeF}_2} &= \text{mole fraction of BeF}_2, \\ x_{\text{ThF}_4} &= \text{mole fraction of ThF}_4. \end{aligned}$$

⁶J. H. Shaffer, D. M. Moulton, and W. R. Grimes, MSR Program Semiann. Progr. Rept. Aug. 31, 1968, ORNL-4344, pp. 176-78.

We have calculated the maximum free-fluoride concentration that is obtainable by single-stage distillation and the processing rate that one might expect in attaining this enhancement of free-fluoride content for various initial salt compositions, using equilibrium separation factors and mass balances. The composition of the bottoms and the free-fluoride content were calculated for vaporization of 2 to 50% of the feed salt. In all cases studied, the bottoms showed a maximum in free-fluoride content at a fractional vaporization between 10 and 40%. A description of the calculation procedure is given below.

In order to apply Eq. (3.1) to the calculation of the processing rate at the fractional vaporization necessary to attain the maximum free-fluoride concentration in the bottoms, the vapor pressure of the salt, p_t , must be calculated. (The condenser pressure, p_c , was assumed to be 0.07 mm Hg, which is the average condenser pressure used in the experiments represented in Fig. 3.1.) For vapor at very low pressure, Dalton's law is applicable and states that

$$p_{\text{LiF}} = p_t y_{\text{LiF}}, \quad (3.3)$$

where p_{LiF} is the partial pressure of LiF, and y_{LiF} is the mole fraction of LiF in vapor. For a nonideal solution,

$$p_{\text{LiF}} \approx p_{\text{LiF}}^* \gamma_{\text{LiF}} x_{\text{LiF}}, \quad (3.4)$$

where

- p_{LiF}^* = the vapor pressure of pure LiF at 1000°C \approx 0.48 mm Hg,
- γ_{LiF} = the activity coefficient of LiF in solution,
- x_{LiF} = mole fraction of LiF in solution.

Thus,

$$P_t \approx \frac{P_{\text{LiF}}^* \gamma_{\text{LiF}} x_{\text{LiF}}}{y_{\text{LiF}}} \quad (3.5)$$

The activity coefficient, γ_{LiF} , can be obtained from the following empirical expression:⁷

$$\ln \gamma_{\text{LiF}} = 0.336 \left[1 - (5.71 x_{\text{ThF}_4} - 1)^2 \right], \quad (3.6)$$

where

x_{ThF_4} = mole fraction of ThF_4 in solution.

The mole fraction of LiF in the vapor, y_{LiF} , needed to solve Eq. (3.5) is obtained from the empirical separation factors,⁷

$$\alpha_{\text{ThF}_4\text{-LiF}} \equiv \frac{y_{\text{ThF}_4} x_{\text{LiF}}}{x_{\text{ThF}_4} y_{\text{LiF}}} \approx 1.5 \left(x_{\text{ThF}_4} \right)^2 \quad (3.7)$$

and

$$\alpha_{\text{BeF}_2\text{-LiF}} \equiv \frac{y_{\text{BeF}_2} x_{\text{LiF}}}{x_{\text{BeF}_2} y_{\text{LiF}}} \approx 3.5 \left[1 + 100 \left(x_{\text{ThF}_4} \right)^2 \right] \quad (3.8)$$

by recognizing that

$$y_{\text{LiF}} = 1 - y_{\text{ThF}_4} - y_{\text{BeF}_2} \quad (3.9)$$

The final equation for the vapor pressure of salt in the still pot, obtained by combining Eqs. (3.5) - (3.9), is then:

$$P_t = \gamma_{\text{LiF}} P_{\text{LiF}}^* \left(x_{\text{LiF}} + \alpha_{\text{BeF}_2\text{-LiF}} x_{\text{BeF}_2} + \alpha_{\text{ThF}_4\text{-LiF}} x_{\text{ThF}_4} \right) \quad (3.10)$$

⁷J. R. Hightower, ORNL, personal communication.

The empirical expressions for γ_{LiF} , $\alpha_{\text{BeF}_2-\text{LiF}}$, and $\alpha_{\text{ThF}_4-\text{LiF}}$ were used in the actual calculations.

These relations were used to predict approximate distillation performance at 1000°C for feed-salt compositions in which the initial BeF_2 and ThF_4 concentrations ranged from 0 to 30 wt % and from 10 to 15 wt %, respectively, with the remaining material being LiF. Figure 3.2 shows that, for three feed-salt compositions of interest, the free-fluoride content achieves a maximum after 10 to 40% of the salt has been distilled. This general behavior was exhibited by all compositions studied. Figure 3.3 shows the maximum free-fluoride contents that can be attained by distillation at 1000°C. The predicted processing rates (distillation rate divided by fraction vaporized) are also shown.

3.2 Gas-Lift Pumping of Liquid Metals

M. S. Lin L. E. McNeese

Gas-lift pumps are being considered for use with liquid bismuth and molten salt for the Flow Electrolytic Cell Facility. This type of pump is simple, appears to be adequate, and is easily fabricated. Most of the data on gas-lift pumps are limited to the air-water system. A series of experiments to test the feasibility of pumping liquid metals such as bismuth was made with air and mercury at room temperature.

The experimental equipment is shown schematically in Fig. 3.4. Most of the components were made of stainless steel. The pump consists of a lift tube, a submergence leg with a reservoir, and a gas-liquid disengaging head pot. Three sizes of lift tubes (0.375, 0.3, and 0.186 in. ID) were tested. Each tube had three air-injection points, which provide three different submergence depths. Air fed to the system was metered by one of three rotameters. The results of the tests are shown in Figs. 3.5 - 3.10.

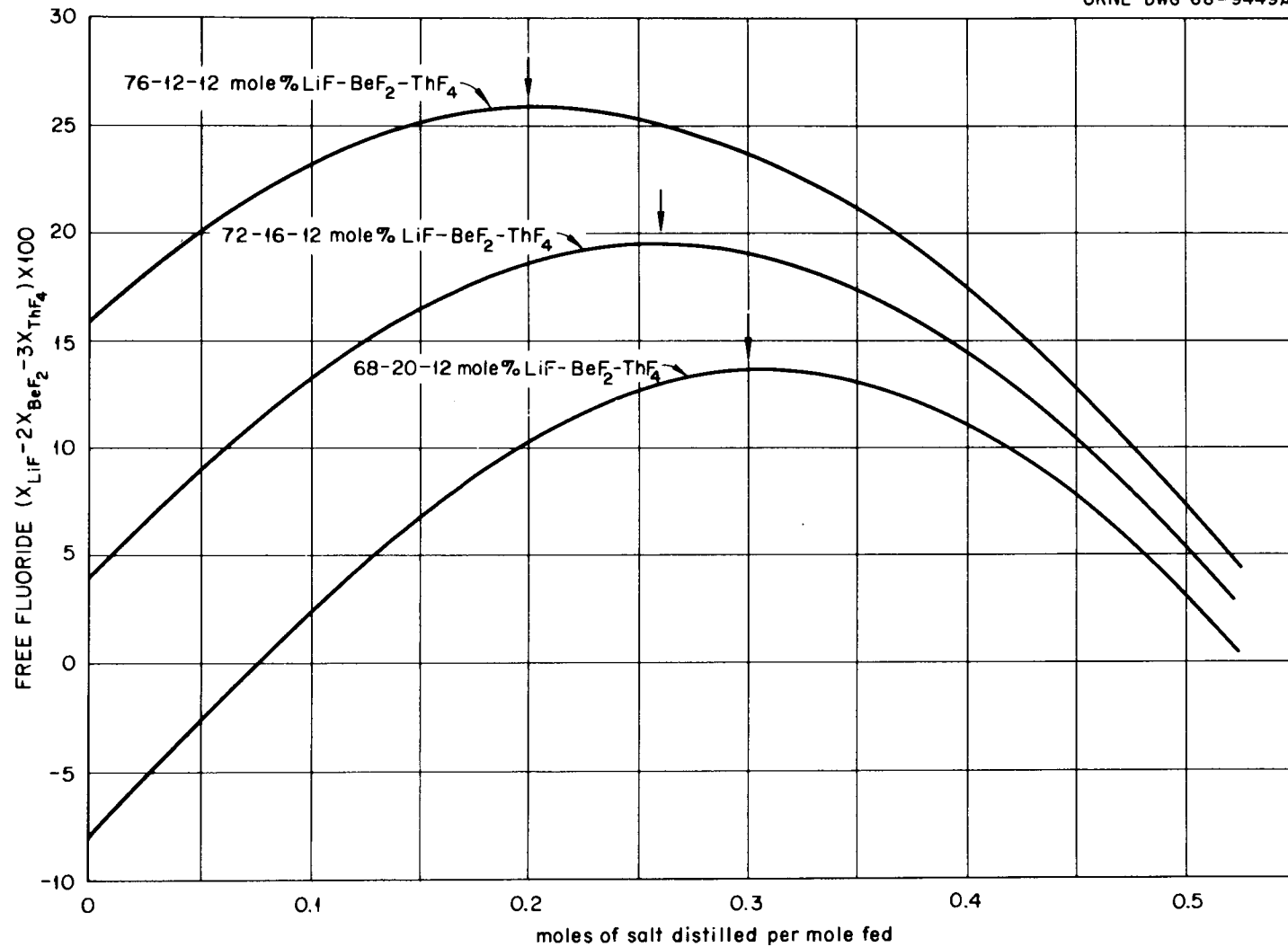


Fig. 3.2 Variation of Free Fluoride with Fraction of Salt Distilled.

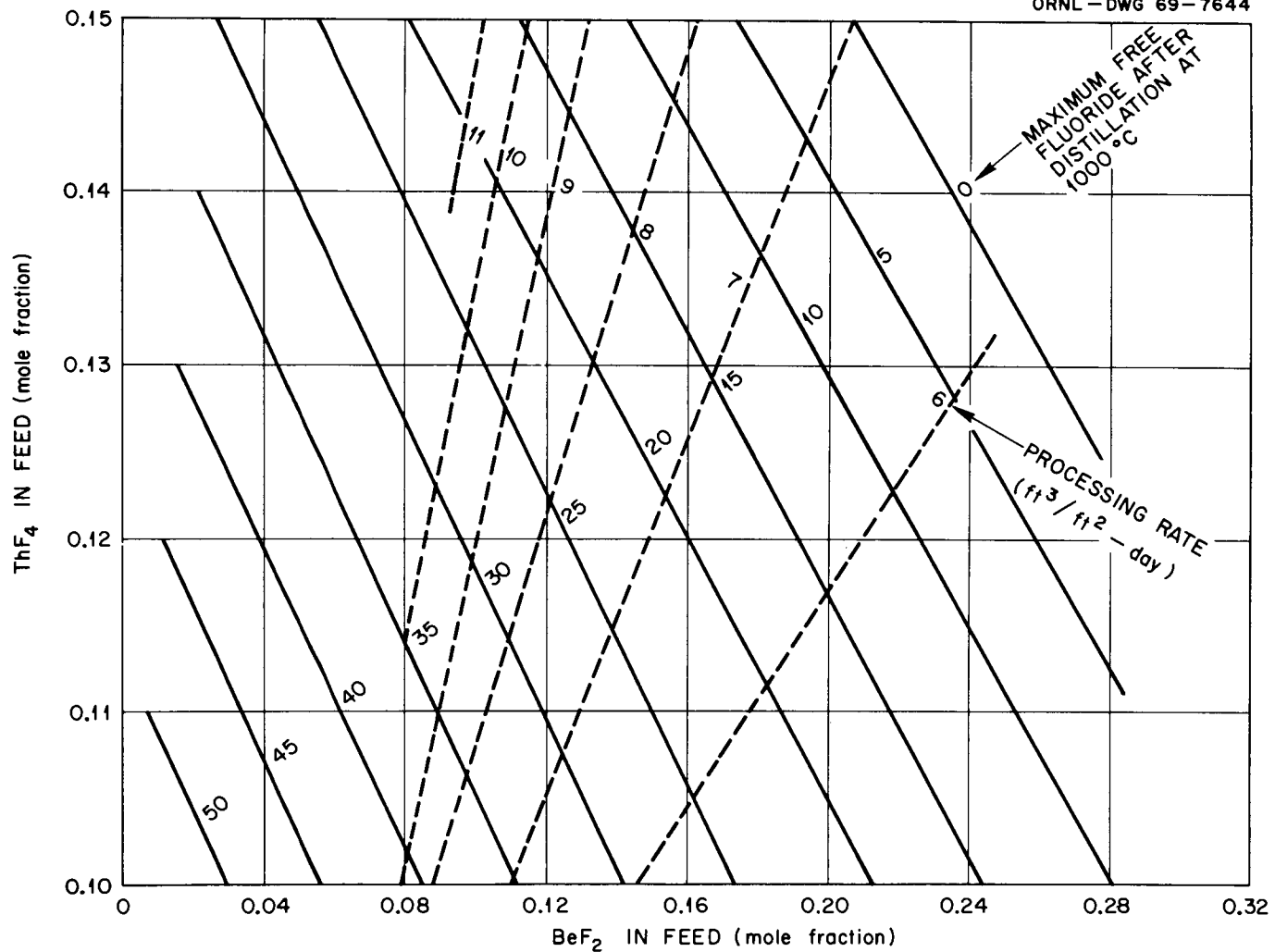


Fig. 3.3 Maximum Free Fluoride Contents and Predicted Processing Rates for Salts Having Various Initial Compositions.

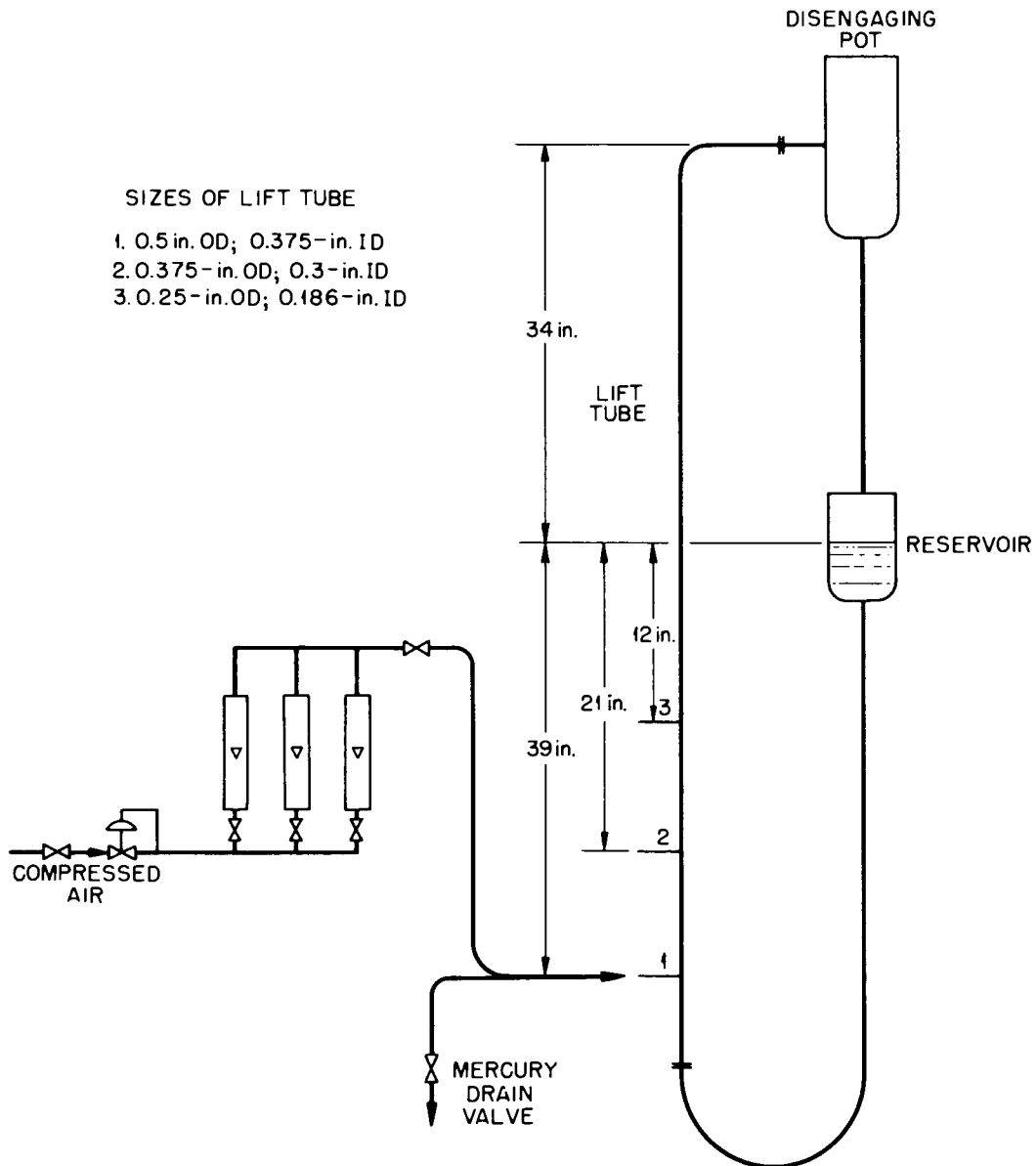


Fig. 3.4 Schematic Diagram of Gas-Lift Pump Test System.

ORNL-DWG 69-7646

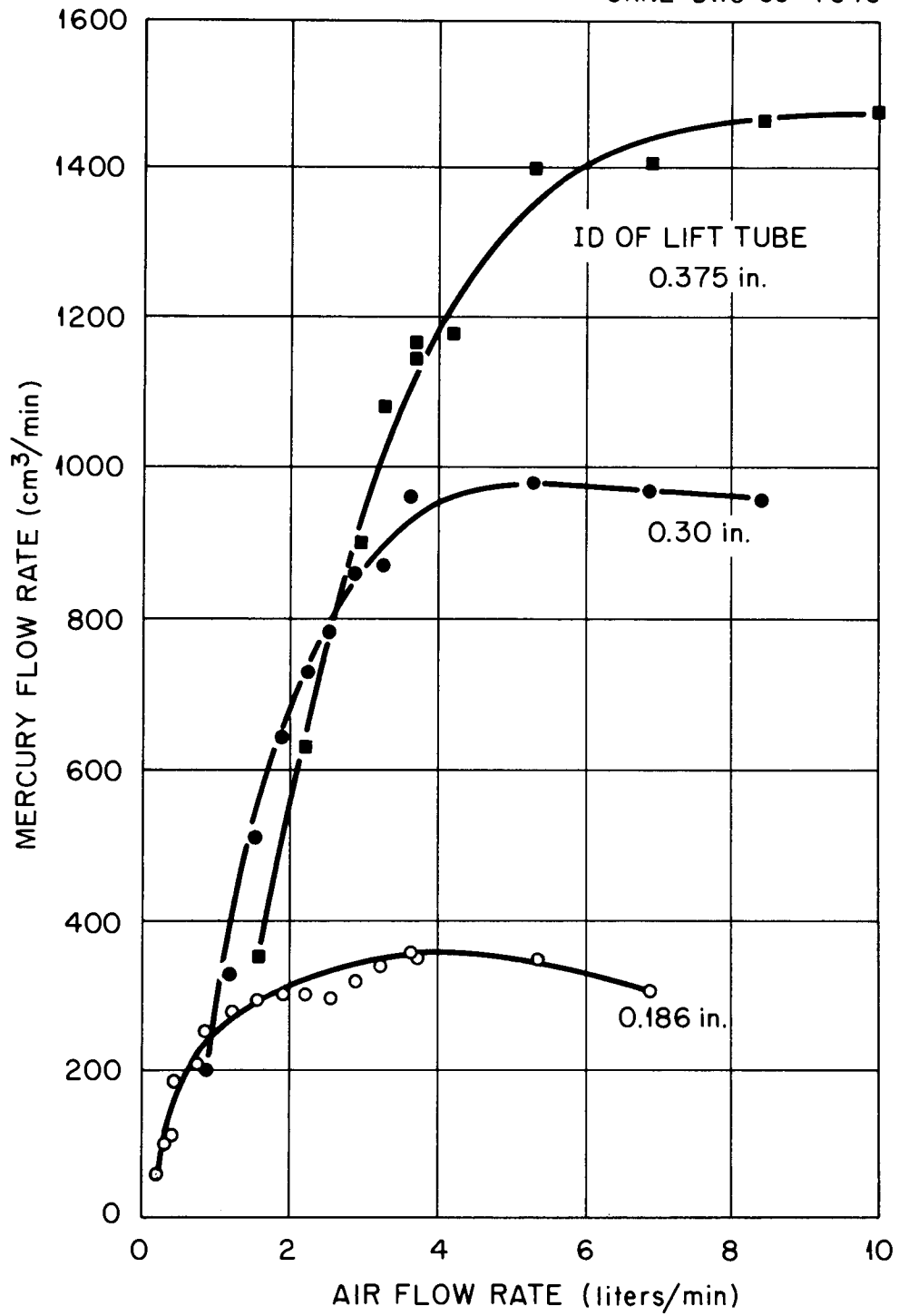


Fig. 3.5 Variation of Mercury Pumping Rate with Air Flow Rate and Lift Tube Size for 53% Submergence. Air flow rate measured at ambient temperature and pressure.

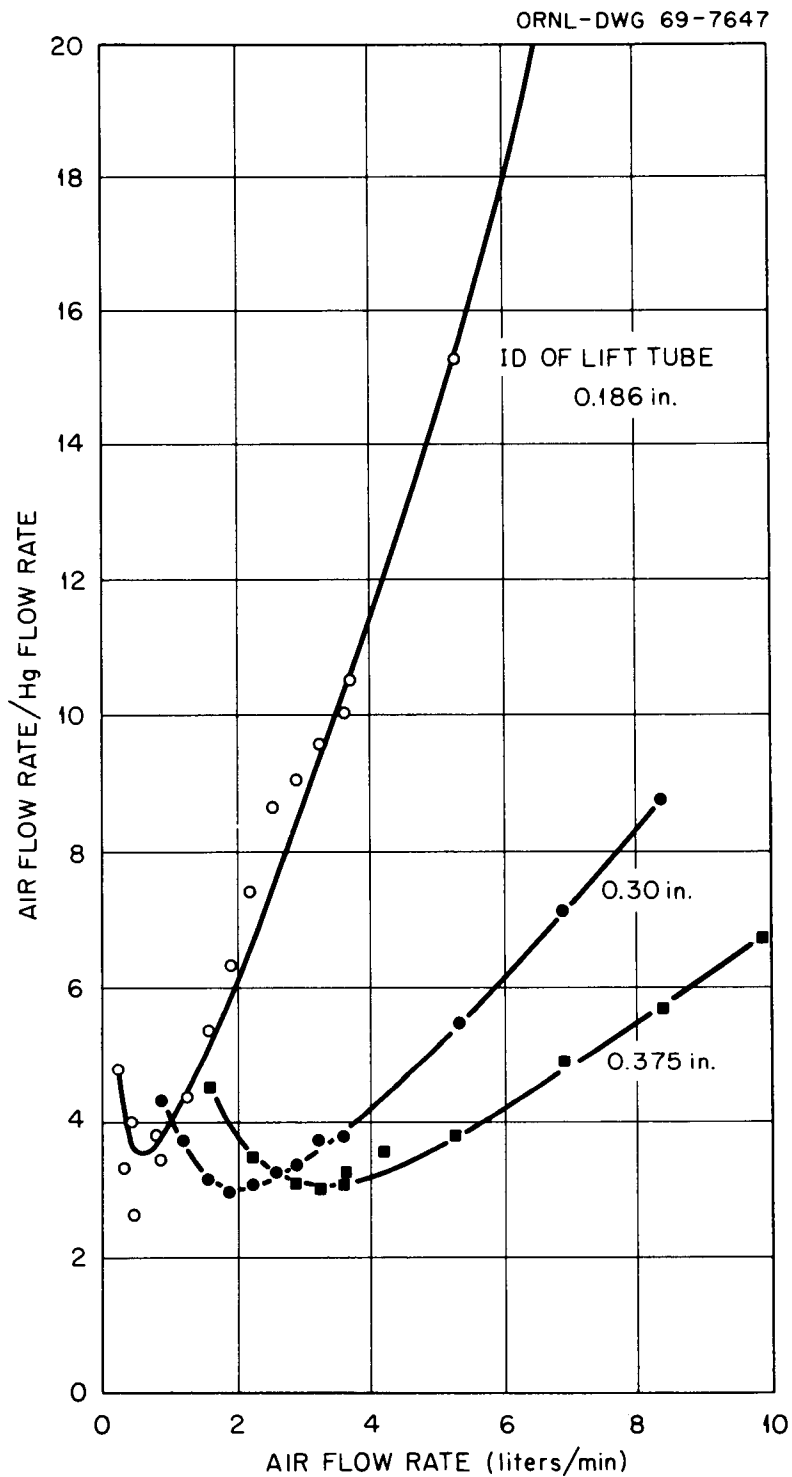


Fig. 3.6 Variation of Ratio of Air Flow Rate to Mercury Flow Rate with Air Flow Rate and Lift Tube Size for 53% Submergence. Air flow rate measured at ambient temperature and pressure.

ORNL-DWG 69-7648

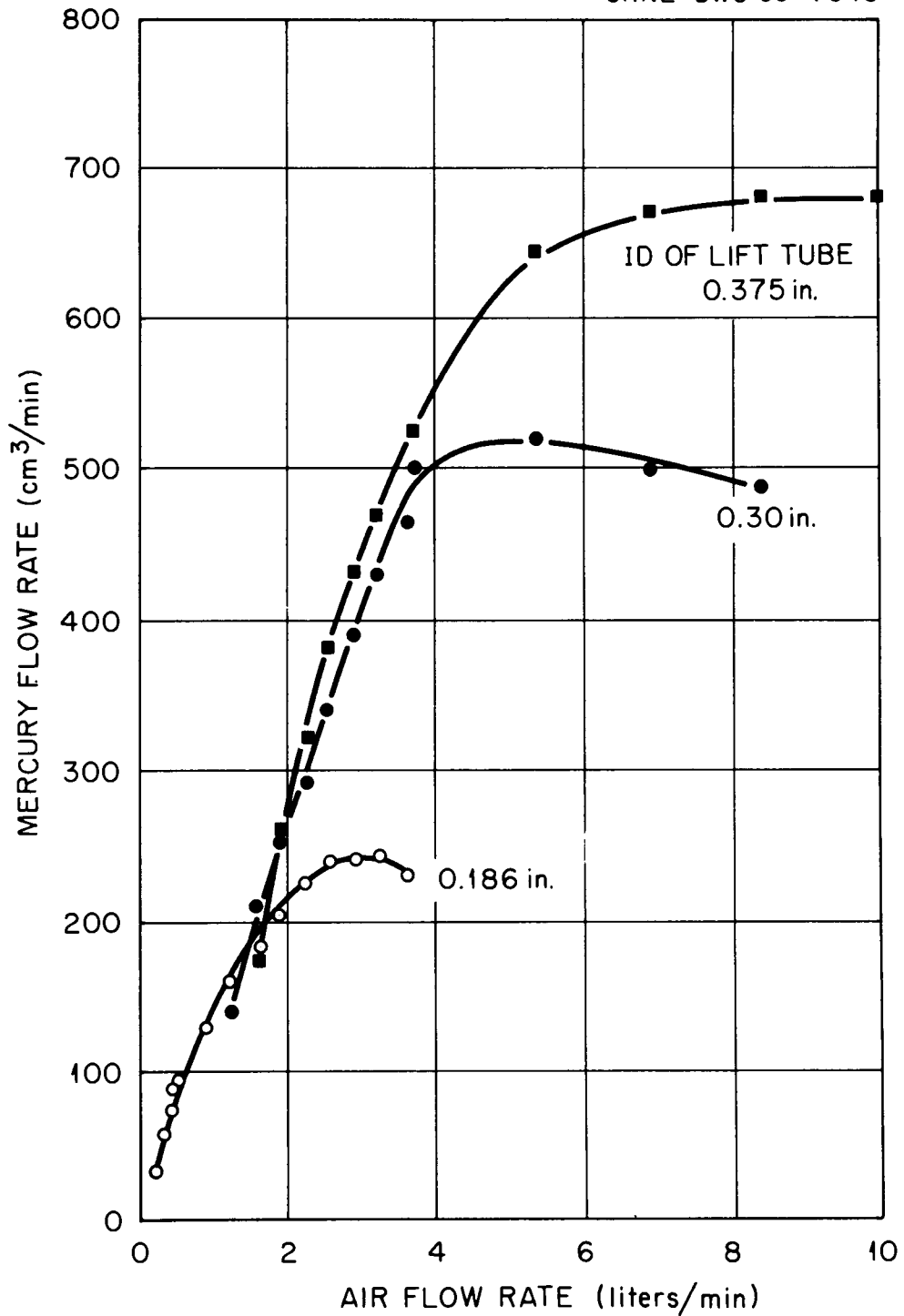


Fig. 3.7 Variation of Mercury Pumping Rate with Air Flow Rate and Lift Tube Size for 39% Submergence. Air Flow rate measured at ambient temperature and pressure.

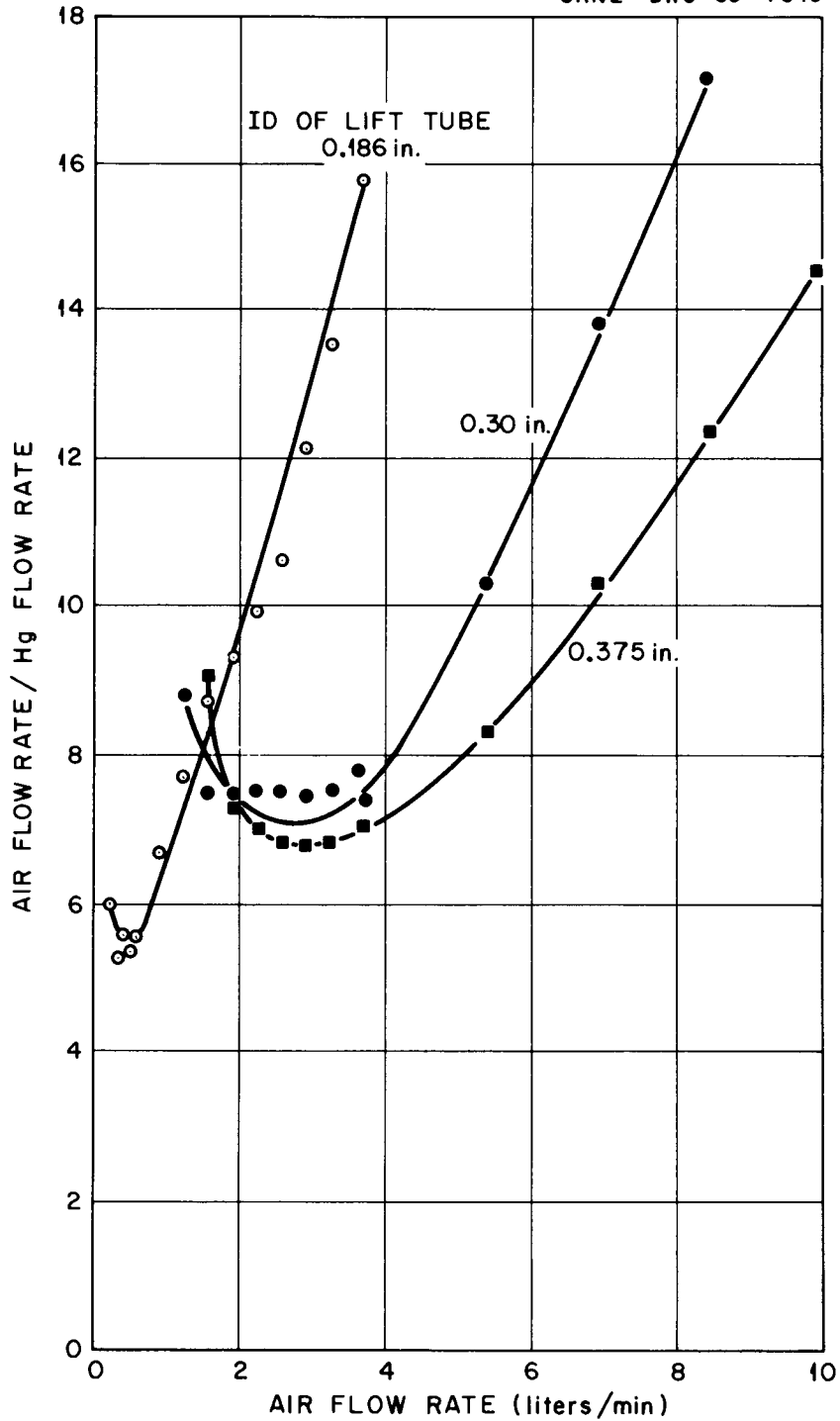


Fig. 3.8 Variation of Ratio of Air Flow Rate to Mercury Pumping Rate with Air Flow Rate and Lift Tube Size for 39% Submergence. Air flow rate measured at ambient temperature and pressure.

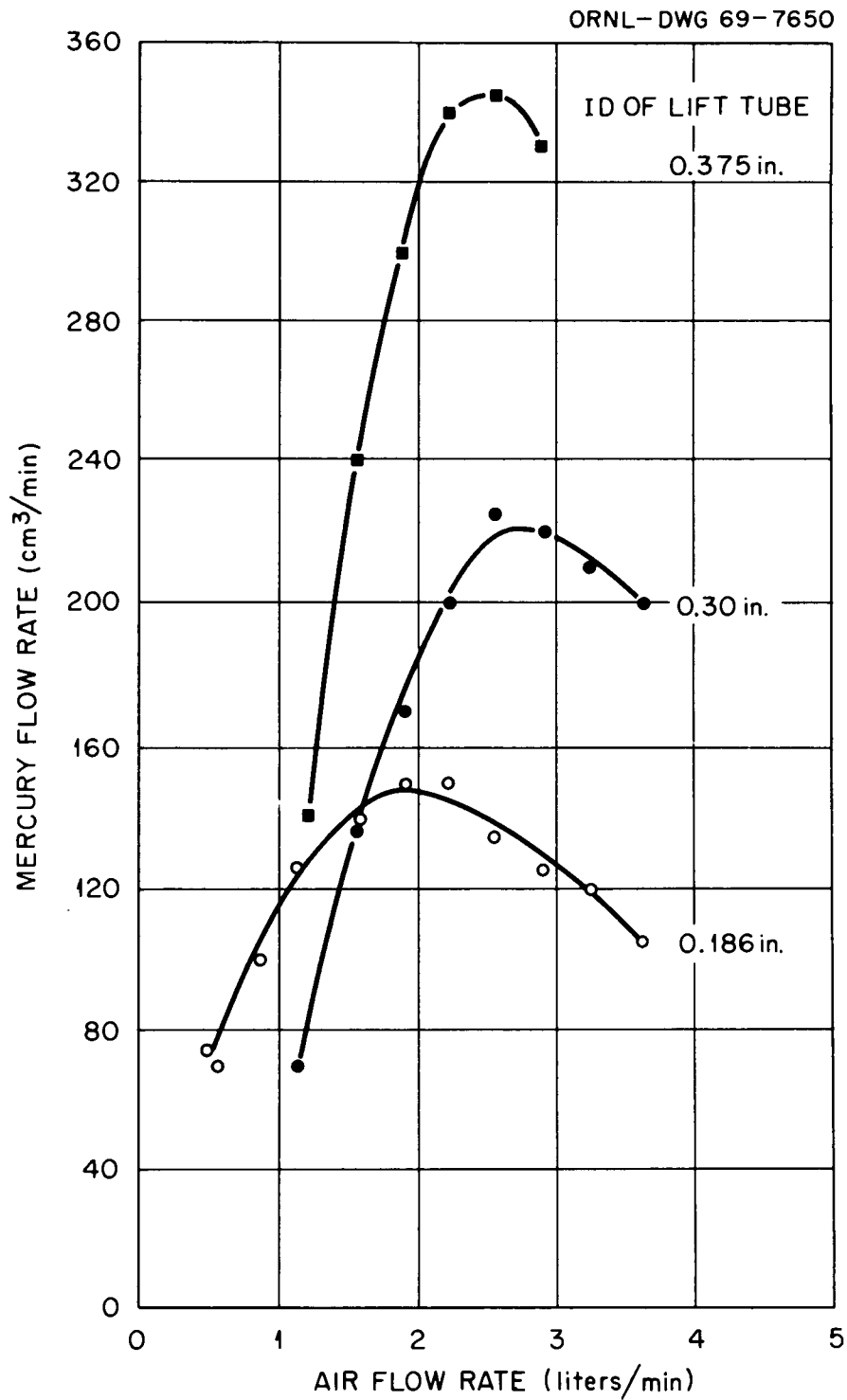


Fig. 3.9 Variation of Mercury Pumping Rate with Air Flow Rate and Lift Tube Size for 26% Submergence. Air flow rate measured at ambient temperature and pressure.

ORNL-DWG 69-7651

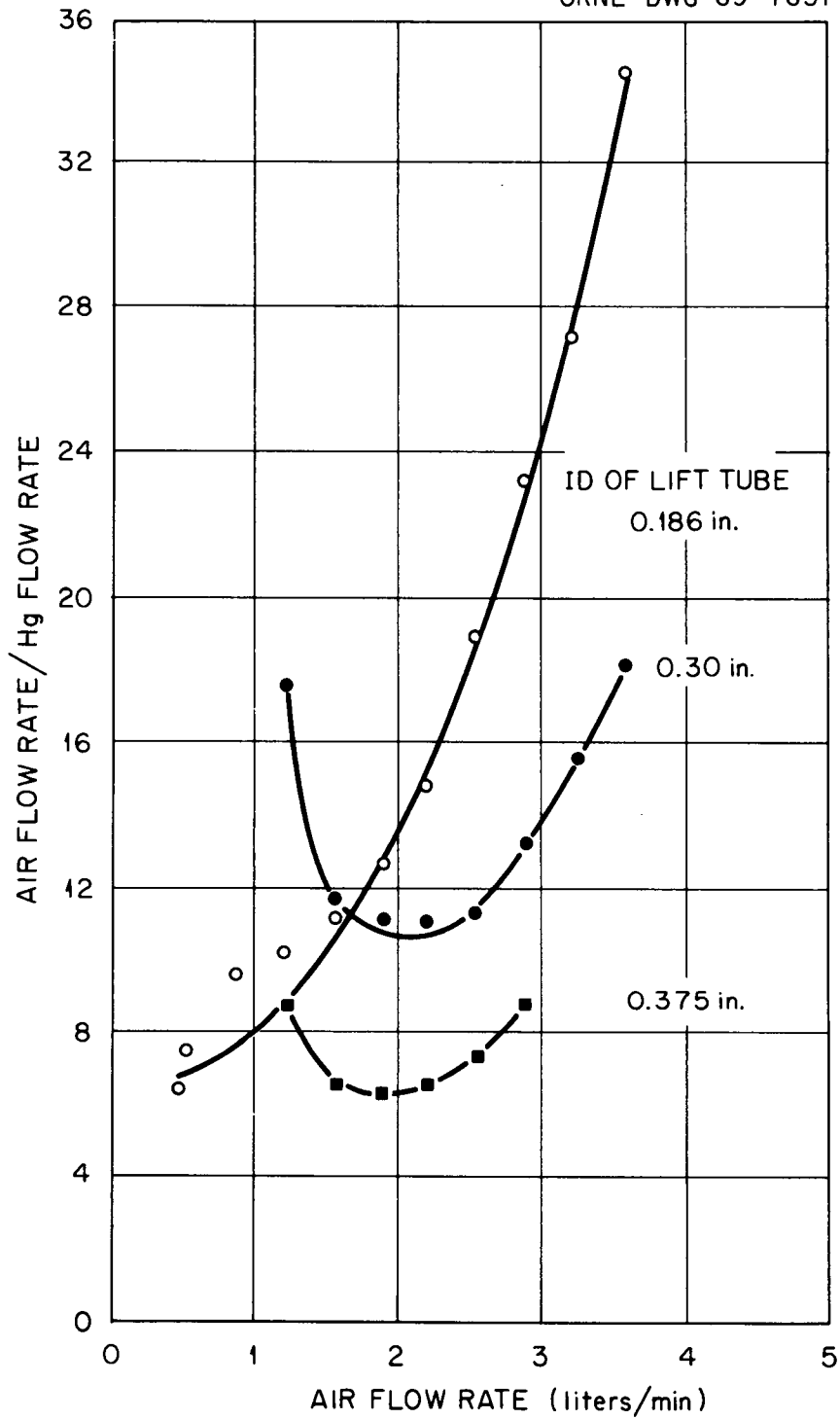


Fig. 3.10 Variation of Ratio of Air Flow Rate to Mercury Pumping Rate with Air Flow Rate and Lift Tube Size for 26% Submergence. Air flow rate measured at ambient temperature and pressure.

For a given size of lift tube with a fixed submergence depth, a maximum mercury pumping rate and a minimum air-to-mercury flow ratio are obtained. The air flow rate yielding the maximum pumping rate is always greater than the air rate that yields the maximum air-to-mercury flow ratio. For a given submergence depth, the pumping capacity increases as the diameter of the lift tube increases. However, as this diameter is increased, the metal flow rate becomes less stable.

It was concluded that gas-lift pumping of bismuth is feasible for the Flow Electrolytic Cell Facility and that two 3/8-in.-OD lift tubes would provide the desired maximum flow of 0.5 gpm.

3.3 Simulated Salt-Metal Contactor Studies

J. S. Watson L. E. McNeese

The flowsheets currently proposed for processing the fuel stream of molten salt breeder reactors (MSBR's) to remove protactinium and rare-earth fission products involve reductive extraction of these elements into molten bismuth containing lithium and thorium metals as reductants. Multistage, countercurrent contactors for bismuth and molten salt to be used in this process present several unique difficulties or requirements. First, the requirements as to temperature and material of construction dictate a reasonably simple design. Second, the high densities of the fluids and the high interfacial tension between the phases make design data and experience from conventional aqueous-organic liquid contactors of little, if any, use. Finally, the rare-earth-removal system requires very high flow ratios, for which conventional columns (packed or spray) have relatively large stage heights because of axial mixing in the continuous phase (i.e., the phase having the lower throughput).

3.3.1 Use of Simulated System for Contactor Development

Contactors development is being studied initially with a low-temperature (i.e., room-temperature) system, mercury-water, which has physical

properties similar to those of the bismuth-salt system. Extrapolation from mercury-water to bismuth-salt conditions is expected to be much easier and more reliable than extrapolations of water-organic phase data.

Although meaningful mass-transfer experiments with mercury and water may not be possible, most properties related to the hydrodynamics of the systems can be studied. To date, quantitative measurements have been made of flooding rates, dispersed-phase holdup, and pressure drop. In addition, by using glass or Lucite columns, interesting and significant visual observations of droplet size (or interfacial area) and flow patterns have been made. In the near future, axial diffusion in the continuous phase will be studied.

These experiments are providing much of the data needed to design bismuth-salt contactors. Hopefully, only a few high-temperature experiments will be required with contactors that have previously been evaluated in the simulated system.

Comparison of Physical Properties in Actual and Simulated Systems.--

Mercury and water were chosen as the two components for the simulated system because they are readily available, can be used at room temperature, and have many physical properties that are similar to those of bismuth and molten salt respectively. Of course, the density difference between mercury and water, 12.5 g/ml ($\rho_{\text{Hg}} = 13.5$ and $\rho_{\text{H}_2\text{O}} = 1.0$), is somewhat greater than that between bismuth and salt, 6.36 g/ml ($\rho_{\text{Bi}} = 9.66$ and $\rho_{\text{salt}} \approx 3.30$).⁸ However, most of the data applicable to the design of contactors have been obtained with organic-water systems in which the density differences are 0.05 to 0.2 g/ml. If data from a simulated system, such as the mercury-water system, were not available, an extrapolation of about 50-fold in density difference would be required. Data from the mercury-water system will be used to obtain improved correlations, which should predict the behavior of bismuth-salt systems.

⁸S. Cantor, Physical Properties of Molten-Salt Reactor Fuel, Coolant, and Flush Salts, ORNL-TM-2316 (1968).

The viscosities of bismuth and mercury are similar; for example, they are reported to be 1.45 (at 365°C)⁹ and 1.5 centipoises (at 25°C),¹⁰ respectively. On the other hand, the viscosity of a typical molten salt at 600°C is approximately 12 centipoises,⁸ whereas the viscosity of water at 25°C is only 0.9 centipoise. The latter values represent a significant difference in viscosity; however, the effect of viscosity is probably fairly well understood because the available data from conventional organic-water systems cover a wide range of viscosities.

The remaining physical property of interest, interfacial tension, presents a problem because no reliable data relative to it are available for bismuth and molten salt. The interfacial tension between mercury and water is approximately 370 dynes/cm.¹⁰ The interfacial tension between bismuth and KCl-LiCl eutectic salt at 810°F has been reported¹¹ to be about 240 dynes/cm. Interfacial tension values for most organic-water systems lie between 1 and 30 dynes/cm. Thus, we are interested in a system having an interfacial tension at least ten times those of systems for which contactor data are available.

3.3.2 Experimental Equipment and Method

The first part of the simulated contactor study involved measurement of dispersed-phase holdup and flooding rates. These measurements were made using a 1-in.-diam, 2-ft-long glass column. The end sections of the column expanded to a 2-in. diameter to allow space for the inlet and outlet lines and to reduce entrainment. Packing material was restrained in the column by screens having openings slightly smaller than the packing (different screen sizes were used with each size of packing). Ball

⁹N. A. Lange, Handbook of Chemistry, 7th ed., Handbook Publishers, Inc., Sandusky, Ohio, 1949.

¹⁰J. W. Mellor, Inorganic and Theoretical Chemistry, Vol. IV, pp. 711-14, Longmans, Green, and Co., New York, 1952.

¹¹N. S. Shaikhmahmud and C. F. Bonilla, Interfacial Tensions of Molten Metal-Molten Salt Systems: Bismuth Against KCl-LiCl Eutectic Mixture, NYO-3093 (1953).

valves (1-in.-diam opening) were located at each end of the 2-ft section of 1-in. glass pipe to allow holdup measurements. Screens located above and below each valve prevented the packing material from entering the valves. The short section through each valve (approximately 2 in. in length) contained no packing; although the flow patterns (e.g., droplet sizes) may have been altered in these sections, the effect was believed to be minor. Flooding-rate measurements (using 3/16-in. Raschig ring packing) made with and without the ball valves were in agreement within experimental error.

The dispersed-phase holdup of the contactor was measured by suddenly closing both ball valves and determining the volume of mercury thus trapped within the column. For large holdup fractions (i.e., large volumes of mercury), the mercury was simply allowed to drain to the bottom of the isolated (valved off) column section, and the interface height was measured. Measurements of the column void fraction and the volume between the top of the valve and the packed column were also made. With small packing sizes or with ring-type packing, a correction was required because water, which was trapped in the column below the nominal mercury surface, made the apparent holdup larger than the actual holdup. A separate 1-in.-diam column was used to measure the retained water volume, which was assumed to be independent of operating conditions.

When the mercury holdup volume was very small, it was difficult to obtain accurate measurements in the above manner because the mercury level was too low to be viewed. In such instances, the mercury was drained from the isolated section of column through a small hole just above the valve and then the resulting volume was measured. Both methods were used over a range of holdup values that allowed a comparison of the methods, and satisfactory agreement was obtained.

Mercury was pumped with a diaphragm pump,^{*} and the pulsation in flow was reduced by a surge chamber. Some fluctuations in the mercury rate to the column were detected, although flow within the column appeared to be

* Masterline Model, manufactured by the Hills-McCanna Co., Carpenterville, Ill.

steady. The packing in the 2-in. expanded section appeared to damp the remaining fluctuations in the mercury rate. The mercury rate, which was determined by setting the stroke length of the pump, was reproducible. It could not be varied continuously, since only four settings were available. The flow rate of the distilled water, circulated through the column via a centrifugal pump, was measured by rotameters.

To date, four types of packing materials have been used. Each has been made either of polyethylene or of Teflon because these materials are not wetted by water or mercury. Materials with this characteristic were chosen because neither the bismuth nor the molten salt is expected to wet the packing (probably graphite or molybdenum) in the high-temperature system. (Although pure bismuth does not wet either of these materials, impurities, such as the reductants in the process, have been reported to cause bismuth to wet some metals. If later evidence shows that the bismuth solution wets the packing materials proposed for the high-temperature system, simulation experiments with wetted packing will be needed.)

3.3.3 Visual Observation of Column Operation

Figures 3.11 and 3.12 are photographs of the column packed with 1/4-in. Raschig rings and 1/4-in. solid right circular cylinders, respectively. The mercury superficial velocities were 186 ft/hr in each case; the corresponding water velocities were 42 and 37 ft/hr. It is obvious that the mercury is well dispersed, and that the interfacial area is reasonably large. At very high flow rates (i.e., when the column is near the flooding point), some larger drops are seen. This is illustrated in Fig. 3.13, which shows the column packed with 1/4-in. rings; the mercury and water velocities were 256 ft/hr and 55 ft/hr, respectively. The flow patterns in the column are dramatically affected by the size of the packing. Figures 3.14 and 3.15 show the column operating with 3/16-in. Raschig rings and 1/8-in. solid cylindrical

PHOTO 95899



Fig. 3.11 Countercurrent Flow of Mercury and Water Through a 1-in.-diam Column Packed with 1/4-in. Raschig Rings. Superficial water and mercury velocities were 42 and 186 ft/hr, respectively.

PHOTO 95901

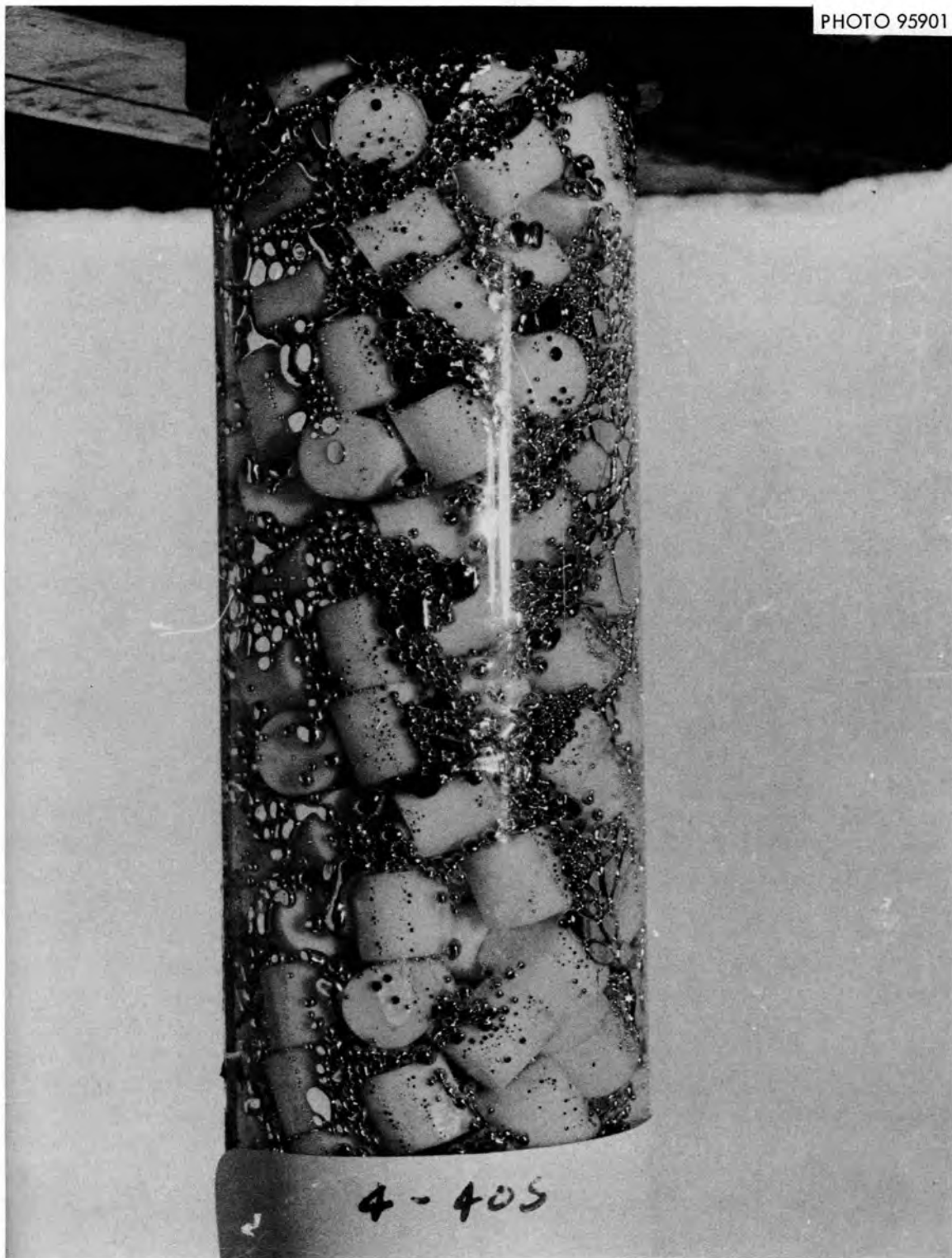


Fig. 3.12 Countercurrent Flow of Mercury and Water Through a 1-in.-diam Column Packed with 1/4-in. Solid Right Circular Cylinders. Superficial water and mercury velocities were 37 and 186 ft/hr, respectively.



Fig. 3.13 Countercurrent Flow of Mercury and Water Through a 1-in.-diam Column Packed with 1/4-in. Raschig Rings. Superficial water and mercury velocities were 55 and 256 ft/hr, respectively.

PHOTO 95897



Fig. 3.14 Countercurrent Flow of Mercury and Water Through a 1-in.-diam Column Packed with $3/16$ -in. Raschig Rings. Superficial water and mercury velocities were 27 and 186 ft/hr, respectively.

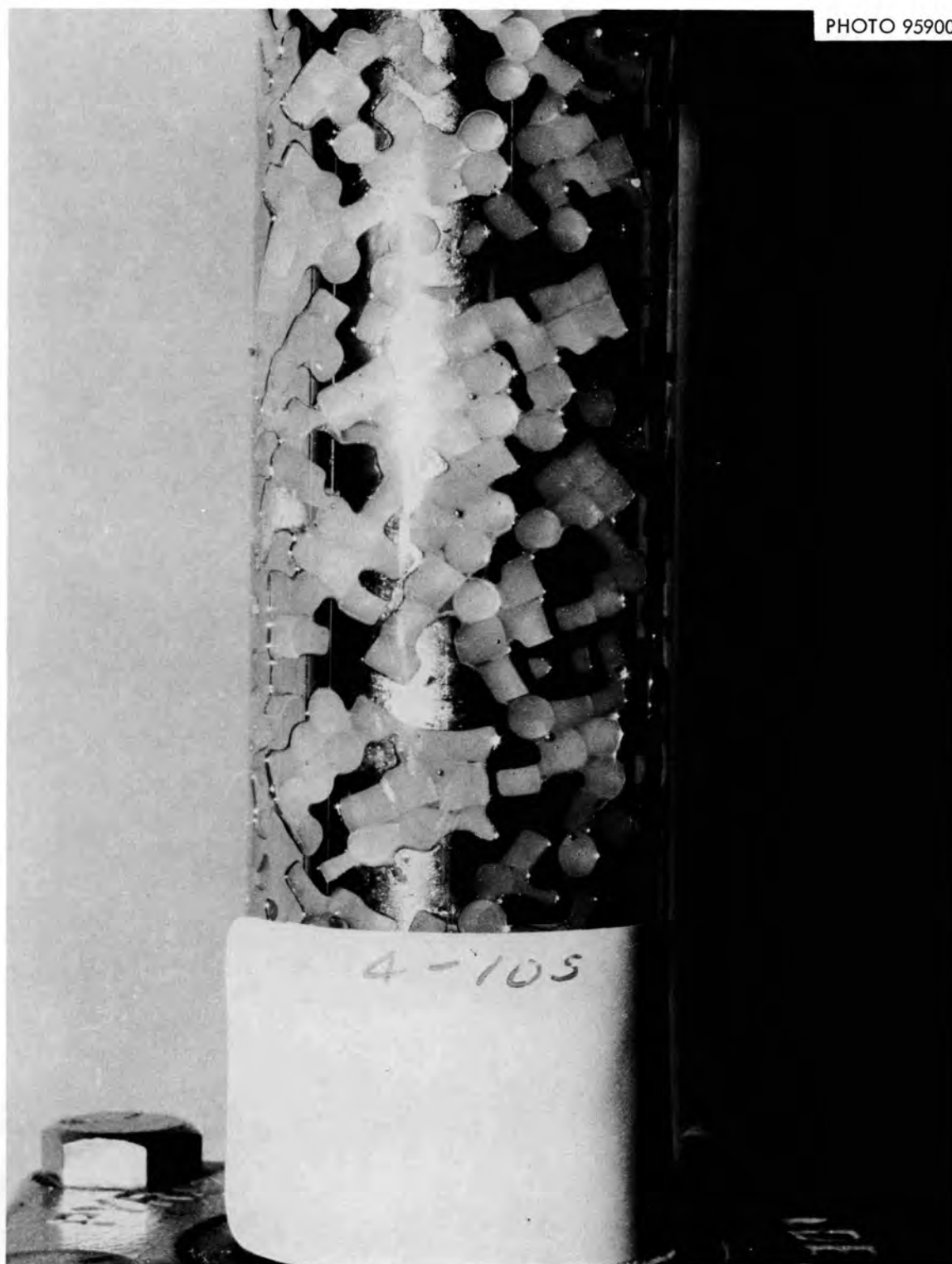


Fig. 3.15 Countercurrent Flow of Mercury and Water Through a 1-in.-diam Column Packed with 1/8-in. Solid Right Circular Cylinders. Superficial water and mercury velocities were 9.3 and 186 ft/hr, respectively.

packing. A 25% reduction in the size of the packing caused the mercury to become essentially coalesced; this, in turn, reduced the interfacial area drastically.

The dependence of flow behavior upon packing size has been reported in other studies.¹²⁻¹⁴ In studies with organic-water systems, Gayler, Roberts, and Pratt¹⁵ showed that dispersed flow is maintained only if the packing diameter is greater than a critical value, d_{pc} , which is defined as follows:

$$d_{pc} = 2.42 \frac{\sigma}{g\Delta\rho}, \quad (3.11)$$

where

- d_{pc} = packing size, cm,
- σ = interfacial tension, dynes/cm,
- g = gravitational constant, cm/sec²,
- $\Delta\rho$ = difference in density of phases, g/cm³.

This equation appears to apply in a general way to the present high-density system; this is rather surprising since the equation is only approximate (e.g., no distinction is made between different types of packing materials). Equation 3.11 predicts dispersed flow with 1/4-in. and 3/16-in. packing and coalesced flow with 1/8-in. packing. Figures 3.16 and 3.17 illustrate the dramatic effect of flow rate on flow patterns and interfacial area in a column with baffles. Figure 3.16 shows the column with

¹²F. R. Dell and H. R. C. Pratt, "Flooding Rates in Packed Columns," *Trans. Inst. Chem. Engrs. (London)* 29, 89-109 (1951).

¹³E. H. Hoffing and F. J. Lockhart, "A Correlation of Flooding Velocities in Packed Towers," *Chem. Eng. Progr.* 50, 94-103 (1954).

¹⁴T. R. Johnson, F. G. Teats, D. R. Gorth, and P. J. Mack, "Studies of Extraction Columns," p. 31 in Chemical Engineering Division Semiannual Report, July-December 1966, ANL-7325 (April 1967).

¹⁵R. Gayler, N. W. Roberts, and H. R. C. Pratt, "Liquid-Liquid Extraction. Part IV. A Further Study of Hold-Up in Packed Columns," *Trans. Inst. Chem. Engrs. (London)* 31, 57-68 (1953).

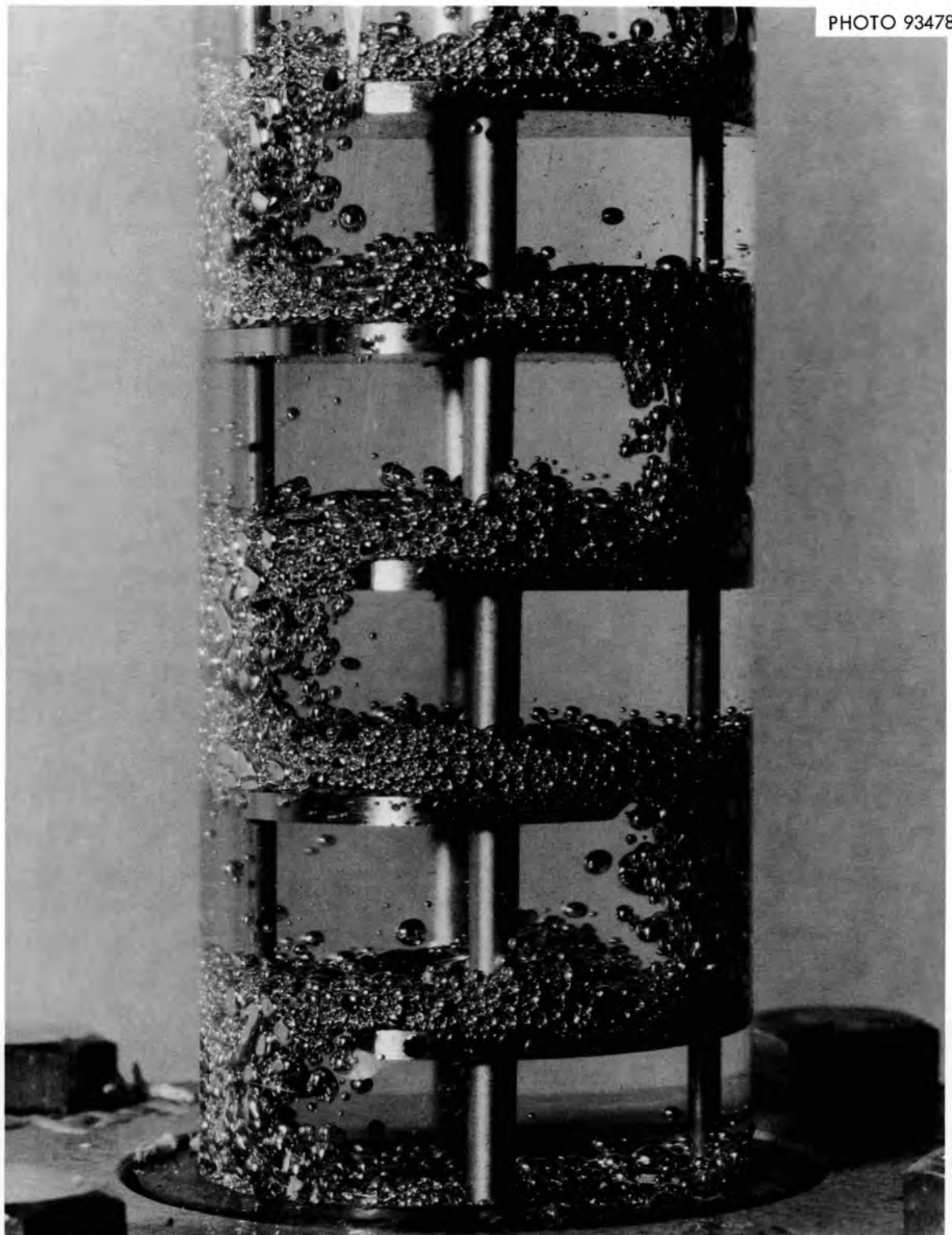


Fig. 3.16 Countercurrent Flow of Water and Mercury in a 1-in.-diam Column Containing Baffles Spaced at $1/2$ -in. Intervals. Superficial water and mercury velocities were 19.4 and 186 ft/hr, respectively.

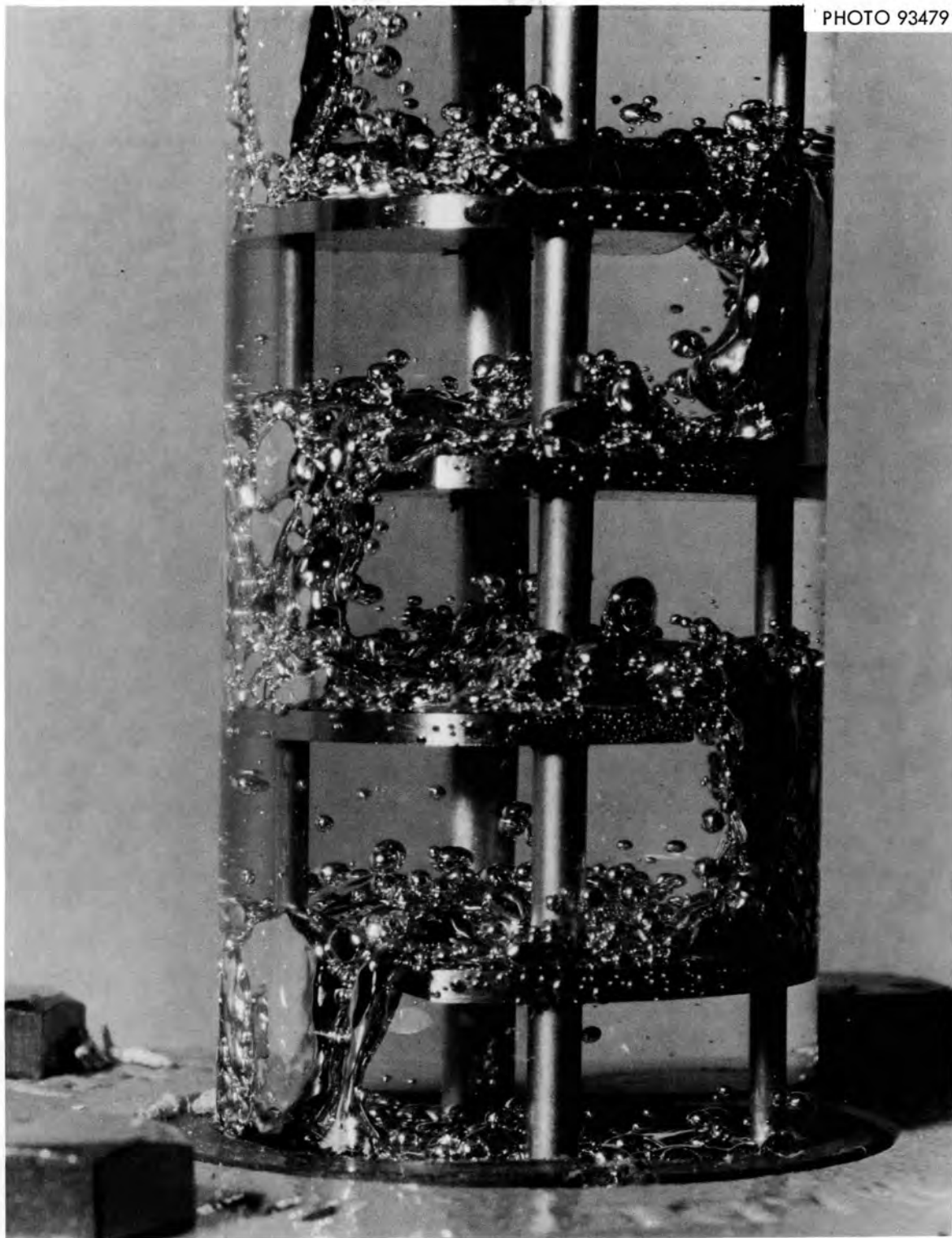


Fig. 3.17 Countercurrent Flow of Water and Mercury in a 1-in.-diam Column Containing Baffles Spaced at $1/2$ -in. Intervals. Superficial water and mercury velocities were 19.4 and 256 ft/hr, respectively.

superficial water and mercury velocities of 19.4 and 186 ft/hr, respectively. The mercury is well dispersed into small drops, and the interfacial area is reasonably high. When the mercury superficial velocity is increased to 256 ft/hr (while the water rate remains constant), the column behavior changes dramatically (Fig. 3.17). The mercury becomes essentially coalesced, and a reduction in interfacial area is observed.

The dependence of flow mode upon flow rate has not been discussed in other studies. The present data with water and mercury were obtained using packing with a diameter near the critical packing diameter, d_p , whereas most studies have been made with packing sizes substantially larger than the critical diameter (since coalesced flow is not desired). When packing having a diameter near the critical diameter is used, the flow mode appears to be dependent on the flow rates.

3.3.4 Experimentally Measured Flooding Rates

The flooding rates observed with two sizes of Raschig rings, two sizes of solid cylindrical packing, and one baffled column are shown in Figs. 3.18-3.22. In these figures, the square root of the superficial velocities of the two phases at flooding are plotted against each other. This type of plot was chosen because previously reported studies have shown that such plots are usually linear.

Our results are shown as bars or bracketed values. A series of runs was made at each available mercury flow rate. The water flow rate was incrementally increased until flooding was observed. The right side of the bracket represents the highest flow rate at which flooding was detected. The brackets, which should contain the flooding rate, were not always in agreement. This is illustrated most clearly in Fig. 3.18, which gives the results from 3/16-in. Raschig rings. More runs were made with this material than with any other packing; thus these results represent the scatter or precision of the measurements. Flooding rates are inherently difficult to measure, mainly because it is often difficult to decide when a column is flooded. In this study, the columns were

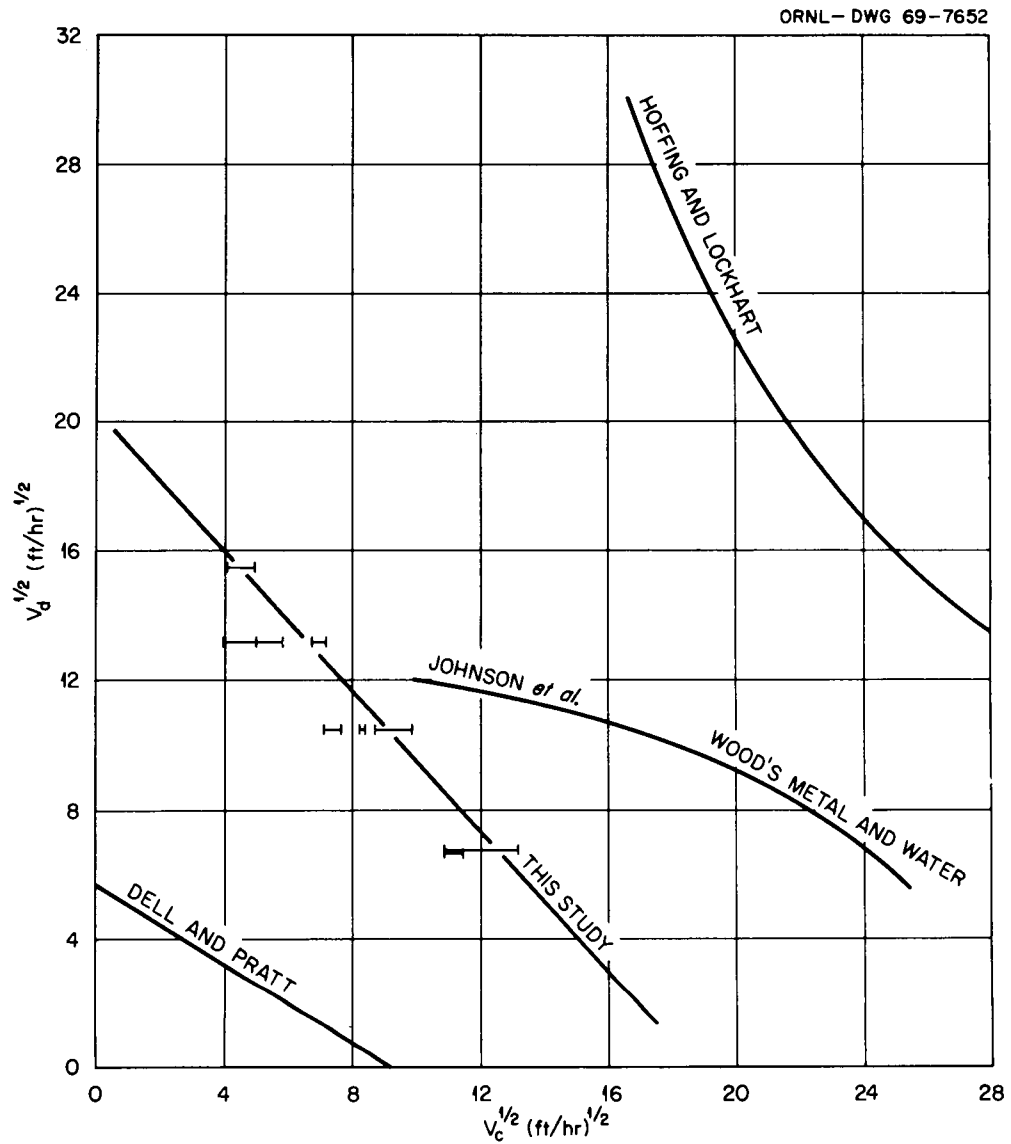


Fig. 3.18 Flooding Rates in Columns Packed with 3/16-in. Raschig Rings.

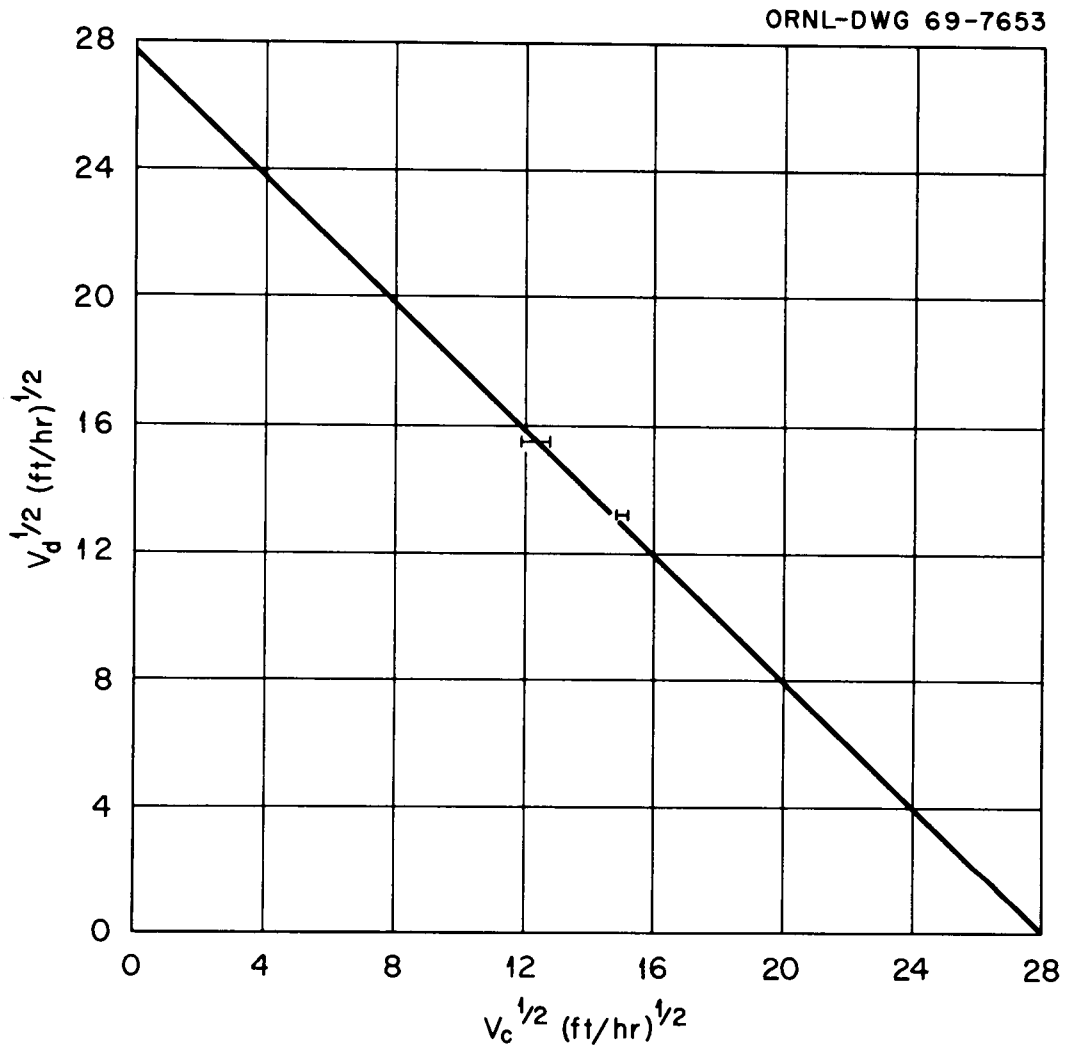


Fig. 3.19 Flooding Rates in a Column Packed with 1/4-in. Raschig Rings.

ORNL-DWG 69-7654

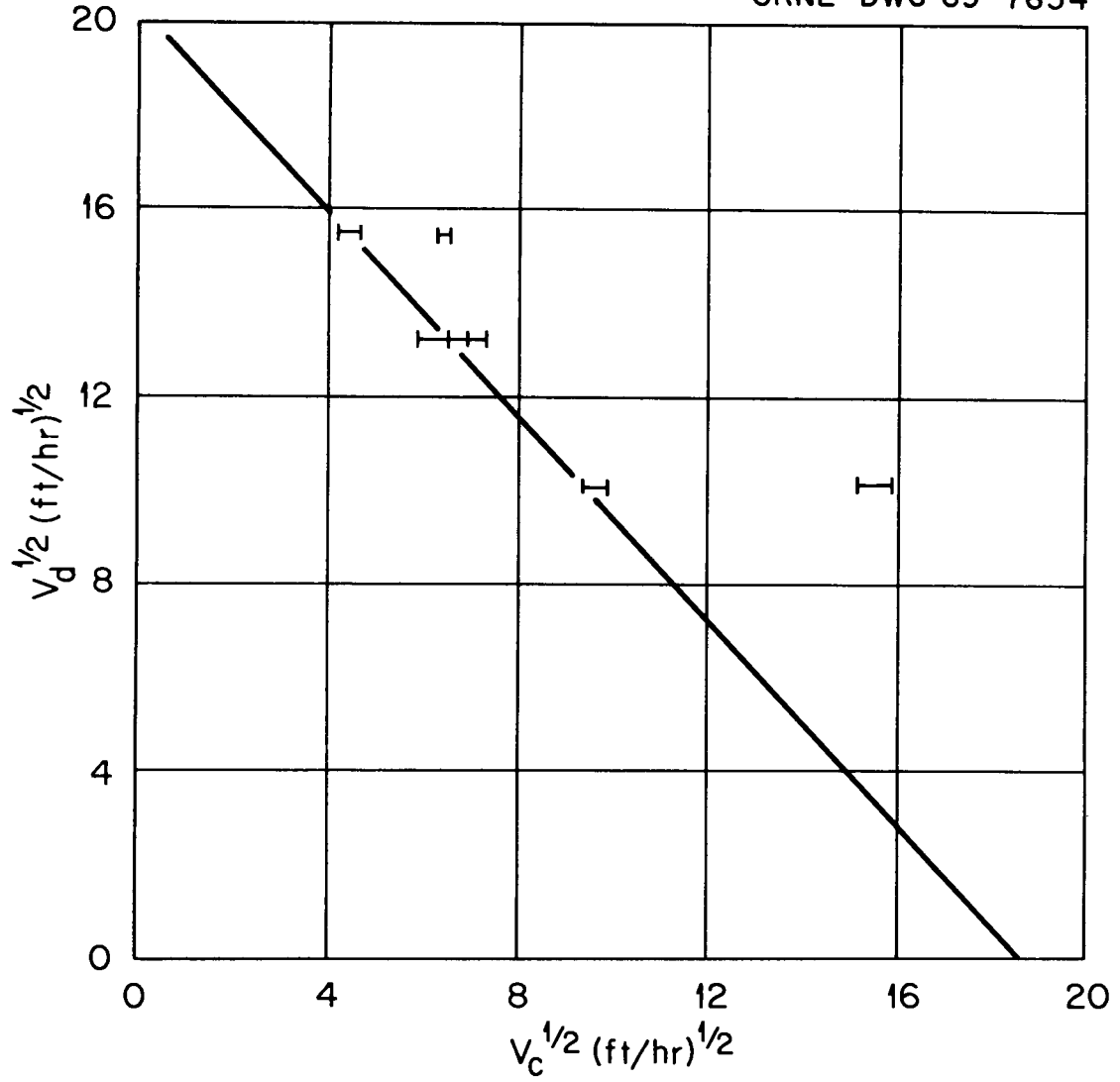


Fig. 3.20 Flooding Rates in a Column Packed with 1/4-in. Solid Right Circular Cylinders.

ORNL-DWG 69-7655

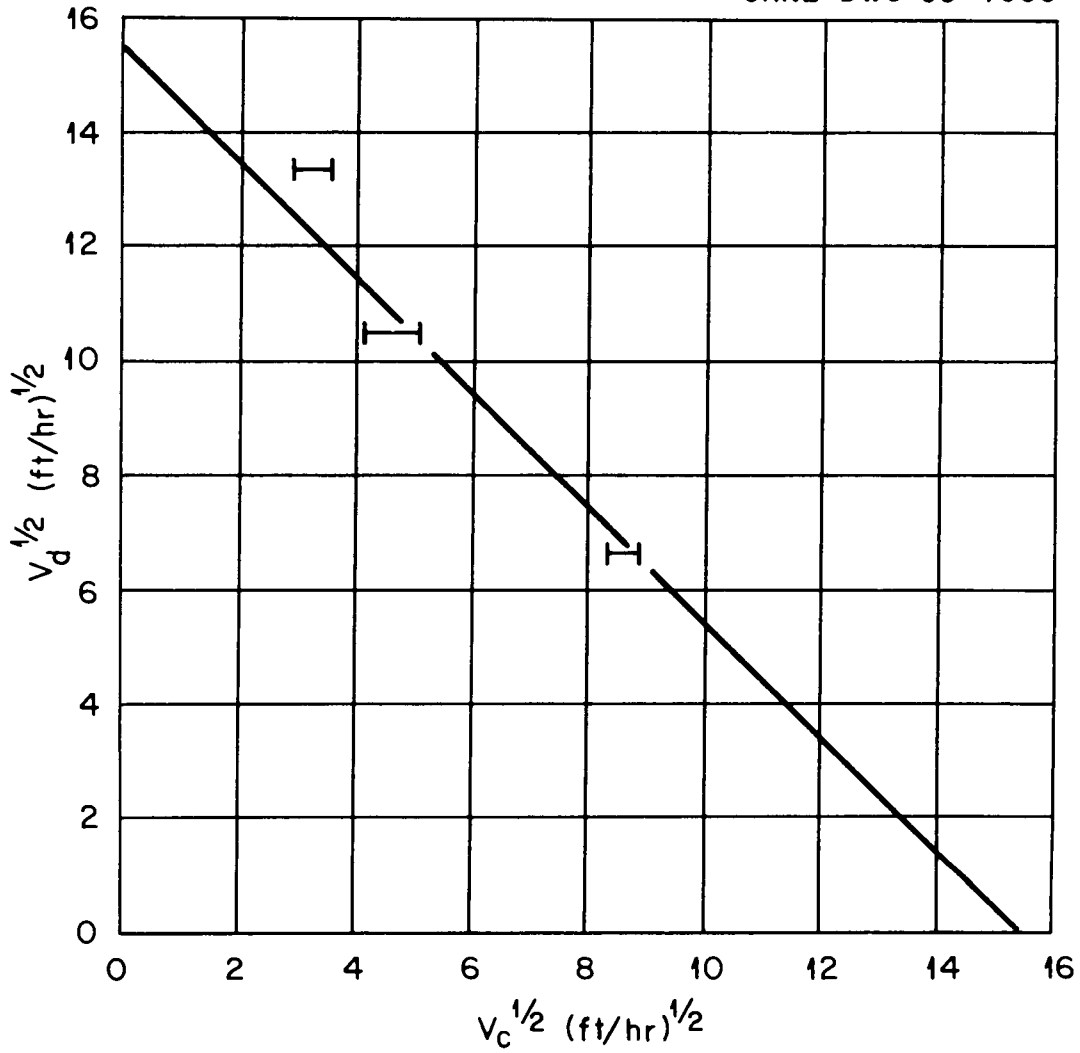


Fig. 3.21 Flooding Rates in a Column Packed with 1/8-in. Solid Right Circular Cylinders.

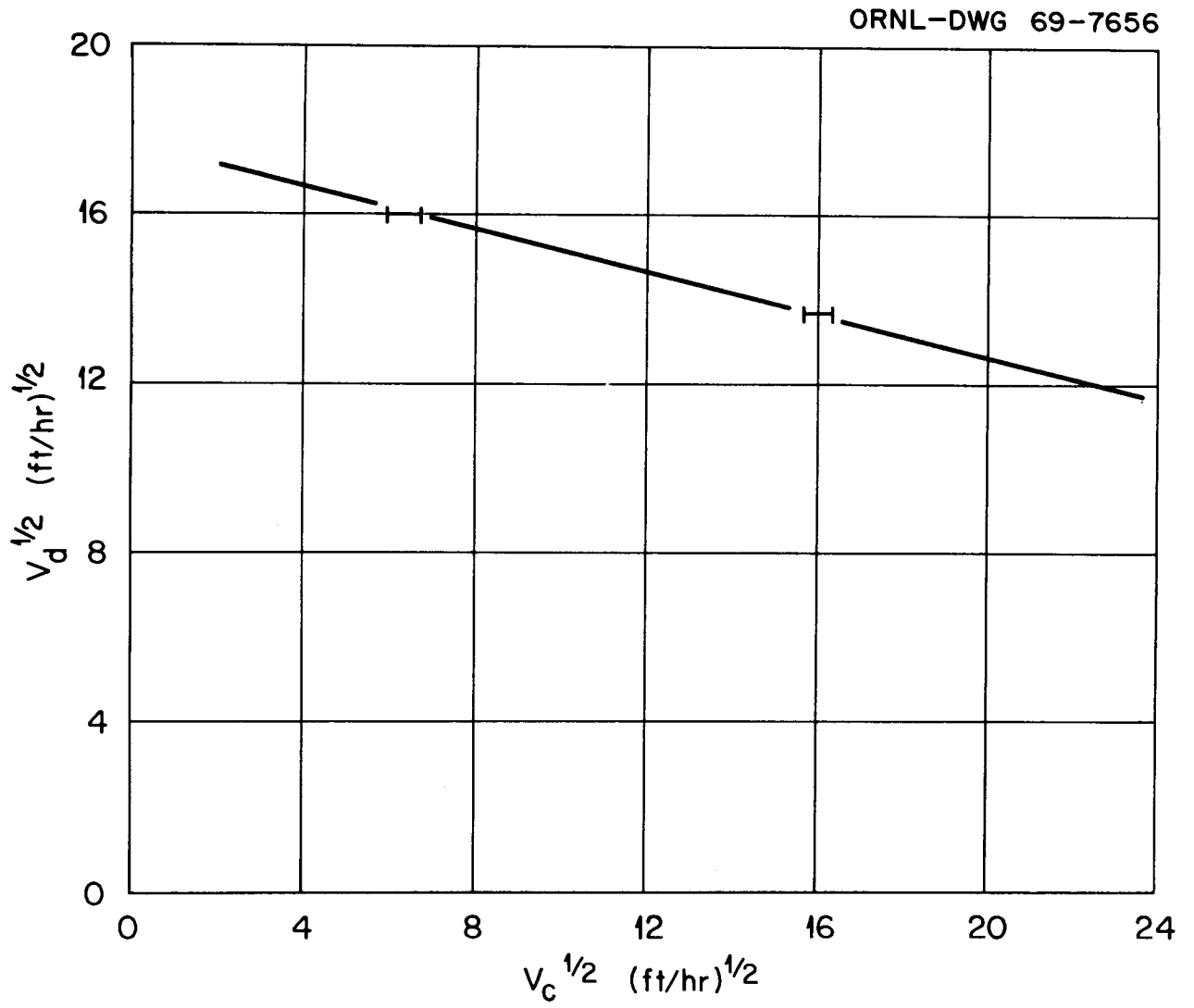


Fig. 3.22 Flooding Rates in a 1-in.-diam Column Containing Baffles Spaced at 1/2-in. Intervals.

considered to be flooded when a constant mercury holdup could not be maintained in the column, that is, when the mercury holdup continued to increase with time. Sometimes this was observed by following the pressure drop (continuous or water phase) across the column; in some cases, the accumulation of mercury within the column could be noted visually. It was necessary to allow operation to proceed for several minutes to ensure that the column was not slowly accumulating mercury. Often the column would operate stably for a time and then suddenly flood, apparently because of some undetected disturbance. If the column could be operated for 10 to 15 min under steady conditions (flow rates and pressure drop), it was not considered to be flooded.

The screens located above and below the ball valves, which were necessary for holdup measurements, represented a potential problem; that is, it was possible for the screens, rather than the packing, to cause flooding. The openings in these screens were only slightly smaller than the packing, and the wires represented a small portion of the column cross section (relative to the solid packing fraction of the column). With the 1/4-in. packing, two different screen sizes were used; no detectable difference in the flooding rates or holdup was observed.

The results with 3/16-in. Raschig rings are compared with two frequently used correlations (Dell and Pratt, and Hoffing and Lockhart) in Fig. 3.18. The correlations are based on data from organic-water systems for which the density differences and the interfacial tension values are much lower than in salt-bismuth or water-mercury systems. Although the two correlations are in reasonably good agreement when applied to organic-water systems, use in the region of interest with mercury and water is not possible since neither of the curves falls near the data of this study and since the predicted results are not in agreement with each other.

3.3.5 Dispersed-Phase Holdup

The fraction of the column void volume that is occupied by the dispersed phase (referred to as holdup) is important for two reasons.

First, for a given drop size, the interfacial area is proportional to holdup; thus it is desirable to operate with a significant holdup. Interfacial area is important because the mass-transfer rate between the two phases is directly dependent on this area. Holdup is also important in that the variation of holdup with flow rate is related to the flooding rate or column capacity. Experimentally determined data on holdup are given in Figs. 3.23-3.25.

With unpacked columns and very low holdup, drops of the dispersed phase do not interact with each other but move through the column with a constant slip velocity (velocity relative to the continuous phase). This, of course, assumes uniform drop size. Under these conditions,

$$\frac{V_d}{X} + \frac{V_c}{1 - X} = V_s, \quad (3.12)$$

where

- V_d = dispersed-phase superficial velocity, ft/hr,
- V_c = continuous-phase superficial velocity, ft/hr,
- X = dispersed-phase holdup, ft³ per ft³ of open column = x/ϵ ,
- x = dispersed-phase holdup, ft³ per ft³ empty column,
- ϵ = column void fraction,
- V_s = slip velocity, ft/hr.

When the holdup in the column becomes significant, drops of the dispersed phase will interact because the flow around each drop will be influenced by the wakes from adjacent drops. To take into account the effect of packing on holdup, one can use a limited form of the Zenz¹⁶ relation for settling particles. The slip velocity is not assumed to be a constant, but a function of the holdup instead. That is,

$$\frac{V_d}{X} + \frac{V_c}{1 - X} = V_s \approx V_o (1 - X), \quad (3.13)$$

where V_o is a constant. For low values of holdup X , Eq. (3.13) reduces to Eq. (3.12). Although Eq. (3.13) has been used to correlate results from several organic-water systems¹³ (despite the presence of packing),

¹⁶F. A. Zenz, *Petrol. Refiner* 36, 147-55 (1957).

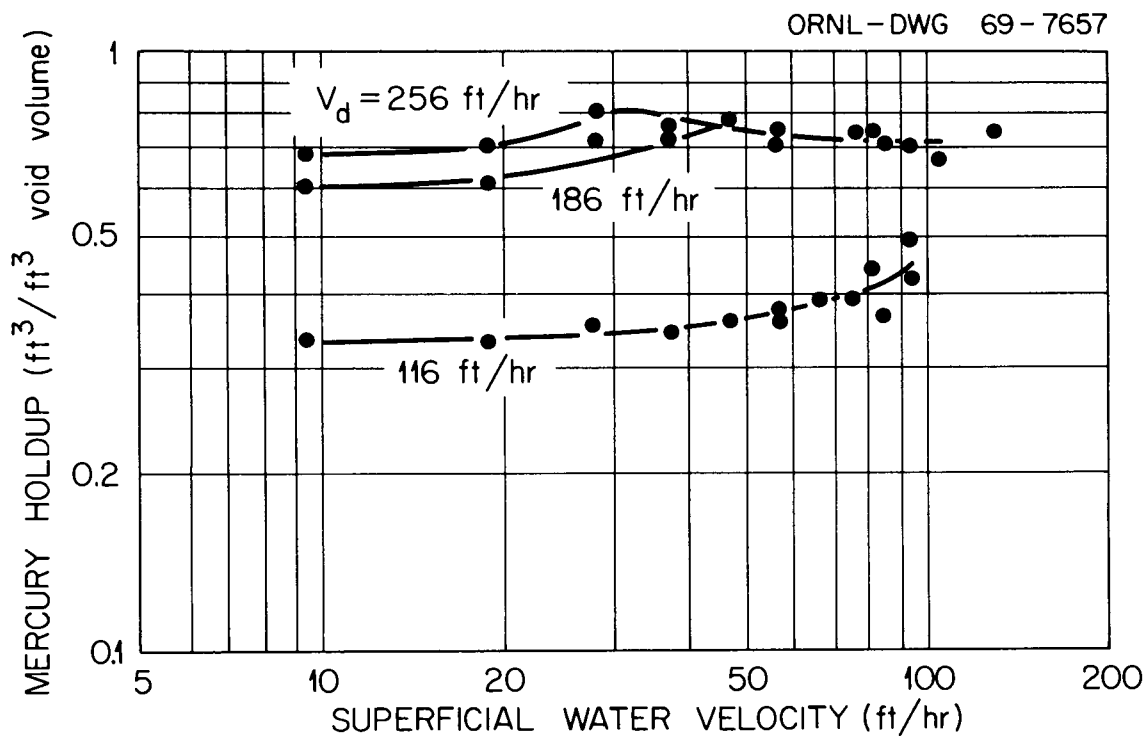


Fig. 3.23 Dispersed-Phase Holdup in a Column Packed with 1/4-in. Solid Right Circular Cylinders.

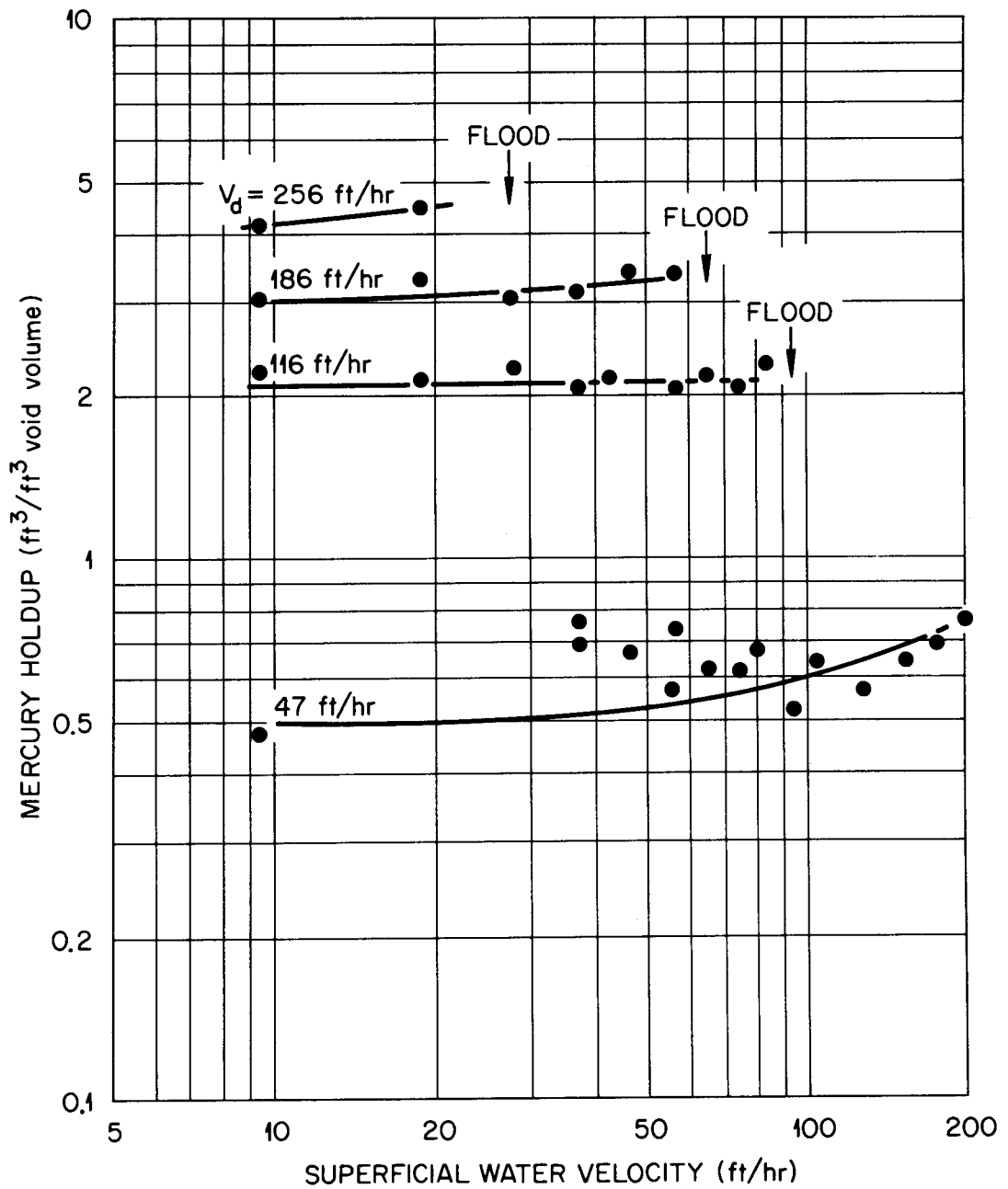


Fig. 3.24 Dispersed-Phase Holdup in a Column Packed with 3/16-in. Raschig Rings.

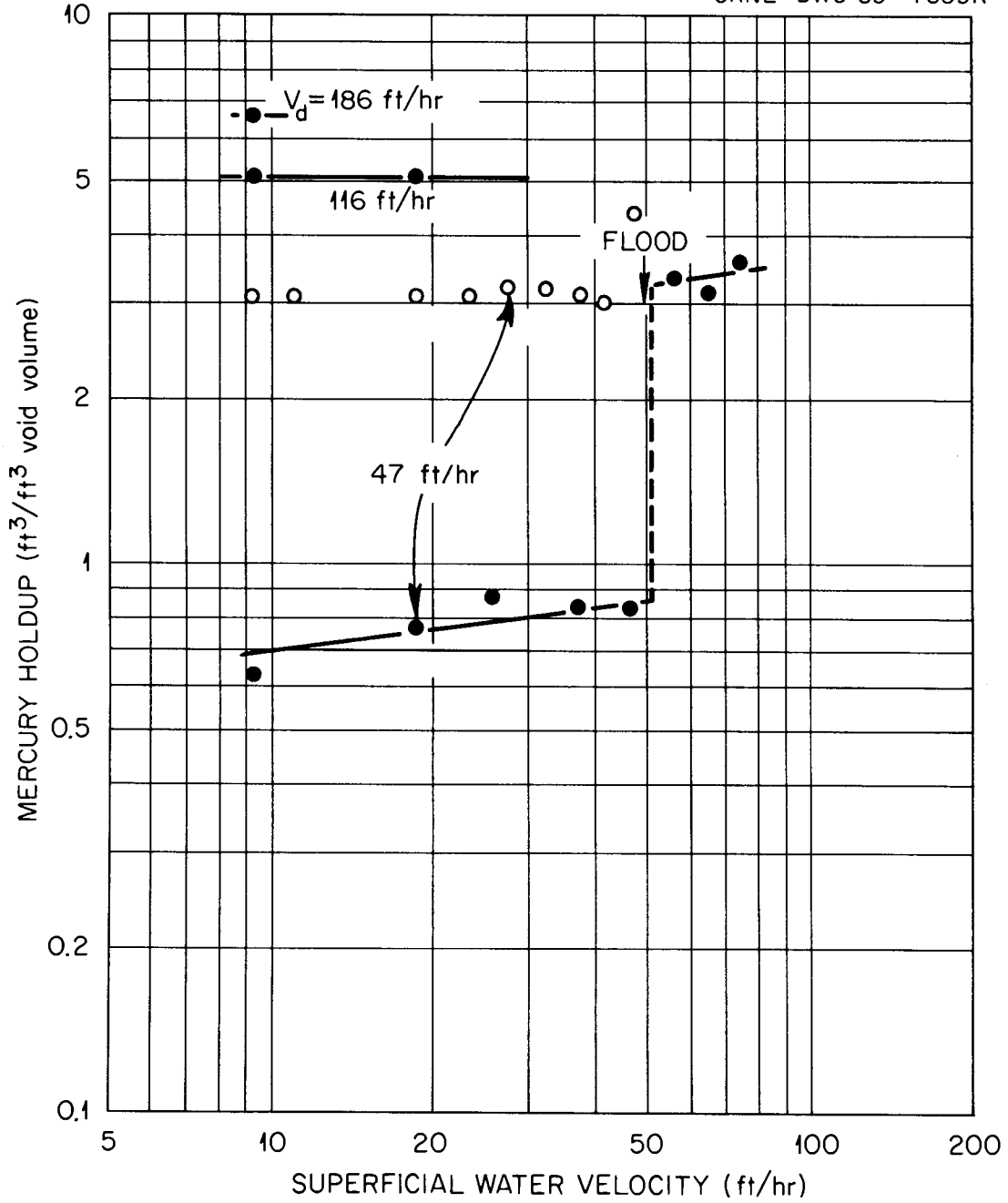


Fig. 3.25 Dispersed-Phase Holdup in a Column Packed with 1/8-in. Solid Right Circular Cylinders.

it does not fit the data obtained from the present study. Figure 3.26 shows V_o and V_s as a function of holdup when 1/4-in. rings are used as the column packing and indicates that V_o is dependent on holdup. The slip velocity, V_s , also appears to be dependent on holdup, although the dependence is slight. Evidently, in high-density systems, holdup is more complicated than Eq. (3.12) or (3.13) would imply.

3.3.6 Pressure Drop in the Continuous Phase

The pressure drop in the continuous phase is important for three reasons: (1) it determines the degree of difficulty of maintaining the bottom interface at an acceptable position in the column; (2) it affects the pump requirements in a plant or experimental system; and (3) it is related to holdup in the column. The relationship between pressure drop and holdup is important since, in salt-metal systems, holdup will be difficult, if not impossible, to measure. Much of the data on column behavior must be inferred from pressure-drop measurements, which will require knowledge of the dependence of holdup on pressure drop.

For the packing materials studied, pressure drop was quite dependent on holdup. This is not surprising since one cause of the pressure drop is the interaction of the water with the mercury phase. These data are shown in Figs. 3.27 - 3.30.

Relationships Between Holdup, Pressure Drop, and Flooding Rates. - To understand the relationship between holdup and pressure drop, a force balance was made for both the dispersed phase and the continuous phase. Forces acting upon the dispersed-phase drops arise from gravity, shear with the continuous phase, the pressure gradient in the column, and shear with the packing and walls. If the forces on the dispersed phase at a point in the column are time-averaged, the sum of these forces will be zero if the dispersed phase is not (on the average) accelerating as it moves through the column. Then,

$$\frac{g}{g_c} A_d \Delta \rho - \tau_i A_i - A_d \frac{dP^*}{dZ} - \tau_{sd} A_{sd} = 0, \quad (3.14)$$

ORNL-DWG 69-7660R

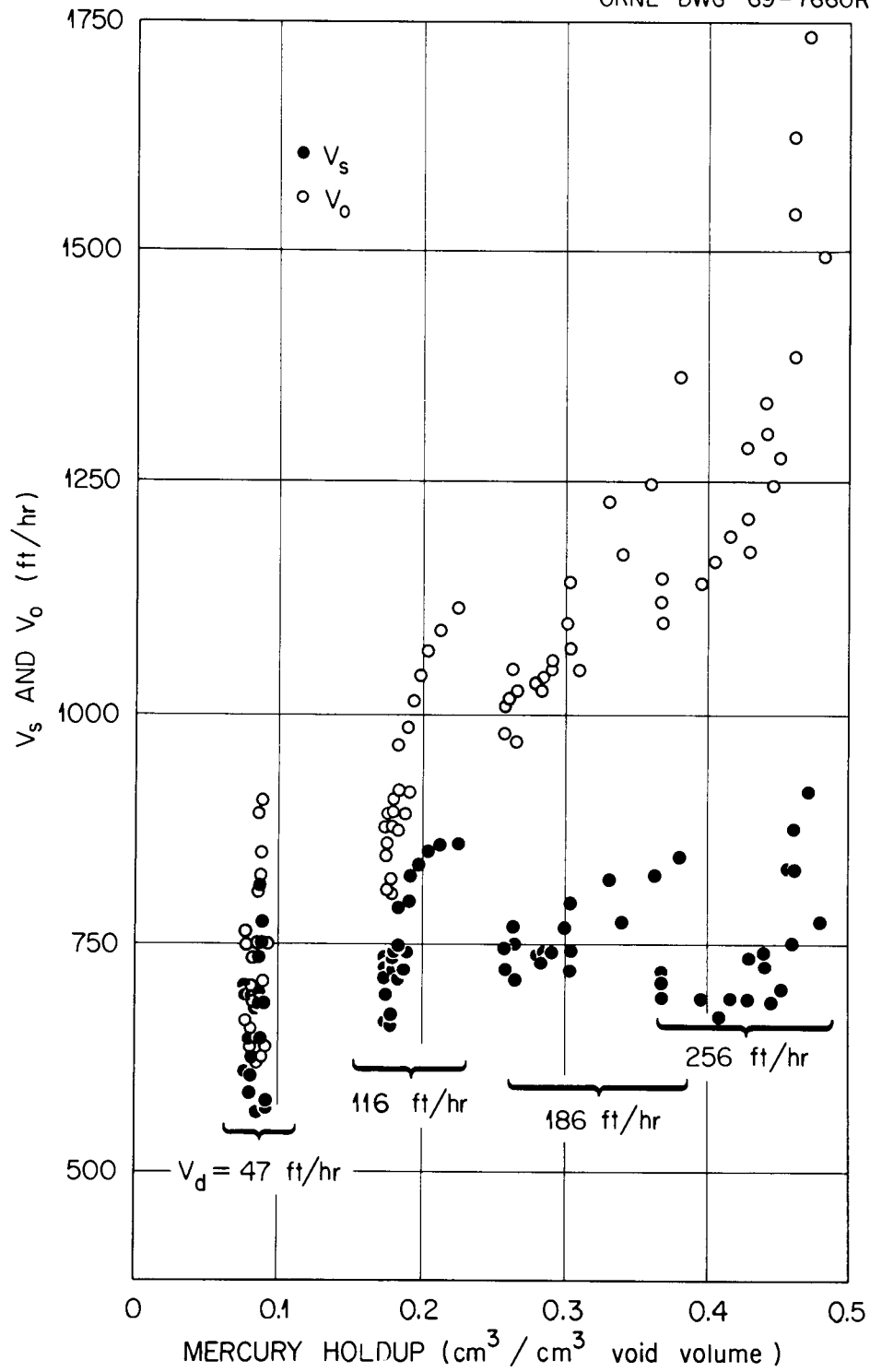


Fig. 3.26 V_o and V_s as a Function of Holdup when 1/4-in. Raschig Rings Are Used as the Column Packing.

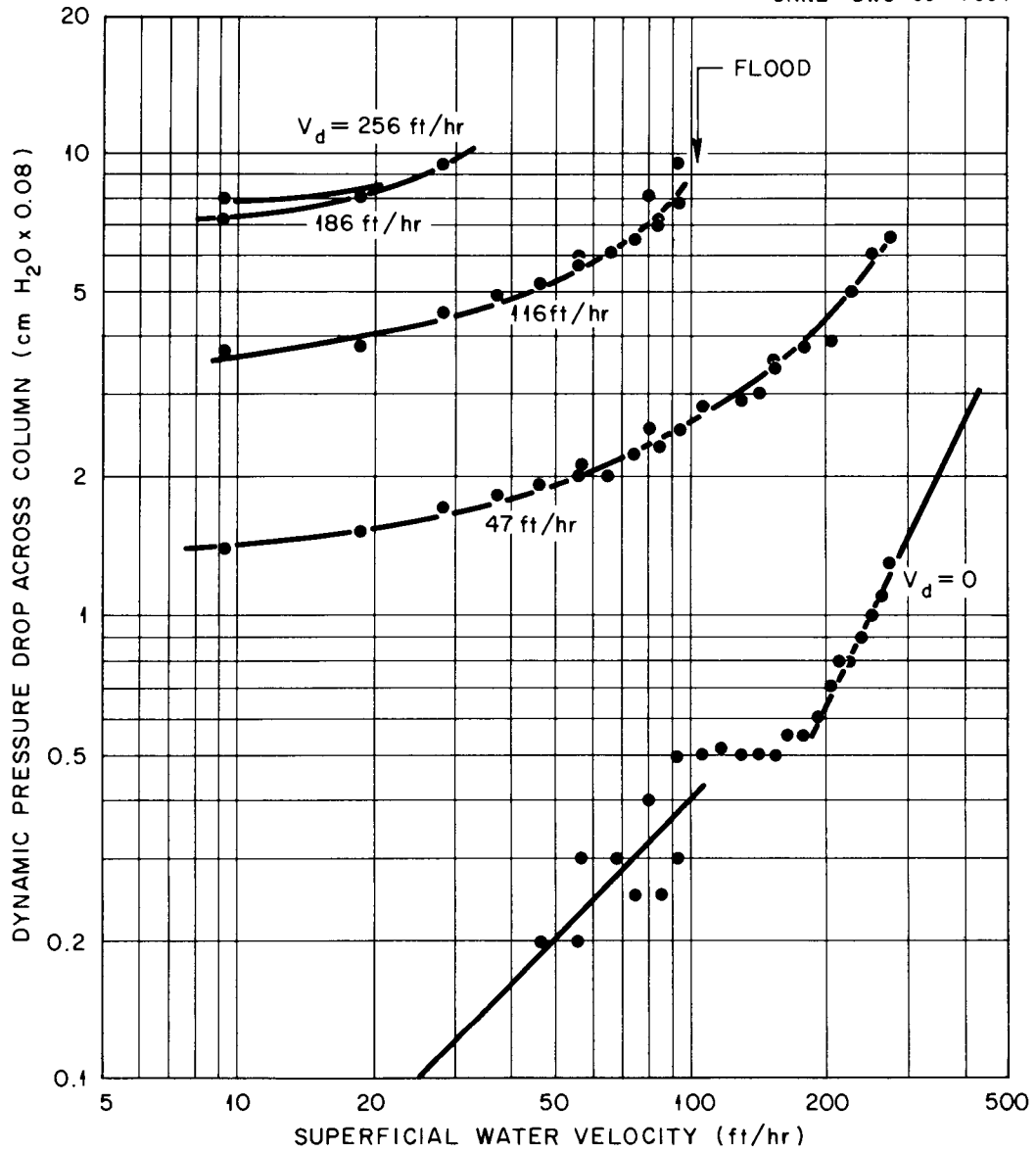
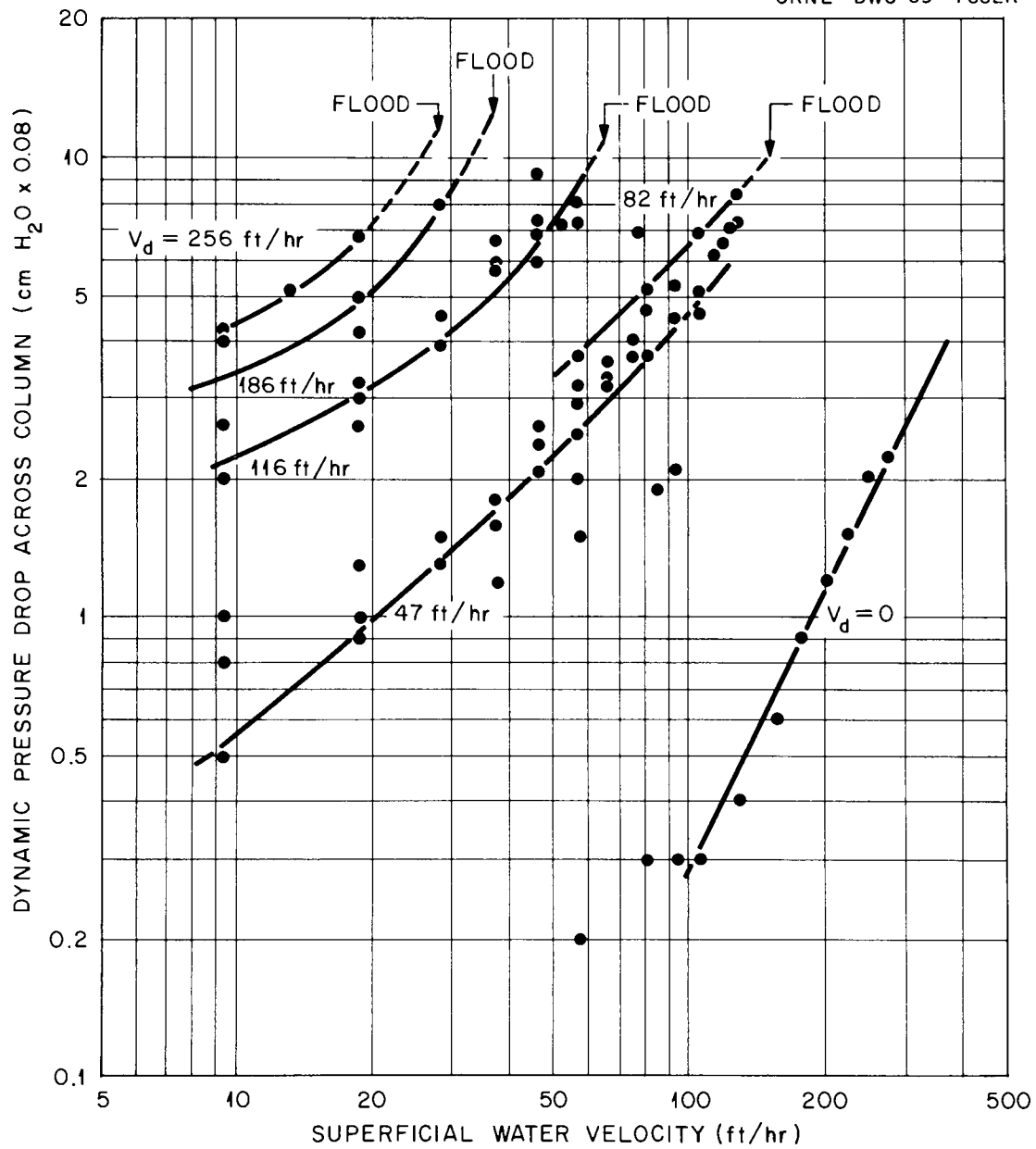


Fig. 3.27 Dynamic Pressure Drop Across a 2-ft-long Column Packed with 1/4-in. Solid Right Circular Cylinders.



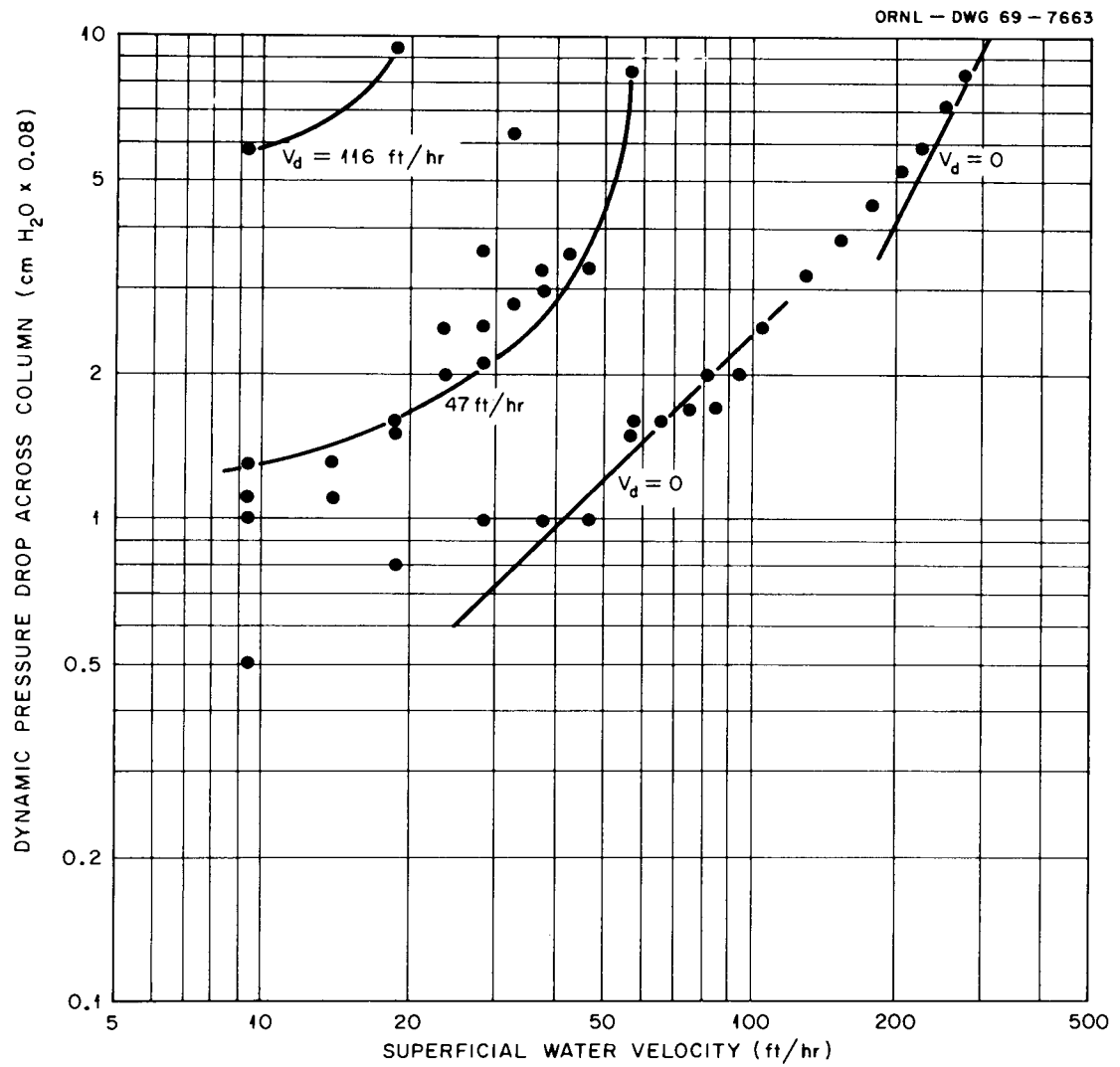


Fig. 3.29 Dynamic Pressure Drop Across a 2-ft-long Column Packed with 1/8-in. Solid Right Circular Cylinders.

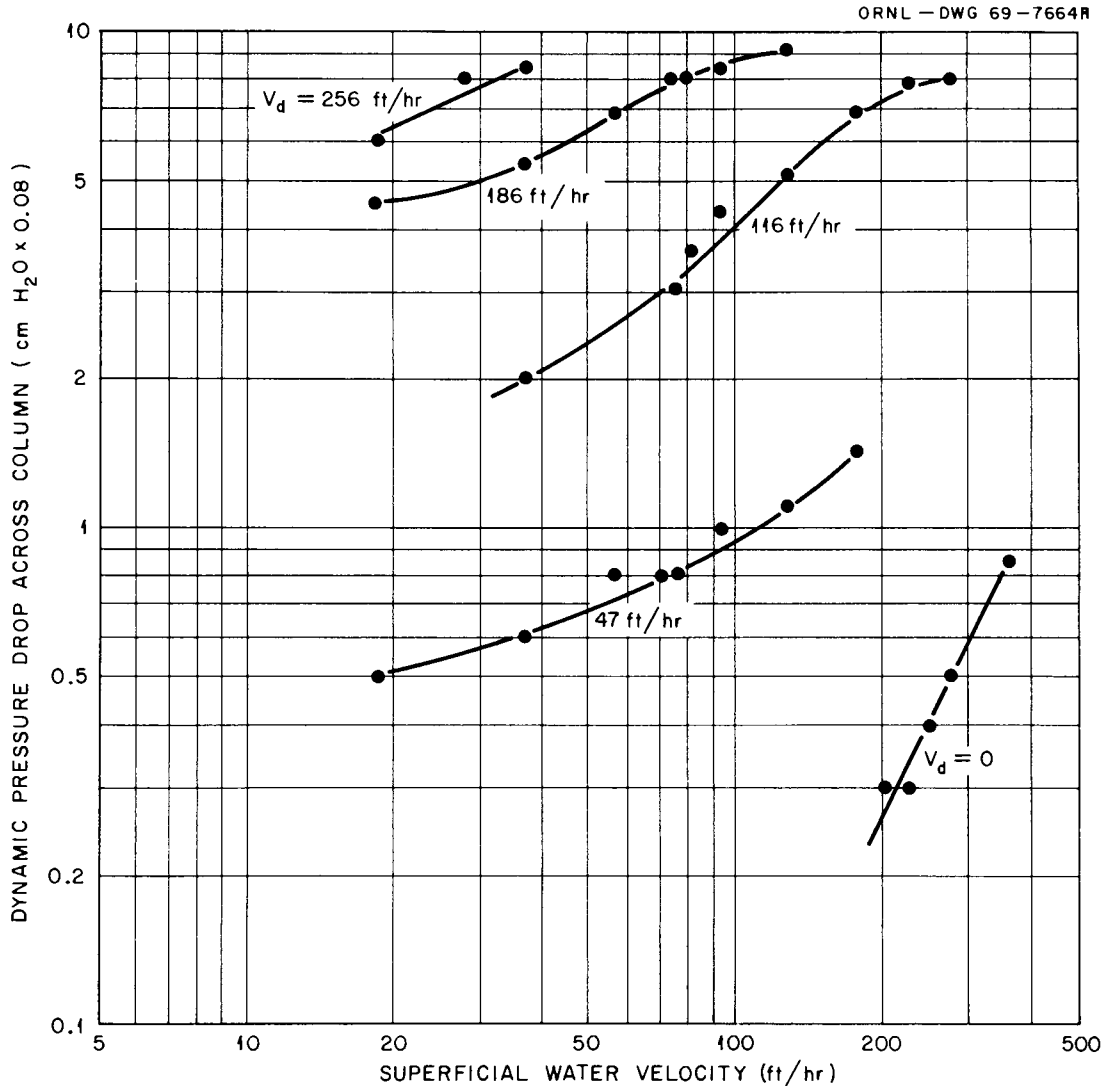


Fig. 3.30 Dynamic Pressure Drop Across a 2-ft-long Column Containing Baffles Spaced at 1/2-in. Intervals.

where

g = acceleration of gravity,

g_c = conversion factor,

A_d = cross-sectional area of dispersed phase,

$\Delta\rho$ = density difference between dispersed and continuous phases,

τ_i = shear stress at liquid-liquid interface,

A_i = interfacial area,

P^* = pressure in the column minus the pressure which would exist in a stagnant column filled with continuous phase,

Z = elevation in the column,

τ_{sd} = shear stress between the dispersed phase and the packing (and wall),

A_{sd} = area of packing (and wall) touched or wetted by the dispersed phase.

For convenience, P^* rather than the absolute pressure in the column was chosen. The continuous-phase pressure (under static conditions) is taken into account in the first term since $\Delta\rho$ is used instead of ρ .

Such a force balance is not useful until the area and shear stress terms are understood. Assume that Eqs. (3.15) and (3.16) are the shear stress terms:

$$\tau_i = k'_i V_s \quad (3.15)$$

$$\tau_{sd} = k'_{sd} \frac{V_d}{X}, \quad (3.16)$$

where V_d is the superficial dispersed-phase velocity and the k 's are constants. Then, dividing Eq. (3.14) by A_d yields:

$$\frac{g}{g_c} \Delta\rho - k'_i \frac{A_i}{A_d} V_s - \frac{dP^*}{dZ} - k'_{sd} \frac{A_{sd}}{A_d} V_d = 0. \quad (3.17)$$

Assume that A_i/A_d is constant and set

$$k_i = k_i' \frac{A_i}{A_d} \quad (3.18)$$

and

$$k_{sd} = k_{sd}' \frac{A_{sd}}{A_d} . \quad (3.19)$$

After rearrangement, Eq. (3.17) becomes:

$$V_s = \frac{g}{g_c} \frac{\Delta\rho}{k_i} - \frac{1}{k_i} \frac{dP^*}{dZ} - \frac{k_{sd}}{k_i} \frac{V_d}{X} . \quad (3.20)$$

A similar force balance on the continuous phase yields:

$$\frac{dP^*}{dZ} = \frac{A_i}{A_c} \tau_i + \frac{A_{sc}}{A_c} \tau_{sc} , \quad (3.21)$$

where A_c is the cross-sectional area of the continuous phase, A_{sc} is the area of packing that is touched or wetted by the continuous phase, and τ_{sc} is the shear stress between the continuous phase and the packing (and the wall).

Note that

$$\frac{A_i}{A_c} = \frac{A_i}{A_d} \cdot \frac{A_d}{A_c} = \frac{A_i}{A_d} X$$

and that A_{sc}/A_c is a constant. Then

$$\frac{A_i}{A_c} \tau_i = k_i X V_s , \quad (3.22)$$

where X is the holdup. Experimental data indicate that

$$\frac{A_{sc}}{A_c} \tau_{sc} = k_{sc} \left(\frac{V_c}{1-X} \right) X , \quad (3.23)$$

where V_c is the continuous-phase superficial velocity. Thus,

$$\frac{dP^*}{dZ} = k_{iS} V_c X + k_{sc} \left(\frac{V_c}{1-X} \right) X. \quad (3.24)$$

No attempt will be made to obtain a rigorous development for the second term in Eq. (3.24); however, a crude justification can be given. Pressure drop associated with flow of fluids through packed beds can be correlated by the Ergun equation,¹⁷ which contains two terms: a viscous term, and an inertial term. With relatively small channels (which would resemble the region between the mercury drops and the wall) and at low velocity, the viscous term dominates. In this case, the Ergun equation becomes:

$$\frac{dP^*}{dZ} \propto v_c^2 \frac{1}{N_{Re}} \propto \frac{v_c^2}{d_c v_c} \propto \frac{v_c}{d_c}, \quad (3.25)$$

where v_c is the velocity of the fluid through the channel. Note that v_c and V_c are related as follows:

$$v_c = \frac{V_c}{1-X},$$

and d is the effective diameter of the channel. If the mercury drops are small, the average distance from the wall to a drop will vary inversely with the concentration of drops. As an approximation, d_c will be assumed to be inversely proportional to X . Using these two approximations, one obtains the second term of Eq. (3.24).

The justification for using Eq. (3.24) rests upon its ability to correlate the experimental data. Figures 3.31 and 3.32 show pressure-drop measurements made with no water flow. Only data for the large-size packing (1/4-in. rings and solid cylinders), where dispersed flow occurs, are presented. Under these conditions, only the first term of Eq. (3.24) is nonzero. Within experimental error, straight lines are obtained. The

¹⁷S. Ergun, Chem. Engr. Progr. 48, 89 (1952).

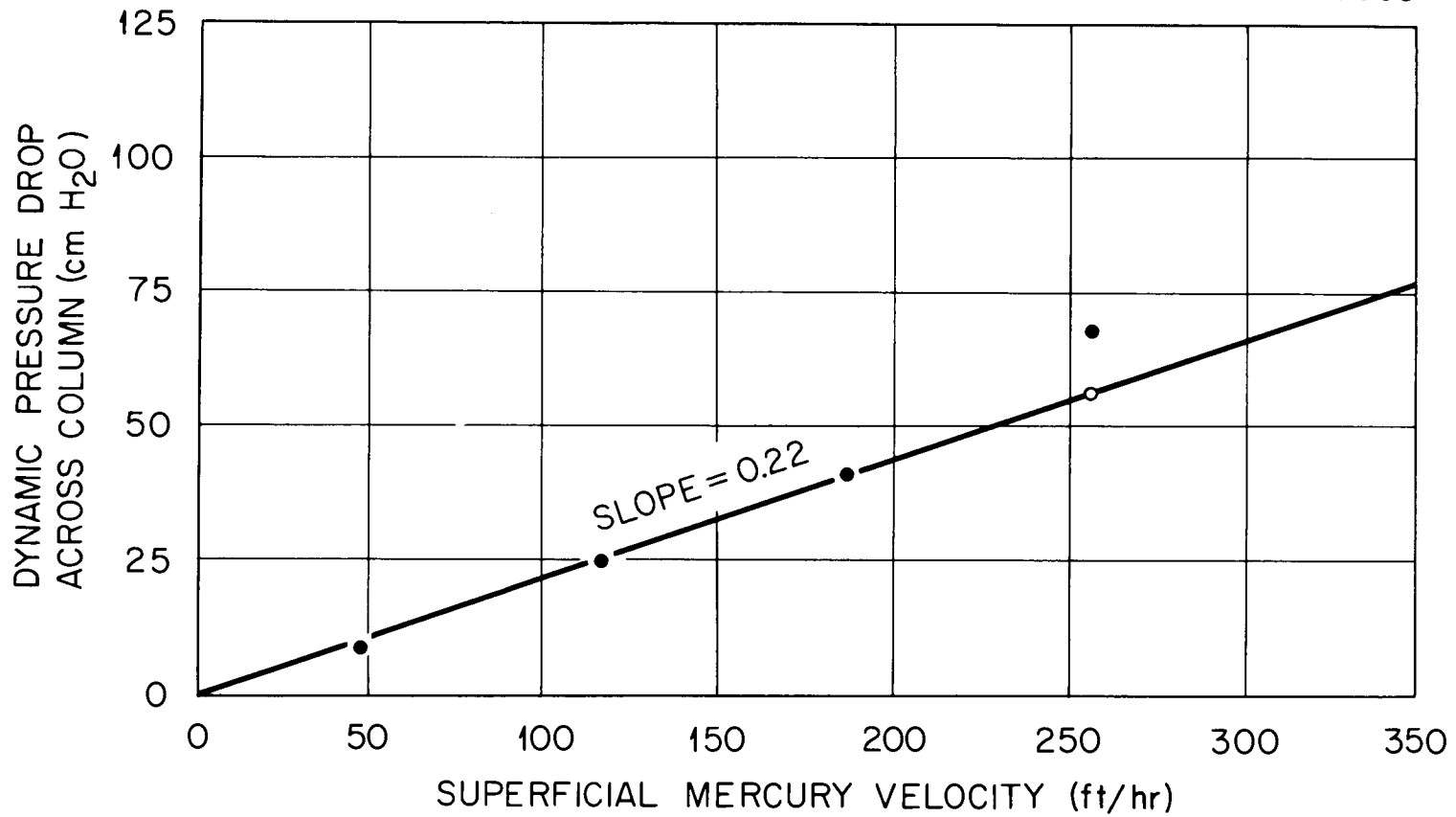


Fig. 3.31 Dynamic Pressure Drop Across a 2-ft-long Column Packed with 1/4-in. Raschig Rings. No water flow.

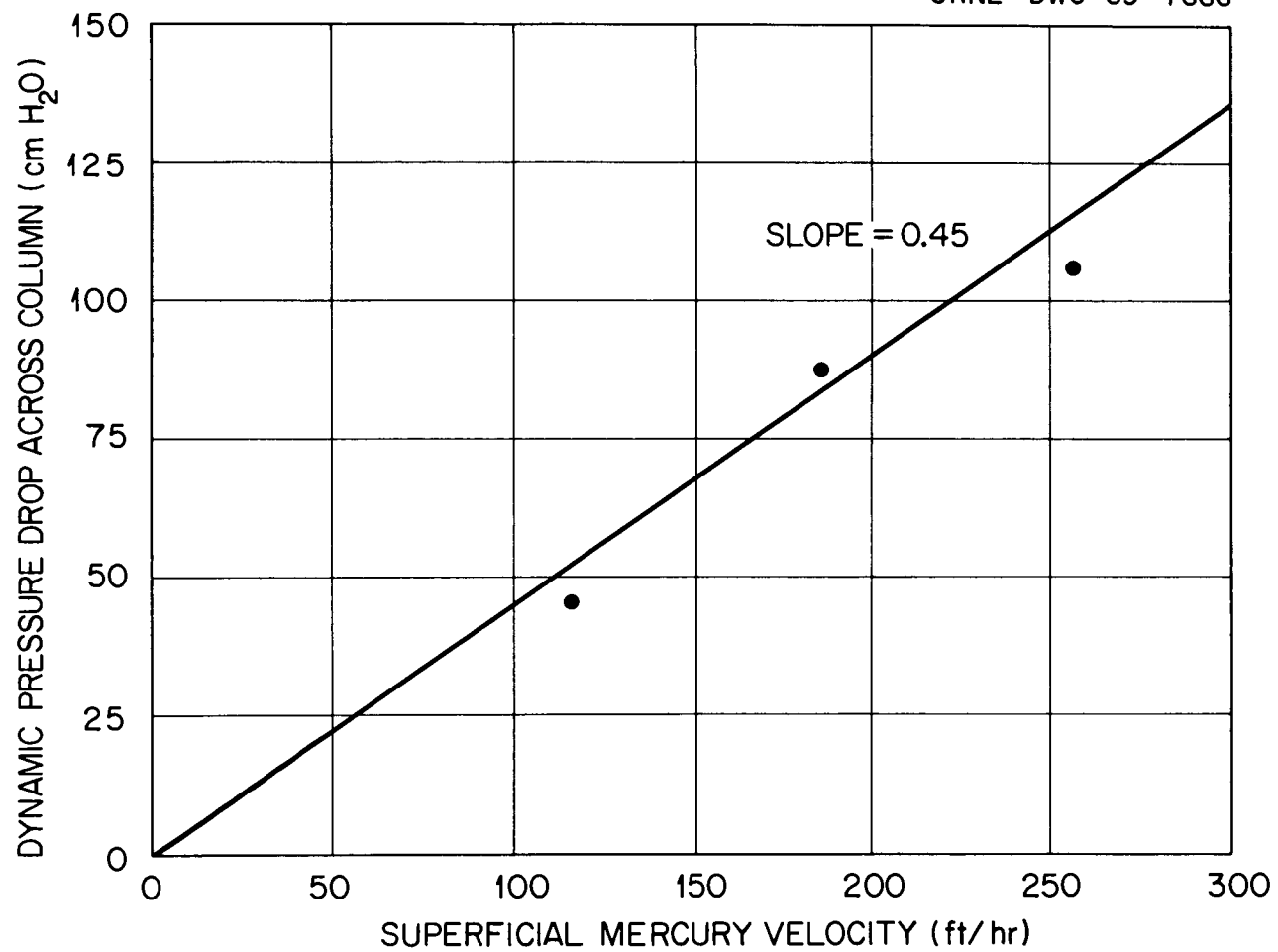


Fig. 3.32 Dynamic Pressure Drop Across a 2-ft-long Column Packed with 1/4-in. Solid Right Circular Cylinders. No water flow.

slopes of the lines are equal to $k_i X$ and can be used for determining k_i . Similarly, in Fig. 3.33, $(\Delta P - k_i V_s X)$ is plotted versus $V_c X / (1 - X)$ for 1/4-in. rings. This plot gives a straight line with a slope of k_{sc} . Although more scatter is evident in this plot, it shows no significant trend; that is, there is no detectable dependence of the data on the mercury flow rate. With 1/4-in. solid cylinders, the slope is essentially zero. Data obtained by using small packing cannot be correlated in a similar manner. This is not surprising since, with packing 1/4 in. or larger in size, the dispersed phase exists as small droplets, whereas with smaller packing it coalesces (Fig. 3.14).

The third constant, k_{sd} , is difficult to evaluate. In principle [from Eqs. (3.13) and (3.20)], one could plot

$$\frac{g \Delta \rho}{g_c k_i} - \frac{\Delta P}{k_i} - \frac{V_c}{1 - X}$$

vs V_d/X , which would yield a straight line with a slope of $(k_{sd}/k_i) + 1$. This approach is limited by the fact that the experimental data do not cover a wide range of V_d/X . Although this does not affect the accuracy with which k_{sd} can be evaluated, it does prevent a satisfactory evaluation of the assumed linear relation for shear between the dispersed phase and the packing. With 1/4-in. Raschig rings, the data appear to form essentially a straight line (Fig. 3.34), and the use of Eq. (3.20) appears valid. Less data have been obtained with 1/4-in. solid packing, and the results are somewhat more scattered (see Fig. 3.35).

Having evaluated the three constants, k_i , k_{sc} , and k_{sd} , we can, in principle, now calculate the holdup, pressure drop, and flooding curves from Eqs. (3.20) and (3.24). Since pressure drop and holdup were used directly to evaluate the constants, the flooding curve affords an independent check of Eqs. (3.20) and (3.24). There is, of course, an obvious danger in this approach because the flow patterns often change near the flooding point. To evaluate the flooding curve, Eqs. (3.21) and (3.24) were combined in order to eliminate the pressure drop. The

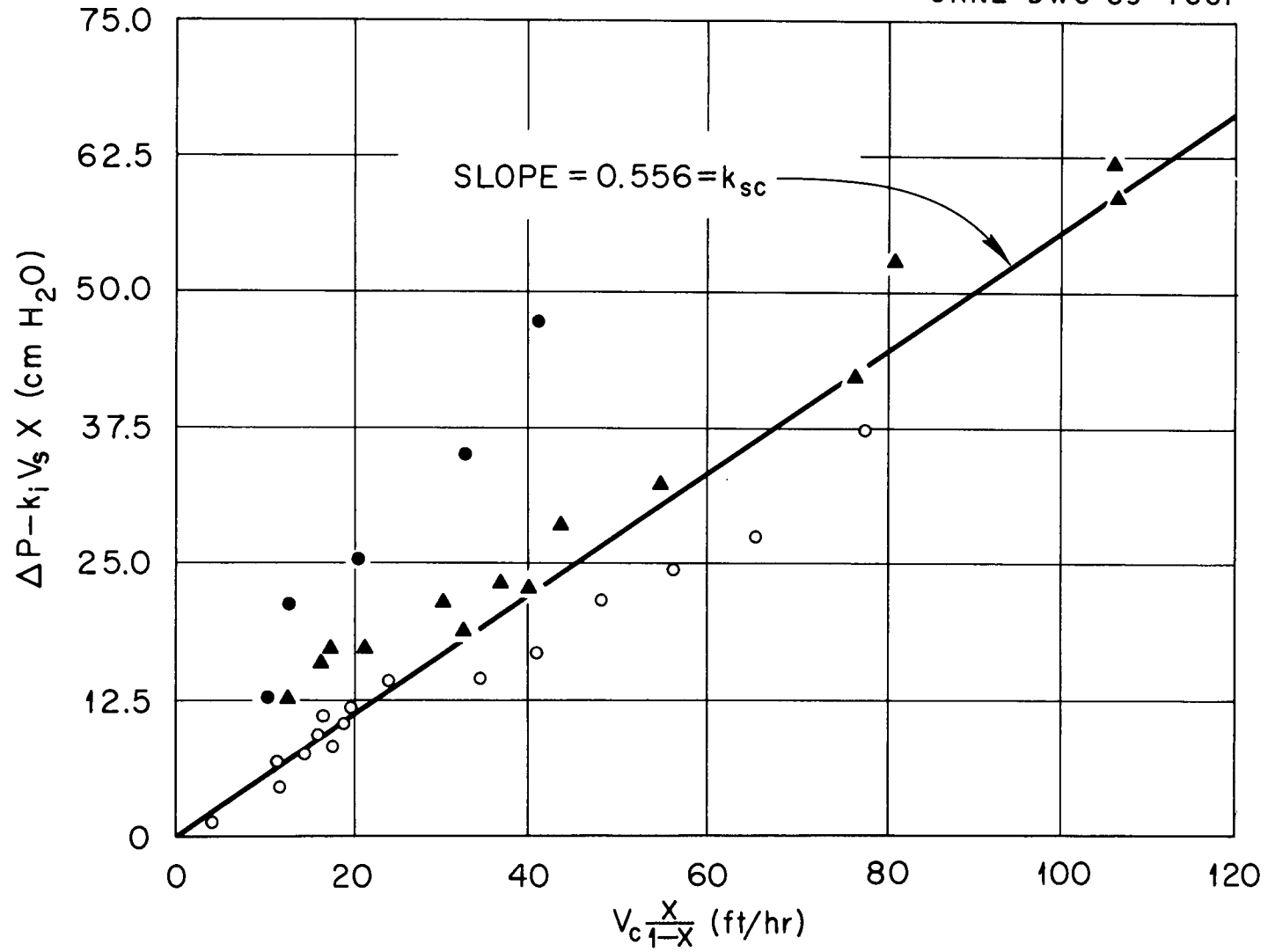


Fig. 3.33 Evaluation of k_{sc} for 1/4-in. Raschig Rings.

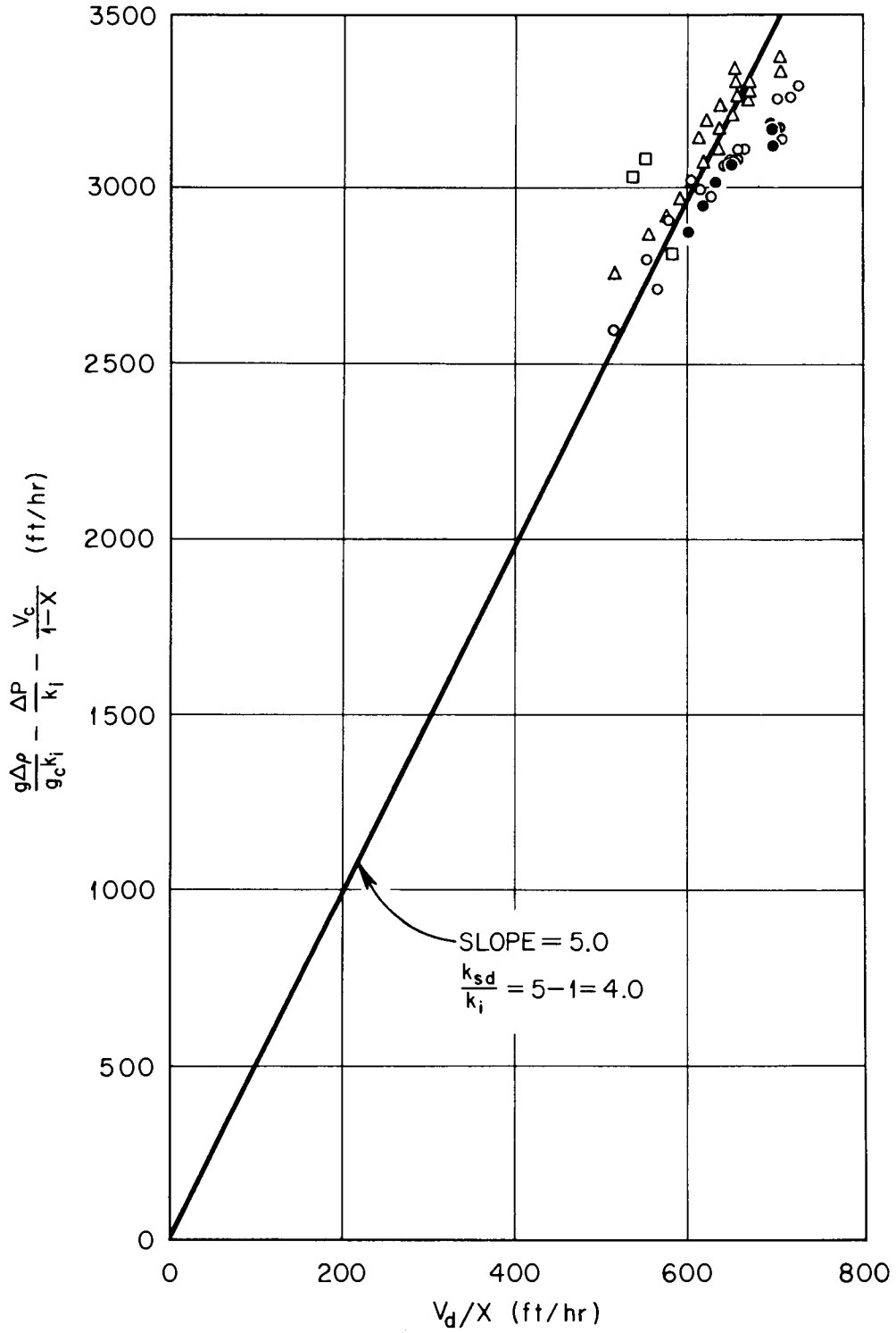


Fig. 3.34 Evaluation of k_{sd} for 1/4-in. Raschig Rings.

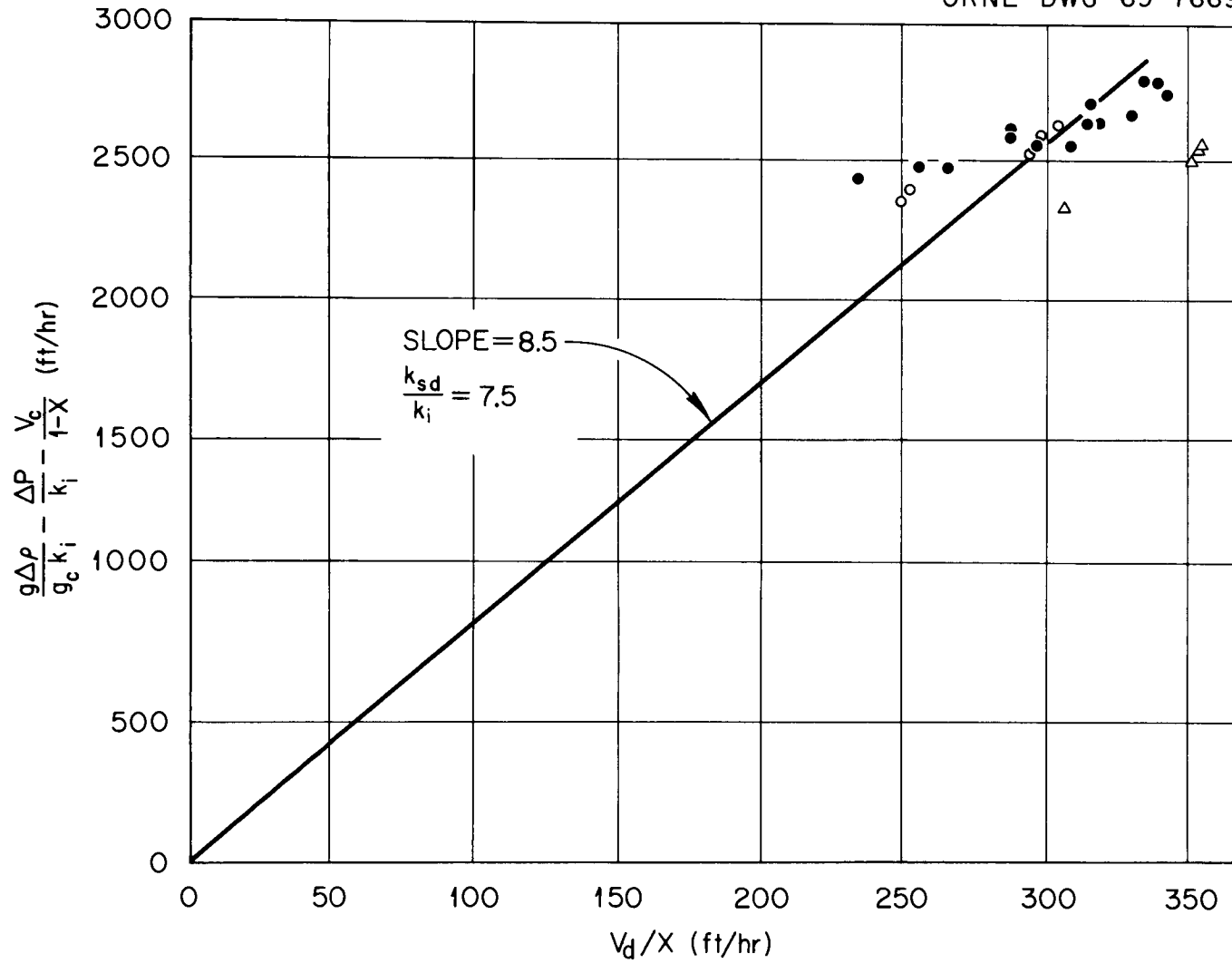


Fig. 3.35 Evaluation of k_{sd} for 1/4-in. Solid Cylindrical Packing.

quantities V_c and V_d then become functions of holdup. For a given value of V_d , a trial-and-error procedure was used to determine the maximum value of V_c . This maximum value of V_c was considered to be the flooding rate; that is, $\partial V_c / \partial X = \partial V_d / \partial X = 0$ at flooding. For a given dispersed rate, V_d , we look for a holdup X that will yield the maximum V_c , or where $\partial V_c / \partial X = 0$. The results of these calculations are given in Figs. 3.36 and 3.37, and the agreement with the experimental flooding curve is encouraging.

In principle, it is possible to use only pressure drop data (no holdup data) to evaluate the three constants. Although the calculations would be more complicated than those just described, the approach should be useful in evaluating or estimating holdup and flooding rates in salt-metal systems.

Data from smaller packing materials (3/16-in. rings and 1/8-in. solid packing) are not correlated by the above model. To date, a model that satisfactorily describes the data from both of these smaller packing materials has not been found. This study, like studies in the past, has concentrated upon larger packing materials, which are of more interest for operating systems.

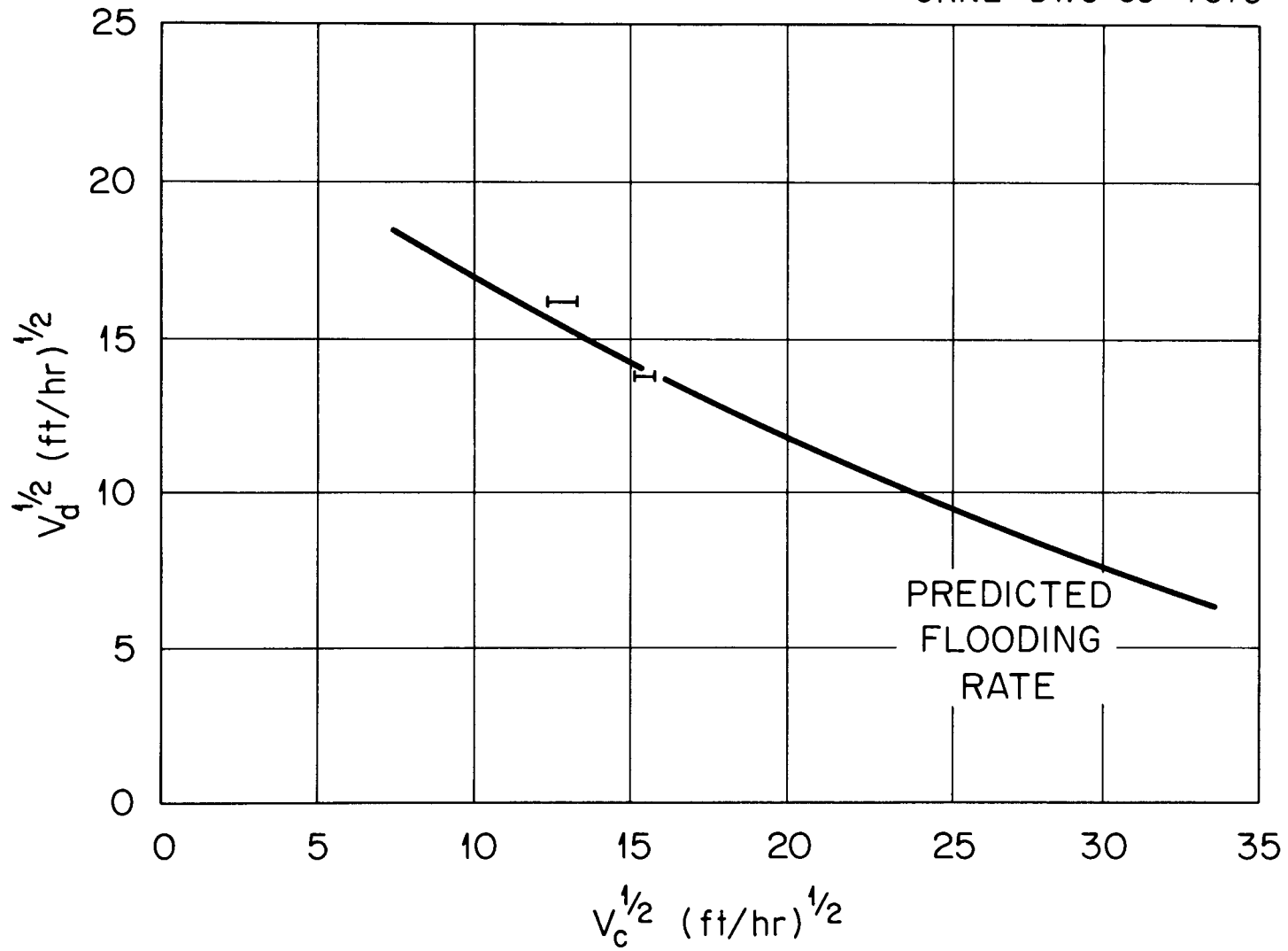


Fig. 3.36 Comparison of Predicted and Measured Flooding Rates in a Column Packed with 1/4-in. Raschig Rings.

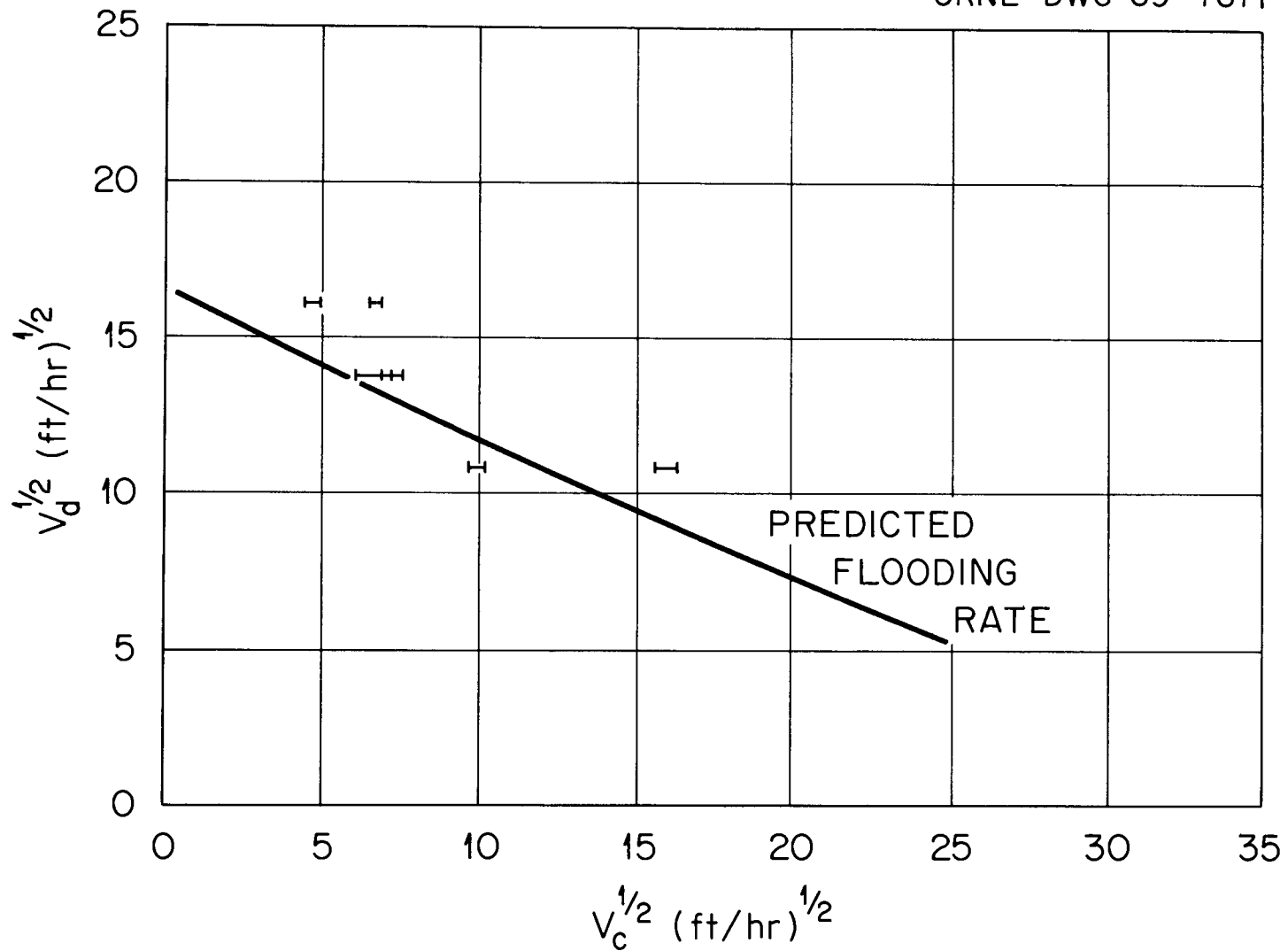


Fig. 3.37 Comparison of Predicted and Measured Flooding Rates in a Column Packed with 1/4-in. Solid Right Circular Cylinders.

86

INTERNAL DISTRIBUTION

- | | |
|-------------------------------------|----------------------------------|
| 1. Biology Library | 73. D. M. Lang |
| 2-4. Central Research Library | 74. R. E. Leuze |
| 5-6. ORNL - Y-12 Technical Library | 75. R. B. Lindauer |
| Document Reference Section | 76. H. G. MacPherson |
| 7-41. Laboratory Records Department | 77. G. M. Marrow (Y-12) |
| 42. Laboratory Records, ORNL R.C. | 78. J. L. Matherne |
| 43. R. E. Blanco | 79. J. P. McBride |
| 44. J. O. Blomeke | 80. W. T. McDuffee |
| 45. R. E. Brooksbank | 81. W. H. McVey |
| 46. K. B. Brown | 82. J. P. Nichols |
| 47. F. R. Bruce | 83. E. L. Nicholson |
| 48. W. D. Burch | 84. F. L. Parker |
| 49. W. H. Carr | 85. J. R. Parrott |
| 50. G. I. Cathers | 86. J. H. Pashley (K-25) |
| 51. J. M. Chandler | 87. F. S. Patton, Jr. (Y-12) |
| 52. W. E. Clark | 88. R. H. Rainey |
| 53. K. E. Cowser | 89. A. D. Ryon |
| 54. D. J. Crouse | 90. W. D. Schaffer, Jr. |
| 55. F. L. Culler, Jr. | 91. M. J. Skinner |
| 56. W. Davis, Jr. | 92. Martha Stewart |
| 57. D. E. Ferguson | 93. J. C. Suddath |
| 58. L. M. Ferris | 94. D. A. Sundberg |
| 59. J. R. Flanary | 95. W. E. Unger |
| 60. H. E. Goeller | 96-117. Unit Operations Section |
| 61. J. M. Googin (Y-12) | 118. C. D. Watson |
| 62. P. A. Haas | 119. A. M. Weinberg |
| 63. F. E. Harrington | 120. M. E. Whatley |
| 64. R. F. Hibbs | 121. R. H. Winget |
| 65. R. W. Horton | 122. R. G. Wymer |
| 66. G. Jasny (Y-12) | 123. E. L. Youngblood |
| 67. H. F. Johnson | 124. P. H. Emmett (consultant) |
| 68. W. H. Jordan | 125. J. J. Katz (consultant) |
| 69. S. H. Jury | 126. J. L. Margrave (consultant) |
| 70. L. J. King | 127. E. A. Mason (consultant) |
| 71. B. B. Klima | 128. R. B. Richards (consultant) |
| 72. E. Lamb | |

EXTERNAL DISTRIBUTION

129. E. L. Anderson, Atomic Energy Commission, Washington
130. A. L. Babb, University of Washington
131. F. P. Baranowski, Atomic Energy Commission, Washington
132. W. G. Belter, Atomic Energy Commission, Washington
133. S. Bernstein, Union Carbide Corporation, Paducah
134. J. M. Berty, Research and Development Department, Union Carbide Corporation, P. O. Box 8361, South Charleston, West Virginia 25314
135. D. E. Bloomfield, Battelle Northwest, Richland, Washington

136. J. A. Buckham, Idaho Chemical Processing Plant
137. J. T. Christy, Richland Operations Office
138. C. R. Cooley, Pacific Northwest, Richland, Washington
139. Kermit Laughon, ORNL, RDT Site Office
140. E. R. Gilliland, Massachusetts Institute of Technology
141. W. W. Grigorieff, Assistant to the Executive Director, Oak Ridge
Associated Universities
142. M. J. Harmon, Pacific Northwest, Richland, Washington
143. L. P. Hatch, Brookhaven National Laboratory
144. O. F. Hill, Pacific Northwest, Richland, Washington
145. C. H. Ice, Savannah River Laboratory
146. E. R. Irish, Pacific Northwest, Richland, Washington
147. B. M. Legler, Idaho Chemical Processing Plant
148. J. A. Lieberman, Atomic Energy Commission, Washington
149. B. Manowitz, Brookhaven National Laboratory
150. J. A. McBride, DML, Atomic Energy Commission, Washington
151. J. W. Nehls, Atomic Energy Commission, Oak Ridge
152. C. M. Nicholls, AERE, Harwell, England
153. E. O. Nurmi, Babcock and Wilcox Company
154. H. Pearlman, Atomics International
155. A. M. Platt, Pacific Northwest, Richland, Washington
156. R. A. Proebstle, Knolls Atomic Power Laboratory
157. J. W. Pollock, Idaho Operations Office
158. K. L. Rohde, Idaho Chemical Processing Plant
159. C. A. Rohrman, Pacific Northwest, Richland, Washington
160. C. M. Slansky, Idaho Chemical Processing Plant
161. M. Smutz, Ames Laboratory, Ames, Iowa
162. C. E. Stevenson, Idaho Division, Argonne National Laboratory,
P. O. Box 2528, Idaho Falls, Idaho
163. K. G. Steyer, General Atomic
164. J. A. Swartout, Union Carbide Corporation, New York
165. C. D. Tabor, Goodyear Atomic
166. V. R. Thayer, Du Pont, Wilmington
167. R. C. Vogel, Argonne National Laboratory, 9700 South Cass Ave.,
Argonne, Illinois
168. G. H. Wagner, General Electric Company, Santa Clara, California
169. D. C. Webster, Associate Director of Chemical Engineering
Division, Argonne National Laboratory, 9700 South Case Ave.,
Argonne, Illinois
170. Laboratory and University Division, AEC, ORO
- 171-360. Given distribution as shown in TID-4500 under Chemistry category
(25 copies - CFSTI)